CHOLESTEROL ESTER METABOLISM GOVERNS INTRACELLULAR CHOLESTEROL CRYSTAL FORMATION

A Thesis Submitted to the College of Graduate and Postdoctoral Studies
In Partial Fulfillment of the Requirements
For the Degree of Master of Science
In the Department of Anatomy, Physiology and Pharmacology

University of Saskatchewan
Saskatoon, Saskatchewan, Canada

By

Jordan Anthony Bairos

Permission to Use

In presenting this thesis in partial fulfillment of the requirements for a Graduate degree from the University of Saskatchewan, I agree that the Libraries of this University may make it freely available for inspection. I further agree that permission for copying of this thesis in any manner, in whole or in part, for scholarly purposes may be granted by the professor or professors who supervised my thesis work or, in their absence, by the Head of the Department or the Dean of the College in which my thesis work was done. It is understood that any copying or publication or use of this thesis or parts thereof for financial gain shall not be allowed without my written permission. It is also understood that due recognition shall be given to me and to the University of Saskatchewan in any scholarly use which may be made of any material in my thesis.

Requests for permission to copy or to make other uses of materials in this thesis in whole or in part should be addressed to:

Head of Department of Anatomy, Physiology and Pharmacology
University of Saskatchewan
2D01 Health Sciences Building
107 Wiggins Road
Saskatoon, Saskatchewan S7N 5E5 Canada

OR

Dean of College of Graduate and Postdoctoral Studies
University of Saskatchewan
116 Thorvaldson Building
110 Science Place
Saskatoon, Saskatchewan S7N 5C9 Canada

Abstract

Free cholesterol (FC) accumulation underlies cholesterol crystallization, yet the mechanistic factors contributing to this process are unknown. The presence of cholesterol crystals (CC) in atherosclerotic lesions has been recognized to increase risk of thrombosis leading to major adverse cardiovascular events. Likewise, recent studies on patients with non-alcoholic steatohepatitis (NASH) indicate that CC in hepatocyte lipid droplets distinguish NASH from benign steatosis. *In vitro* investigations attempting to recapitulate the effects of CC on macrophages in the context of atherosclerosis demonstrate that CC activate inflammatory signaling and remodel macrophage metabolism. A wealth of literature has reported the production of intracellular CC by incubating macrophages, smooth muscle cells, and endothelial cells with modified lipoproteins. In addition, electron microscopy has provided evidence that CC nucleate intracellularly on macrophage lipid droplet surfaces. However, few studies have explored intracellular CC formation in hepatocytes, despite a strong link to NASH. Whether hepatocyte crystals actively contribute to liver disease pathogenesis and progression remains to be investigated. Due to the ability of lipid droplets to concentrate cholesterol in the form of esters, we reasoned cholesterol esterification, subsequent lipid droplet localization, and then de-esterification will concentrate FC at the lipid droplet surface to drive cholesterol nucleation and crystal formation. Hence, we hypothesized that enzymes that mediate cholesterol esterification and enzymes that de-esterify lipid droplet cholesterol ester (CE) are required for intracellular CC formation. To investigate this, human hepatocytes and mouse macrophages were loaded with cholesterol or acetylated low-density lipoprotein (acLDL), respectively, and were imaged under polarized light to detect CC. Crystals formed reliably in a time- and dose-dependent manner in both cell types. Fluorescence imaging and polarized light microscopy reveal that these crystals are associated with lipid droplets, but not lysosomes. Inhibiting acyl-coenzyme A: cholesterol acyltransferase 1 (ACAT1) using pharmacologic and genetic methods diminished cholesterol crystallization and CE production. Remarkably, nonselective ACAT inhibition prevented plate-like CC cleft formation in hepatocytes. Also, blocking the de-esterification of lipid droplet CE with neutral CE hydrolase 1 (nCEH1) inhibitor JW480 blunted CC formation, but was more effective in hepatocytes than in macrophages. Collectively, we identify ACAT1 and nCEH1 as critical factors that function in series to drive intracellular CC formation. Our results provide needed mechanistic insight into cholesterol crystallization and highlight potential targets to prevent CC formation in human disease.

Acknowledgements

First and foremost, I would like to extend my sincerest gratitude to my supervisor Dr. Scott Widenmaier for taking a chance on me as an undergraduate student and welcoming me into the lab even though I had no research experience. I am grateful for your mentorship and support over the past three years. Having the opportunity to learn from you has been a pleasure.

Thank you to all past and present members of the Widenmaier lab: Dr. Lei Li, May Akl, Mike Trites, Uche Njoku, Alireza Ahadiabhari, Sharmili Prathap, Aidan Hydomako, Maria Zafar, Sherin McDonald, and Brynne Stebbings for your feedback during lab meetings and the countless lab hours spent together. Sherin, I appreciate your guidance and the time you spent training me during my early days in the lab. May, thank you for your assistance with cholesterol crystal imaging and quantification. Lei, thank you for performing the genomic cleavage assay and preparing samples to be sequenced for this project.

Thank you to my research advisory committee for their valuable insights and feedback throughout my program: Dr. Changting Xiao and Dr. Asmahan AbuArish. I'd also like to thank our collaborators Dr. Ana Paula Arruda and Dr. Gunes Parlakgul from the University of California Berkeley for their assistance in acquiring electron microscope images. Special thank you to Dr. Scot Stone for allowing access to your microscope and to Heather Neufeld for initial lab training and keeping our work environment organized and safe.

Thank you to the University of Saskatchewan College of Medicine for providing financial support through an Anatomy, Physiology and Pharmacology Devolved scholarship and to Dr. Widenmaier for supporting my stipend.

Lastly, I would like to thank my parents, siblings, and friends for their ongoing support and encouragement throughout my MSc program.

Table of Contents

Permission to use……..……i

Abstract……ii

Acknowledgements……iii

Table of contents……..……iv

List of tables……..……vii

List of figures……viii

List of abbreviations……...……x

Chapter 1: Thesis Introduction and Rationale……..……1

Chapter 2: Literature Review……...……3

2.1: Properties, functions, and regulation of cellular cholesterol……3
2.1.1: Properties……...……3
2.1.2: Functions……3
2.1.3: Regulation……..……4
2.2 Cholesterol ester homeostasis……...……5
2.2.1: Acyl-CoA:Cholesterol Acyltransferase 1 and 2……5
2.2.2: Neutral CE hydrolase 1……..7
2.2.3: Lipid droplets……8
2.3: Atherosclerosis and cholesterol crystals……...……9
2.3.1: Atherosclerosis……...……9
2.3.2: Identification of cholesterol crystals in atherosclerotic plaques……9
2.3.3: NLRP3 inflammasome……11
2.3.4: Metabolic reprogramming……...……12
2.3.5: Plaque destabilization……..……13
2.3.6: Targeting ACAT in atherosclerosis…….……14
2.4: Fatty liver disease and cholesterol crystals…….……19
2.4.1: Fatty liver disease……19
2.4.2: Cholesterol crystal nucleation……..……19
2.4.3: Cholesterol crystallization in hepatocytes……...……20
2.4.4: A potential pathway coupled to cholesterol crystallization in liver…..……22
2.5: Hypothesis and objectives……..……22

Chapter 3: Materials and Methods……24

3.1: Reagents……..……24
3.2: MβCD-Cholesterol complexing…….……24

3.3: Cell culture……..……24
3.4: CRISPR/Cas9-based gene editing……..……24
3.5: Cholesterol crystal formation and imaging…….……25
3.6: Cholesterol crystal area quantification……...……26
3.7: Fluorescence imaging…….……26
3.8: Live/dead imaging assay…….……27
3.9: Cholesterol crystal solubilization assay……..……27
3.10: Lipid extraction and cholesterol quantification……27
3.11: Immunoblot analysis…….……28
3.12: Gene expression analysis……..……30
3.13: Electron microscopy…….……31
3.14: Genomic cleavage detection and sequencing…...……31
3.15: Statistical analysis…….……32

Chapter 4: Cholesterol Crystallization Model and Intracellular Localization……..……33

4.1: Introductory rationale…….……33
4.2: Results…….……33
4.2.1: Cholesterol crystallization model characterization…..……33
4.2.2: Intracellular cholesterol crystal localization……41
4.3: Conclusion……..……42

Chapter 5: The Role of Cholesterol Ester Metabolism in Cholesterol Crystal Formation.43

5.1: Introductory rationale…….……43
5.2: Results…….……43
5.2.1: Evidence that ACAT1 is required for cholesterol crystal formation…...…43
5.2.2: The contribution of autophagy to cholesterol crystal formation……..……54
5.2.3: Evidence that nCEH1 is required for cholesterol crystal formation……57
5.2.4: Replication of results from hepatocytes in macrophages……60
5.3: Conclusion and proposed mechanism…….……62

Chapter 6: Discussion……..……64

6.1: Cholesterol crystallization in hepatocytes and NASH……64
6.1.1: General discussion……...……64
6.1.2: Targeting the liver to treat heart disease……..……68
6.1.3: Potential of targeting ACAT in cancer……69
6.1.4: Role of nCEH1 in cancer…….……70
6.2: Cholesterol crystallization in macrophages and atherosclerosis…….……72
6.2.1: General discussion……...……72
6.2.2: CE hydrolysis in macrophages……72
6.2.3: A potential downstream pathway of cholesterol crystallization……..……73
6.3: Limitations……..……73
6.4: Future directions…….……74
6.5: Conclusions…….……75

References………………………..…………………………………………………………76

Appendix……………………….....……………………………………………………………87

List of Tables

Table 2.1: Summary of key studies targeting ACAT in atherosclerosis……16

Table 3.1: Antibodies used for immunoblotting……29

Table 3.2: DNA primer sequences used in qPCR……..……30

Table 3.3: PCR primer sequences used for genomic cleavage detection and sequencing……..…32

List of Figures

Chapter 4

Figure 4.1: Cholesterol loading induces cholesterol crystal formation in a time-dependent manner in hepatocytes……..……34

Figure 4.2: Cholesterol esterification is associated with cholesterol crystal formation……35

Figure 4.3: Transition to cholesterol-free media is sufficient to solubilize pre-formed cholesterol crystals……...……36

Figure 4.4: Cholesterol depletion is sufficient to solubilize pre-formed cholesterol crystals...…38

Figure 4.5: acLDL and cholesterol loading induces cholesterol crystal formation in a time-dependent manner in macrophages……40

Figure 4.6: Hepatocyte lipid droplets support cholesterol crystallization…….……41

Figure 4.7: Macrophage lipid droplets support cholesterol crystallization……42

Chapter 5

Figure 5.1: Cholesterol esterification and subsequent lipid droplet localization is required for cholesterol crystal formation……..……44

Figure 5.2: Cholesterol loaded hepatocytes display expected homeostatic regulation……..…45

Figure 5.3: ACAT inhibition prevents the formation of lipid droplet-associated cholesterol crystals……...……47

Figure 5.4: Intracellular plate-like cholesterol crystal formation in hepatocytes is ameliorated by ACAT inhibition……49

Figure 5.5: Selective ACAT1 inhibition is sufficient to blunt cholesterol crystal formation……50

Figure 5.6: *SOAT1*-deficient hepatocytes exhibit reduced cholesterol crystal formation……..…52

Figure 5.7: *SOAT1*-deficient hepatocytes display altered lipid droplet formation and lack lipid droplet-associated cholesterol crystals……...……53

Figure 5.8: Cholesterol accumulation induces autophagy but is not potentiated by ACAT inhibition……54

Figure 5.9: Cholesterol crystal formation is unaffected by autophagy induction……..…56

Figure 5.10: Lipid droplet cholesterol ester hydrolysis is required for cholesterol crystal formation……58

Figure 5.11: nCEH1 inhibition prevents the formation of lipid droplet-associated cholesterol crystals……..……59

Figure 5.12: ACAT inhibition prevents acLDL-induced cholesterol crystal formation in macrophages……..……60

Figure 5.13: nCEH1 inhibition partially reduces cholesterol crystal formation in cholesterol loaded macrophages…….…..……61

Figure 5.14: Proposed model for intracellular cholesterol crystal formation……63

List of Abbreviations

AADAC	Arylacetamide deacetylase
AADACL1	Arylacetamide deacetylase like 1
ABCA1	ATP-binding cassette subfamily A member 1
ACAT1/2	Acyl-CoA: Cholesterol acyltransferase 1 or 2
acLDL	Acetylated low-density lipoprotein
ACS	Acute coronary syndrome
ANOVA	Analysis of variance
AP	Autophagosome
ApoB	Apolipoprotein B
ApoE	Apolipoprotein E
ATF4	Activating transcription factor 4
ATP	Adenosine triphosphate
A.U.	Arbitrary units
BCA	Bicinchoninic acid
BiP	Binding immunoglobulin protein
BMT	Bone-marrow transplant
BSA	Bovine serum albumin
Cas9	CRISPR-associated protein 9
CC	Cholesterol crystal(s)
CD	Cyclodextrin
cDNA	Complimentary DNA
CE	Cholesterol ester
CESD	Cholesterol ester storage disease
CHO	Chinese hamster ovary
CHOP	C/EBP homologous protein
CLEC4	C-type lectin 4
CRISPR	Clustered regularly interspaced short palindromic repeats
Ct	Cycle threshold
CVD	Cardiovascular disease
CYP3A4	Cytochrome P450 family 3 subfamily A member 4

CYP7A1	Cytochrome P450 family 7 subfamily A member 1
DAMPs	Damage-associated molecular patterns
DHA	Docosahexaenoic acid
DMEM	Dulbecco's modified eagle medium
DMSO	Dimethyl sulfoxide
EM	Electron microscopy
EPA	Eicosapentaenoic acid
ER	Endoplasmic reticulum
FC	Free cholesterol
FDFT1	Farnesyl-diphosphate farnesyltransferase 1
FIT	Fat storage inducing
GAPDH	Glyceraldehyde-3-phosphate dehydrogenase
GFP	Green fluorescent protein
GLUT1	Glucose transporter type 1
HCC	Hepatocellular carcinoma
HFD	High fat diet
HIF1α	Hypoxia inducible factor 1 subunit alpha
HK2	Hexokinase 2
HRP	Horseradish peroxidase
HSCs	Hepatic stellate cells
HSL	Hormone sensitive lipase
H&E	Hematoxylin and eosin
IDOL	Inducible degrader of the LDL receptor
IgG	Immunoglobulin G
IL-1β	Interleukin-1 beta
INDEL	Insertion/deletion
IVUS	Intravascular ultrasound
LC3B	MAP1 light chain 3 beta
LD	Lipid droplet
LDL	Low-density lipoprotein
LDL-C	Low-density lipoprotein cholesterol

LDLR	Low-density lipoprotein receptor
LPS	Lipopolysaccharide
LXR	Liver X receptor
mAb	Monoclonal antibody
MAGE	Monoalkylglycerol ether
MBOAT	Membrane bound O-acyltransferase
MOI	Multiplicity of infection
MPMs	Mouse peritoneal macrophages
mRNA	Messenger RNA
mTORC1	Mechanistic target of rapamycin complex 1
MβCD	Methyl-beta-cyclodextrin
NASH	Non-alcoholic steatohepatitis
NAFLD	Non-alcoholic fatty liver disease
nCEH1	Neutral cholesterol ester hydrolase 1
NLRP3	NLR family pyrin domain containing 3
OA	Oleic acid
oxLDL	Oxidized low-density lipoprotein
PBS	Phosphate buffered saline
PC	Phosphatidylcholine
PDI	Protein disulfide isomerase
PFKFB3	6-phosphofructo-2-kinase/fructose-2,6-bisphosphatase 3
PI	Propidium iodide
PI3K	Phosphatidylinositol-3-kinase
PLM	Polarized light microscopy
PM	Plasma membrane
qPCR	Quantitative polymerase chain reaction
SDS	Sodium dodecyl sulfate
SEM	Standard error of the mean
SMCs	Smooth muscle cells
SOAT1/2	Sterol O-acyltransferase 1 or 2
$SOAT1/2^{KO}$	Sterol O-acyltransferase 1 or 2 knockout

sgRNA	Single guide RNA
SREBP2	Sterol regulatory element binding protein 2
Syk	Spleen associated tyrosine kinase
TBST	Tris-buffered saline containing tween 20
TNFα	Tumor necrosis factor alpha
TG	Triglyceride
2D	Two-dimensional
3D	Three-dimensional

This page is intentionally left blank.

Chapter 1 – Thesis Introduction and Rationale

Metabolism refers to the sum of all chemical reactions that take place within a living organism in order to sustain life[1]. At a basic level, cells require energy in the form of adenosine triphosphate (ATP) to power biochemical reactions that support virtually all cellular functions. ATP is derived from catabolic reactions involving the breakdown of complex molecules like carbohydrates, proteins, and fats in a series of oxidation and reduction reactions[1]. At times during primitive life, mammals experienced environmental challenges such as nutrient and energy scarcity[2]. However, these evolutionary pressures allowed for the development of remarkable adaptations and coordination of metabolic circuits to safeguard survival by promoting energy storage and conservation[2]. Unfortunately, modern society has become increasingly plagued by sedentary lifestyles and chronic overnutrition, both of which contribute to excessive energy storage through anabolic programs leading to metabolic dysfunction and obesity. Simply put, an imbalance between anabolism and catabolism underlies metabolic disease.

Storage of excess energy within the body manifests in the development of obesity, which is accompanied by a myriad of risk factors[3]. Two prominent metabolic diseases that are linked to obesity are cardiovascular and liver disease. Over the last 20 years, diseases of the heart which include stroke and atherosclerosis were reported to be the second leading cause of death in Canada[4] and the leading cause of death worldwide[5]. The failure of low-density lipoprotein-cholesterol (LDL-C) lowering therapies to completely diminish the frequency of cardiovascular events suggests that other risk factors or pathological mechanisms contribute residual risk[6]. On the other hand, non-alcoholic fatty liver disease (NAFLD) is predicted to become the most prevalent cause of hepatocellular carcinoma (HCC)[7]. Non-alcoholic steatohepatitis (NASH) is a subset of NAFLD characterized by steatosis, necroinflammation and fibrosis that frequently progresses to HCC[7]. Moreover, NASH is a prominent contributor to HCC progression in patients that display pre-cirrhotic NAFLD, which is exacerbated by restrictive screening guidelines[7] and limited effective therapies for NASH[8].

Intriguingly, metabolic dysregulation of cholesterol is a hallmark feature of both atherosclerosis and NASH[6,9,10], and cellular cholesterol accumulation is known to lead to multiple pathological consequences[11,12]. One consequence of considerable interest is the formation of

cholesterol crystals (CC). Notably, an abundance of literature suggests that CC are causally associated with atherosclerotic plaque instability and rupture[13–19]. Likewise, the presence of CC has been found to distinguish simple steatosis from NASH in human patients[20]. However, considerably less is known regarding the role of CC in liver disease pathogenesis and progression. Although multiple studies have used cholesterol crystallization as a benchmark for plaque phenotype or atherosclerosis progression, none have directly attempted to define the mechanistic factors that promote CC formation. Based on early observations that free cholesterol (FC) appears to be associated with CC[21,22], we developed an *in vitro* model to explore the mechanisms that link FC accumulation to CC formation. Our interest was directed toward lipid droplets, as cholesterol esterification and subsequent lipid droplet localization defends against FC accumulation[11,23] and CC have been detected in hepatocyte lipid droplets[20,24,25]. Our study was undertaken on human hepatocyte and mouse macrophage cell lines and combines cell/molecular biology techniques with diverse imaging methods to reveal these mechanisms. In addition, we utilize an efficient and reproducible method to quantify CC in these cells. Here, we propose a mechanism wherein two enzymes involved in cholesterol ester metabolism operate in a sequential fashion to support intracellular cholesterol crystallization.

Chapter 2 – Literature Review

2.1: Properties, functions, and regulation of cellular cholesterol

2.1.1: Properties

Cholesterol is a unique lipid that is essential for mammalian biology. Structurally, cholesterol is composed of twenty-seven carbon molecules arranged into four hydrocarbon rings giving it a rigid, planar orientation[26]. Extending from the five-carbon ring is a hydrocarbon tail, and from the six-carbon ring is a polar hydroxyl group[26]. Cholesterol is classified as an amphipathic molecule due to the presence of a single polar hydroxyl group as well as hydrophobic nonpolar regions within its structure, which enables it to intercalate between the phospholipids of mammalian cell membranes. These important biophysical properties of cholesterol are what gives it the ability to provide membranes with distinct characteristics of their own[12].

2.1.2: Functions

Cell membranes intrinsically serve as semi-permeable barriers to a variety of molecules; however, this function is dependent on cholesterol[27]. Interestingly, cholesterol modulates both extremes of membrane fluidity, and some organisms can even adjust the sterol content of their membranes in response to environmental temperature variability[28]. In phospholipid regions containing an abundance of unsaturated fatty acids, cholesterol functions to rigidify the bilayer, while it will increase the fluidity of regions rich with saturated phospholipids[27].

Besides structural aspects, cholesterol plays an integral role in systemic metabolism. Steroid hormones are synthesized from pregnenolone which is derived from cholesterol via oxidative cleavage of its hydrophobic tail[9]. These hormones synthesized from cholesterol have diverse roles ranging from salt and water balance to glucose metabolism, and sexual differentiation in development[26]. Additionally, vitamin D synthesis relies on the presence of cholesterol-derived precursors in the skin to form calcitriol in the kidney[26]. In the gut, bile acids derived from liver cholesterol aid dietary fat digestion and absorption into enterocytes by supporting emulsification[9].

Within the cell, cholesterol predominately exists in two forms. Unesterified or “free” cholesterol is the main structural form of cholesterol and the majority of FC is located in the plasma membrane (PM)[29]. Conversely, the endoplasmic reticulum (ER) membrane contains a significantly

lower concentration of FC[29]. As such, this feature gives the ER the unique ability to sense small changes in cellular FC abundance and respond accordingly to maintain homeostasis by fine tuning cholesterol synthesis, uptake, efflux, or modification[9]. Achieving cholesterol homeostasis is complicated by the fact that cells do not contain enzymes to directly catabolize cholesterol, and therefore it must be converted to different forms within the cell. For example, excess FC can be converted to bile acids in the liver by rate-limiting enzyme CYP7A1 which are subsequently excreted into the feces[30]. In addition, the ER contains cholesterol esterifying enzymes known as acyl-CoA: Cholesterol acyltransferase 1 and 2 (ACAT1 and ACAT2, encoded by the *SOAT1* and *SOAT2* genes) that convert FC to cholesterol esters (CE) to prevent FC accumulation[9]. Compared to FC, CE are more hydrophobic requiring them to be stored within the internal core of lipid droplets or lipoproteins, rather than the organelle membrane. Thus, CE are typically deemed less cytotoxic and play a more significant role in cholesterol storage and transport. The inability to control cholesterol abundance results in FC accumulation, leading to pathological consequences such as induction of apoptosis, oxysterol formation, and cholesterol crystallization[11].

2.1.3: Regulation

The liver plays a central role in systemic cholesterol homeostasis. It is composed of various cell types including Kupffer cells, hepatic stellate cells (HSCs), sinusoidal endothelial cells, and hepatocytes[31]. The Kupffer cells are liver-resident macrophages that are intimately linked to host defence and various toxic insults[32], whereas hepatic stellate cells store retinol and participate in antigen presentation[33]. Sinusoidal endothelial cells play a structural role by separating hepatocytes from the sinusoidal lumen[31]. Hepatocytes are the most abundant cell type in the liver and are the main regulators of hepatic cholesterol metabolism. Their lipid-related functions include facilitating lipoprotein and bile acid synthesis and secretion, as well as directing the uptake of remnant chylomicron and lipoprotein particles from the circulation for storage of excess cholesterol and other lipids[34]. For these reasons, hepatocytes are considered to be the primary cells involved in the regulation of cellular and systemic cholesterol metabolism.

Notably, the ER is particularly sensitive to cholesterol fluctuations. Transcriptional control of cholesterol homeostasis is governed by cholesterol metabolic events at the ER that modulate sterol regulatory element binding protein 2 (SREBP2) and liver X receptor (LXR). These transcription factors direct the transcription and processing of genes that function in cholesterol

biosynthesis, uptake, and efflux[9]. As such, they are able to sense fluctuations in cholesterol levels[9] and integrate this information to direct adaptive mechanisms to conserve homeostasis. An intricate balance within the cell exists between de novo synthesis, receptor-mediated uptake, removal from the cell, and conversion to esters, bile acids, and steroid hormones[9]. However, dysregulation of cellular cholesterol abundance contributes to metabolic disease pathogenesis such as atherosclerosis and fatty liver disease[6,8].

An interesting link between the above diseases is the presence of CC in the advanced stages of these conditions. Excessive cholesterol accumulation in macrophages and hepatocytes in the context of atherosclerosis and fatty liver disease, respectively, results in the precipitation of CC[20,21,24,25,35–37]. At the molecular level, these crystals are thought to form due to the inability of the phospholipid headgroups to shield the overabundance of cholesterol molecules within the membranes of these cells[20]. Yet, the factors that underpin CC formation have not been thoroughly investigated. Some studies have explored intracellular CC formation in the context of atherosclerosis by treating macrophages, smooth muscle cells (SMCs), and endothelial cells with modified lipoproteins to cause crystallization. However, insufficient cell-based work has been done to delineate the fundamental processes that underlie intracellular CC nucleation and formation. Further studies on cell culture model systems are needed to gain such understanding.

2.2: Cholesterol ester homeostasis

2.2.1: Acyl-CoA:Cholesterol Acyltransferase 1 and 2

ACAT1 and ACAT2 are membrane bound proteins and part of the membrane-bound O-acyltransferase (MBOAT) enzyme family that are encoded by two different genes[38,39]. Using long-chain fatty acyl-CoA and cholesterol as substrates, they convert FC to CE in order to prevent FC accumulation in membranes[38,39]. Noteworthy is the fact that ACAT enzymes are not under transcriptional regulation by SREBP2 like other enzymes involved in cholesterol homeostasis, but rather are controlled by allosteric regulation[38].

Cloning and functional characterization of human ACAT1 was first carried out by Chang *et al*. using Chinese hamster ovary (CHO) cells[40]. Mutant CHO cells lacking ACAT1 activity exhibited reduced lipid droplet formation detected by differential interference contrast microscopy.

Conversely, transfection of mutant cells with human ACAT1 complimentary DNA (cDNA) from human macrophage rescued this phenotype, which showed abundant lipid droplet formation. These results were confirmed using nonselective ACAT inhibitor Sandoz 58-035 which also reduced lipid droplet accumulation. Additionally, both transient and stable ACAT1 transfection experiments increased rates of CE synthesis measured using an oleate pulse assay. Based on this initial study, it was concluded that ACAT1 catalyzes CE formation and subsequent lipid droplet storage. Later studies by the same group demonstrated that ACAT1 localizes to the ER using indirect immunofluorescence microscopy[41]. Based on these findings, it was reasonable to consider a role for ACAT1 in atherosclerosis. Meiner *et al*. then generated a global ACAT1-deficient mouse model to investigate this and confirmed that these mice displayed reduced CE levels in macrophages. Unexpectedly, their group also found that livers of these animals did not exhibit reduced CE levels, suggesting that there is another cholesterol esterifying enzyme present that had not yet been identified[42].

Through the efforts of three independent research teams, the second ACAT enzyme was identified and named ACAT2. Isolation and cloning experiments showed that ACAT2 also participates in CE formation[43–45]. Contrary to ACAT1, which was found to be expressed in all tissues examined, ACAT2 was expressed primarily in human and mouse liver and intestine[43–45]. Similar to ACAT1, ACAT2 was localized to the ER[43–45]. Based on the tissue expression, it was suggested that ACAT2 functions in hepatic secretion of CE-rich ApoB-containing lipoproteins and aids cholesterol absorption from the gut. Indeed, ACAT2 deficiency in mice limited intestinal cholesterol absorption[46] and reduced CE content in ApoB-containing lipoproteins[47]. However, there is a discrepancy between the relative contributions of ACAT1 and ACAT2 to ACAT activity in the livers of humans compared to mice. In cultured human hepatocytes, ACAT1 was reported to account for 85-90 percent of the total ACAT activity, with the remainder attributed to ACAT2[48]. This is at odds with other studies done in mice which suggest that ACAT2 is the dominant isoform for CE production in the liver[49]. Collectively, the above studies demonstrate that ACAT1-derived CE are sequestered in lipid droplets and ACAT2-derived CE are secreted into ApoB-containing lipoproteins.

2.2.2: Neutral CE hydrolase 1

Compared to the ACATs, enzymes that liberate FC from CE in lipid droplets have not been as well characterized. Ishibashi and colleagues investigated neutral CE hydrolase (nCEH/nCEH1, also known as KIAA1363 and AADACL1) as a potential ester hydrolase in macrophages[50]. Using mouse peritoneal macrophages (MPMs) and subcellular fractionation, they showed high nCEH activity and nCEH protein expression in microsomal fractions. In comparison to the MPMs, cultured RAW 264.7 macrophages displayed lower nCEH expression and higher hormone-sensitive lipase (HSL) expression. RNA silencing of nCEH led to reduced nCEH activity while overexpression significantly reduced CE content. In addition, it was found that nCEH was expressed in macrophage foam cells in the aortas of hypercholesterolemic mice, implicating nCEH in atherosclerosis. As expected, mice lacking nCEH1 exhibited more severe atherosclerosis and it was suggested that nCEH1 is more efficient than HSL at mobilizing CE and promoting cholesterol efflux[51]. However, these findings are in contrast with another group who showed that CE hydrolase activity was reduced in $HSL^{-/-}$ macrophages but not in $nCEH1^{-/-}$ macrophages[52]. Further studies reported that nCEH1 protein expression was greater than HSL in human monocyte-derived macrophages as well as CE hydrolase activity[53]. Another report describes a role for nCEH1, but not HSL, in protecting against oxysterol-induced apoptosis[54]. Despite these findings, there is still much disagreement and controversy as to which is the main CE hydrolase. Sakai *et al*. provide evidence that nCEH1 indeed is the dominant hydrolase[55], while others propose that multiple enzymes function cooperatively with HSL[52].

Likewise, the tissue distribution and subcellular localization of nCEH1 has not been extensively reported. nCEH1 protein was found to be abundantly expressed in heart, adrenal, and kidney tissues, but was not detected in liver[50]. These findings are consistent with those of Nomura *et al.* who also did not detect ample nCEH1 protein in liver[56]. However, the inability to detect nCEH1 in their study could be attributed to differences in glycosylation as Igarashi *et al*. reported that glycosylation at Asn^{389} is needed to visualize the upper 50 kDa band[53], but Nomura *et al*. only identified the lower 45 kDa band. More recently, whole liver nCEH1 expression in mice was also demonstrated to be low, but comparatively was greater in primary HSCs than in primary hepatocytes at the RNA and protein levels[57]. Due to the reported role of nCEH1 as a neutral CE hydrolase in macrophage foam cells, determining its subcellular localization was of critical importance. Based on similarity to other ER-localized AADAC enzymes it was hypothesised that

nCEH1 was also localized to the ER[58,59]. To investigate, Igarashi *et al*. examined endogenous nCEH1 localization in MPMs using immunocytochemistry and immunostaining[59]. nCEH1 was shown to co-localize with ER marker PDI, and its cellular distribution was not altered by incubation with acLDL. Additionally, GFP-tagged nCEH1 also co-localized with PDI but did not co-localize with lipid droplets upon acLDL loading, nor was its distribution affected. Site-directed mutagenesis experiments revealed that nCEH1 contains a critical N-terminal transmembrane domain required for recruitment and localization to the ER. Despite this study, many reviews still suggest that nCEH1 functions at the lipid droplet rather than the ER. A deeper understanding of lipid droplet biogenesis and associations with the ER membrane may reveal important functional characteristics of nCEH1.

2.2.3: Lipid droplets

Lipid droplets are composed of a surface phospholipid monolayer, in contrast to a bilayer typical of membranes, and contain unesterified cholesterol and embedded proteins, as well as a neutral lipid core containing CE and triglycerides (TG)[58,60,61]. It was initially believed that lipid droplets were simple energy storage organelles with passive functions; however, it is now understood that they are dynamic organelles. Besides buffering the accumulation of toxic sterols and free fatty acids by storing these lipids in their esterified forms, lipid droplets also contain enzymes that are under hormonal control that participate in lipid metabolism[58]. In addition, multiple studies have attempted to elucidate the lipid droplet proteome and their analyses suggest that more than 200 proteins are localized to lipid droplets with functions including lipid metabolism, membrane trafficking, and signaling, as well as other canonical ER, cytoskeletal, and chaperone proteins (reviewed by Hodges and Wu)[60]. Diverse roles for lipid droplets in oxidative/ER stress, hypoxia, protein folding, and DNA maintenance have also been identified[62,63]. As is expected from such a dynamic organelle, lipid droplets have also been recognized to form direct membrane contact sites with other organelles enabling them to participate in diverse cellular functions[62]. Furthermore, they appear to be involved in both metabolic disease progression and resistance as lipid droplet accumulation is prominent in heart and liver diseases[64], but lipid droplets have also been found to protect against ER stress and mitochondrial damage[63].

Recent advances in lipid droplet biology have led to a greater understanding of the mechanisms that contribute to lipid droplet formation. The requisite step for lipid droplet

biogenesis is the synthesis of neutral lipids such as CE and TG. As their concentration increases within the ER bilayer leaflets, an oil lens forms due to coalescence of the neutral lipids[62,63]. Budding of lipid droplets from the ER into the cytosol is a consequence of the expansion of the neutral lipid lens and is facilitated by fat storage-inducing (FIT) proteins, seipin, and other proteins[63]. Interestingly, no specific targeting sequence has been identified for lipid droplet-localized proteins. Despite what is currently known, lipid droplet dynamics are not well understood.

2.3: Atherosclerosis and cholesterol crystals

While the primary aim of my thesis focuses on cholesterol crystallization in hepatocytes, there has been little work done on the topic. In contrast, there is an abundance of information on the role of CC in atherosclerotic plaques and in model macrophage systems. This sub-section will review the work relevant to atherosclerosis and glean critical details that will be informative for comparing to liver.

2.3.1: Atherosclerosis

The initiating event that drives atherogenesis is the accumulation and retention of lipoproteins within the intima of human coronary arteries[6,12]. A chronic increase of circulating LDL particles leads to their modification through oxidation, acetylation or aggregation, instigating unregulated uptake by macrophage scavenger receptors[65–67]. Macrophages and SMCs attempt to reduce the lesion lipid burden by ingestion of these modified lipoproteins which leads to massive lipid droplet accumulation, giving rise to characteristic foam cells[6,67,68]. Despite the clearance of lipoproteins from the intima, cholesterol accumulation in these cells can trigger cell death and inflammation[11], contributing to the inflammatory milieu present in atherosclerosis. Furthermore, defective clearance of apoptotic macrophages via efferocytosis is a major contributor to the formation of the necrotic core, increasing the risk of thrombosis[67].

2.3.2: Identification of cholesterol crystals in atherosclerotic plaques

Despite great interest in the presence of CC in atherosclerotic lesions, their discovery is not recent. Initial reports of crystalline cholesterol deposition upon feeding rabbits egg yolk or pure cholesterol was first published in 1916, and appears to be the first report on CC[69]. Since then,

efforts were directed at examining the composition of these crystalline deposits. The identification of cholesterol monohydrate as the culprit has been documented throughout the late 20th century using methods such as X-ray diffraction[70,71] and more recently using stimulated Raman scattering and second-harmonic generation microscopy[72]. Techniques to identify the presence of CC within atherosclerotic lesions have also become more refined within the last twenty-five years. Early reports have noted empty spaces in H&E stained atherosclerotic lesions sectioned in paraffin upon processing with ethanol, which have been described as cholesterol 'clefts'[73].

Polarized light microscopy (PLM) has more recently been used for CC identification based on their unique birefringent properties and their ability to reflect plane-polarized light[74]. Birefringence is defined as a property of materials that result in the splitting of incident light into two rays that are circularly polarized in opposite directions[75]. To detect CC, a series of two polarizing filters is used. Emitted light is linearly polarized by the first filter, and subsequently leads to circular polarization of light due to CC birefringence causing retardation of the incident light. The vertical component of the circularly polarized light (which is absent in non-birefringent materials) is polarized 90° to the emitted light by the second filter and is detected as a crystallized substance. Unfortunately, PLM is not ideal to image advanced atherosclerotic lesions as the presence of collagen, which is also a crystalline material, can interfere with imaging[74].

To avoid this potential confound, some groups have turned to confocal reflection microscopy and differential interference contrast microscopy which can specifically identify crystalline cholesterol[76,77]. Based on the premise that CC surfaces could operate as foreign antigens, one group developed a monoclonal antibody known as 58B1 that selectively targets the crystal surfaces of cholesterol monohydrate (cholesterol microdomains), but not individual cholesterol molecules[78]. This antibody has successfully been used to investigate the formation of 3-dimensional (3D) CC from 2-dimensional (2D) nucleation sites[79–81] and different CC polymorphisms[82,83]. In addition, recent advances in electron microscopy techniques have proven to be value tools to characterize the presence of crystals within lesions and their association with cellular organelles[65,84,85].

Common mouse models used to study cholesterol crystallization in atherosclerotic lesions are apolipoprotein E (ApoE)-null and low-density lipoprotein receptor (LDLR)-null mice, fed a high cholesterol diet. Both models demonstrate robust cholesterol crystallization upon diet feeding

compared to control, and cholesterol clefts have been identified using H&E or osmium tetroxide staining[22,86,87]. Many studies have identified CC or cholesterol clefts in whole tissue in an extracellular context, however, some groups have also assessed intracellular cholesterol crystallization. Production of intracellular CC has been observed by loading macrophages[21,36,37,88], SMC[89], and aortic endothelial cells[90,91] with modified lipoproteins. Baumer and colleagues found that oxidized-LDL (oxLDL) and acLDL-loaded psoriatic macrophages show pro-atherosclerotic phenotypes and exhibit increased CC presence under PLM[35]. This study, along with another done on endothelial cells implicate inflammation in CC formation[91]. Another group developed a method to induce foam cell formation in human THP-1 macrophages using acLDL and 7-ketocholesterol and visualized CC using PLM[92]. Given the relative abundance of crystalline material in atherosclerotic lesions, it is highly likely that this material actively contributes to disease progression rather than being a passive by-product of cholesterol dysregulation.

2.3.3: NLRP3 inflammasome

Immunometabolism is the fundamental interplay between the immune and metabolic systems. One facet of immunometabolism is the study of how metabolic changes influence inflammatory responses and immune cell function. In the case of atherosclerosis, altered cholesterol metabolism can have drastic effects on immune cell function. Duewell and colleagues were the first to report that NLR family pyrin domain containing 3 (NLRP3) inflammasomes are required for atherogenesis and are activated by CC[76]. Upon feeding ApoE-null mice a high cholesterol diet, they observed a time-dependent increase in lesion macrophage content and CC presence compared to regular diet feeding. Interestingly, crystal presence appeared to correlate positively with macrophage content across time on high cholesterol diet. To test the cellular effects of CC, they isolated human peripheral blood mononuclear cells and treated them with synthetic CC. They reported that treatment with exogenous CC was sufficient to activate the NLRP3 inflammasome and trigger interleukin 1β (IL-1β) secretion. Mechanistically, this group reported that exogenous crystals could be taken up by murine macrophages and induce lysosomal damage, thereby activating the NLRP3 inflammasome. Duewell *et al.* also demonstrated that acLDL instead of lipopolysaccharide (LPS) was a sufficient priming signal to trigger IL-1β secretion following activation by CC, indicating that dysregulated cholesterol metabolism alone is sufficient for altered immune cell function[76].

At almost the same time, another group published similar findings and were able to support that CC could activate the NLRP3 inflammasome in human macrophages[77]. Rajamaki and colleagues provided evidence that macrophages accumulate CE following incubation with exogenous CC. In agreement with the findings of Duewell *et al*., they show mechanistically that CC could destabilize lysosomes causing cytoplasmic cathepsin B leakage. These two foundational studies, published almost simultaneously, link cholesterol crystallization to immunometabolic disease development[76,77].

2.3.4: Metabolic reprogramming

Another immunometabolic consequence of CC presence is their effects on macrophage metabolic reprogramming. Atherosclerosis progression and plaque instability is recognized to be associated with increased glycolysis[93]. O'Rourke *et al*. sought to determine whether CC could alter macrophage metabolism and influence their inflammatory M1-like status[93]. Using exogenous CC alike the ones in previous studies (albeit a higher dose), they found that CC incubation in primary human macrophages resulted in upregulation of M1 macrophage markers and damage associated molecular patterns (DAMPs), with a concomitant downregulation of M2 markers. Furthermore, it was found that CC drove the expression of glycolytic markers GLUT1, HK2, HIF1α, GAPDH, PFKFB3, and promoted metabolic reprogramming to favor glycolysis. Treatment with glycolytic inhibitors attenuated CC-induced macrophage polarization and metabolic reprogramming.

In another study, Zimmer and colleagues demonstrated that ApoE-null mice fed a high cholesterol diet alongside cyclic oligosaccharide 2-hydroxypropyl-β-cyclodextrin (CD) injections exhibited impaired atherogenesis compared to control mice[94]. In addition, CD treatment significantly reduced CC area and led to regression of murine atherosclerosis. CD is a known cholesterol solubilizer, and this group investigated the mechanism by which CD reduces atherosclerosis in bone marrow derived macrophages. Remarkably, they discovered that CD could interact with and dissolve both intracellular and extracellular CC, which were imaged using confocal reflection microscopy. Deuterium labeled CC were used to investigate the cellular effects of cholesterol derived from the synthetic crystals. They reported that CD promoted esterification of cholesterol derived from the crystals and reduced the intracellular cholesterol pool. This reduction in cholesterol was due to augmented crystal-derived cholesterol efflux and conversion

to 27-hydroxycholesterol. Based on the ability of CC to reprogram macrophage metabolism as outlined in these two studies, CC likely have profound effects on lesion stability.

2.3.5: Plaque destabilization

In the absence of sufficient crystal solubilization or resolution, CC have been found to exert mechanical stresses that contribute to membrane damage and plaque rupture. Abela and Aziz were the first to suggest that crystalline material in lesions could cause mechanical damage to membranes and speculated that this damage could lead to thrombosis[16]. In their study, they aimed to prove that the conversion of cholesterol from a liquid to a solid crystal state could rupture biological membranes. They demonstrated that a strong positive correlation exists between cholesterol weight (amount) and rate of crystal growth. Further studies using scanning electron microscopy confirmed that CC ruptured biological membranes and human plaques during acute cardiovascular events[18]. Two subsequent reviews discuss the possibility of CC contributing to inflammation and serving as a driving force for atherogenesis[17,95]. To translate their findings, Abela and Aziz *et al*. investigated the effects of CC in arteries of patients who succumbed to acute coronary and cerebrovascular syndromes[96]. Notably, 100% of patients that experienced an acute coronary syndrome (ACS) exhibited presence of CC compared to 0% in patients that did not have an acute coronary syndrome. Moreover, it was reported that increased CC content was associated with a greater risk of thrombosis. In support of these findings, a recent study using optical coherence tomography determined that ACS patients with CC in atherosclerotic lesions had higher NLRP3 and IL-1β expression than those without CC[97]. They speculated that CC may have led to NLRP3 activation, contributing to plaque vulnerability.

As the importance of CC in plaque disruption gained more attention, other groups attempted to model the effects of these crystals on atherosclerotic plaques. Luo *et al*. used micro-optical coherence tomography to assess cross sectional geometric information of CC in human atherosclerotic aortas[19]. They report multiple important findings. First, CC presence at the cap shoulder of the plaque imposes the highest peak stress. Second, crystal growth compromises fibrous cap stability. Last, evenly distributed crystallization exerted less peak stress compared to concentrated crystallization. These data imply that the distribution of CC, rather than presence, is a stronger determinant of potential plaque disruption.

More recently, optical coherence tomography has been used to obtain high-resolution imaging of carotid plaque morphology. Shi *et al*. sought to explore the potential association between CC and clinical/plaque morphological characteristics[15]. Supporting the previous findings of Baumer *et al.*, this group found that the majority (75%) of plaques with CC also had macrophage accumulation and calcification (62.5%). However, no association between plaque rupture and CC was detected. The authors still suggest that CC are substantial components of vulnerable plaques based on their association with macrophages and calcification.

2.3.6: Targeting ACAT in atherosclerosis

A defining feature of atherogenesis is the storage of excess cholesterol and foam cell accumulation[6]. The observation that LDL-derived cholesterol esters rather than endogenously synthesized FC was the substrate for cholesterol esterification[98] prompted investigators to examine ACAT[40]. Global deletion of ACAT1 in mice fed a high-fat diet (HFD) reduced macrophage CE content, which led to considerable interest in targeting ACAT1 to reduce foam cell formation as an anti-atherosclerosis therapy[42]. Nonselective ACAT inhibitors targeting both ACAT1 and ACAT2 were soon developed, and many were found to exert atheroprotective effects in hamsters, mice, and rabbits[87,99–101]. At around the same time, whole body ACAT1$^{-/-}$ mice were generated and crossed with atherogenic and dyslipidemic ApoE$^{-/-}$ mice, which exhibited cutaneous xanthomas despite reduced atherosclerosis[102]. In contrast, reconstitution of LDLR$^{-/-}$ mice with ACAT1$^{-/-}$ bone marrow failed to protect against atherosclerosis but did reduce lesion macrophage content[22,103]. It was theorised that macrophage ACAT1 deficiency triggered FC accumulation and apoptosis[11,22,103].

Despite disagreement between different studies, nonselective ACAT inhibitors were tested in human trials. The Avasimibe and Progression of Lesions on Ultrasound (A-PLUS) trial was the first clinical trial to be conducted and had the main objective of assessing the effects of Avasimibe on the progression of coronary atherosclerosis, assessed by intravascular ultrasound (IVUS)[104]. Unfortunately, it was concluded that administration of Avasimibe did not favorably affect atherosclerosis, and that Avasimibe unexpectedly raised plasma LDL levels. The ACAT Intravascular Atherosclerosis Treatment Evaluation (ACTIVATE) trial was a subsequent phase 3 clinical trial performed using a similar ACAT inhibitor, known as Pactimibe[105]. In a similar fashion, the ACTIVATE trial failed to demonstrate atherosclerosis protection, and some measures

indicate atherogenesis was enhanced. The final clinical study, the Carotid Atherosclerosis Progression Trial Investigating Vascular ACAT Inhibition Treatment Effects (CAPTIVATE) trial, had a devastating outcome[106]. Shockingly, the trial was terminated prematurely as LDL cholesterol levels increased by 7.3%. Pactimibe failed to show a treatment effect on carotid intima media thickness and resulted in a statistically significant greater incidence of major cardiovascular events compared to placebo. The failure of these three human clinical trials is likely rooted in the mechanism of action of Avasimibe and Pactimibe. Both drugs are nonselective inhibitors of ACAT1 and ACAT2 which may result in massive cellular accumulation of free cholesterol, potentially causing cytotoxic effects[11]. Of note, most of the A-PLUS trial participants were simultaneously taking a statin alongside Avasimibe, which is a known CYP3A4 inducer[105,107]. This potential induction may have interfered with statin function, contributing to the reported 10% increase in LDL cholesterol levels from baseline[104].

In contrast with the studies performed in the early 2000s, subsequent studies using nonselective ACAT inhibitors[108,109] and ACAT1 specific inhibitors[110,111] demonstrate a protective effect on atherosclerosis. To precisely investigate the role of ACAT1 in macrophages, Huang *et al.* developed a myeloid-specific ACAT1$^{-/-}$ mouse model. They report reduced atherosclerosis progression and lesion macrophage content upon western diet feeding[112]. Using the same model, Melton *et al.* showed reduced lesion burden in advanced atherosclerosis but failed to demonstrate complete reduction in foam cell presence, implicating the involvement of ACAT2 or SMC ACAT1 in foam cell formation[86]. Melton and colleagues also addressed the discordance between ACAT1$^{-/-}$ mice in bone marrow transplant (BMT) experiments and the myeloid-specific ACAT1$^{-/-}$ model. They posit that lack of ACAT1 in bone marrow cells other than monocytes such as B or T lymphocytes may be responsible for the negative phenotypes observed in the BMT experiments. Wakabayashi and colleagues are in agreement with this postulate, which is supported by a study showing that ACAT1 inhibition potentiated CD8+ effector T cell function and proliferation[113,114]. However, this hypothesis needs to be tested in further studies as transplantation of LDLR$^{-/-}$ mice with ACAT1$^{-/-}$ bone marrow was found to attenuate atherosclerosis aggravated by nCEH1$^{-/-}$[115]. Even more confusing is the fact that the same group used an identical ACAT1$^{-/-}$ BMT model and discovered that loss of ACAT1 in bone marrow-derived cells aggravated atherosclerosis (which was protected by loss of NLRP3)[113]. Furthermore, ACAT1$^{-/-}$ was found to protect against pathological onset in NPC1 mutant mice that exhibit aberrant cholesterol storage[116]. See table 2.1

for a complete summary of selected preclinical and clinical studies targeting ACAT in atherosclerosis.

Author, Year, Journal	Preclinical /Clinical	Model/Patient Characteristics	Treatment/ Intervention	Relevant Finding(s)
Meiner, 1996, PNAS[42]	Preclinical	Whole body ACAT1$^{-/-}$ in mice	HFD	ACAT$^{-/-}$ alone reduced CE in macrophages but not in liver. Speculation of another esterifying enzyme present in liver.
Nicolosi, 1998, Atherosclerosis[101]	Preclinical	F_1B Hamsters	High cholesterol diet + CI-1011 (Avasimibe)	Avasimibe prevented and regressed aortic fatty streak formation.
Bocan, 2000, ATVB[100]	Preclinical	Male New Zealand White Rabbits	Hypercholesterolemic diet feeding + Avasimibe	Avasimibe reduced macrophage presence and MMP expression in atherosclerotic lesions.
Accad, 2000, JCI[22]	Preclinical	Whole body ACAT1$^{-/-}$ on ApoE$^{-/-}$ and LDLR$^{-/-}$ backgrounds, and BMT into LDLR$^{-/-}$ mice	HFD	ACAT1$^{-/-}$ mice did not exhibit reduced atherosclerosis, but reduced macrophage presence, neutral lipids, and cholesterol clefts. Free cholesterol accumulation seems to be associated with cholesterol clefts. Cholesterol clefts present in skin and brain. ACAT1$^{-/-}$ in macrophages was sufficient for dermal xanthomas in LDLR$^{-/-}$ mice.
Yagyu, 2000, JBC[102]	Preclinical	Whole body ACAT1$^{-/-}$ on ApoE$^{-/-}$ and LDLR$^{-/-}$ backgrounds in mice	HFD	Hypercholesterolemic ACAT1$^{-/-}$ mice exhibited reduced atherosclerosis and CE, but cutaneous xanthomas and presence of dermal cholesterol clefts (atherosclerotic

				lesions not examined for clefts).
Fazio, 2001, JCI[103]	Preclinical	WT vs ACAT1$^{-/-}$ BMT into LDLR$^{-/-}$ mice	HFD	Macrophage ACAT1$^{-/-}$ in mice promotes atherosclerotic lesion development, but reduced macrophage content.
Delsing, 2001, Circulation[87]	Preclinical	Female ApoE*3-Leiden mice	HCD + Avasimibe	Avasimibe reduced atherosclerosis and plasma cholesterol.
Perrey, 2001, Atherosclerosis[117]	Preclinical	C57BL/6 mice, ApoE$^{-/-}$ mice, KHC Rabbits	Fat diet + CI-976 (nonselective ACAT inhibitor)	CI-976 had no effect on lesion area.
Kusunoki, 2001, Circulation[99]	Preclinical	ApoE$^{-/-}$ mice	Western diet + F-1394 (nonselective ACAT inhibitor)	ACAT inhibition reduced atherosclerosis, macrophage content, and cholesterol clefts.
Willner, 2003, PNAS[118]	Preclinical	Whole body ACAT2$^{-/-}$ mice on ApoE$^{-/-}$ background	Chow diet	ACAT2 deficiency reduced atherosclerosis and plasma lipid levels. Increased TG in VLDL. ApoB particles containing TG are presumably less atherogenic than those containing CE.
Tardif, 2004, Circulation[104]	Clinical	Patients >30 years of age referred for clinically indicated coronary angiography, LDL-C >3.2 mmol/L and at least 1 coronary artery stenosis.	Avasimibe (50, 250, 750 mg/day)	Avasimibe slightly increased plaque volume, change in atheroma volume and LDL-C. High dose Avasimibe reduced ApoB.
Nissen, 2006, NEJM[105]	Clinical	1 coronary artery stenosis, with clinical indications for coronary angiography.	Pactimibe/ non-selective ACAT inhibitor (100 mg/day)	Pactimibe did not favorably reduce atheroma volume.
Ikenoya, 2007,	Preclinical	F_1B Hamsters	HFD + K604 (ACAT1	K604 suppressed fatty streak lesions without

Atherosclerosis[110]			specific inhibitor)	affecting plasma cholesterol levels.
Terasaka, 2007, Atherosclerosis[109]	Preclinical	ApoE$^{-/-}$ mice	Avasimibe (C-1011) and Pactimibe (CS-505)	Pactimibe reduced and stabilized atherosclerotic lesions to a greater degree than Avasimibe, but similar lowering effects on plasma cholesterol.
Meuwese, 2009, JAMA[106]	Clinical	Patients heterozygous for familial hypercholesterol-emia and carotid atherosclerosis	Pactimibe (100 mg/day)	Pactimibe had no effect on atherosclerosis and significantly increased LDL-C and major cardiovascular events.
Yoshinaka, 2010, Atherosclerosis[111]	Preclinical	ApoE$^{-/-}$ mice	K604 (60 mg/kg/day)	K604 positively alters atherosclerotic plaque phenotype.
Rong, 2013, ATVB[108]	Preclinical	ApoE$^{-/-}$ mice	Western diet + F-1394	F-1394 reduced plaque progression and cholesterol content without systemic toxicity.
Huang, 2016, JBC[112]	Preclinical	Myeloid-specific ACAT1$^{-/-}$ on ApoE$^{-/-}$ in mice	Western diet	Myeloid-specific ACAT1 deficiency reduced atherosclerosis progression and lesion macrophage content.
Melton, 2019, JBC[86]	Preclinical	Myeloid-specific ACAT1$^{-/-}$ on ApoE$^{-/-}$ in mice	Modified Paigen diet	Myeloid-specific ACAT1 deficiency reduced atherosclerotic burden in advanced lesions and reduced macrophage inflammation. Speculated contribution of SMC ACAT1 or ACAT2 in other tissues to atherosclerosis.
Yamazaki, 2019, J Ath Throm[115]	Preclinical	ACAT1$^{-/-}$ and nCEH1$^{-/-}$ BMT into LDLR$^{-/-}$ mice	HCD	ACAT1$^{-/-}$ attenuates atherosclerosis that is aggravated by nCEH1$^{-/-}$.
Rogers, 2022, PNAS[116]	Preclinical	ACAT1$^{-/-}$ and NPC1 mutant mice and MEF	N/A	ACAT1$^{-/-}$ reduced cholesterol storage phenotypes in NPC mutant cells.

Table 2.1: Summary of key preclinical and clinical studies targeting ACAT in atherosclerosis.

2.4: Fatty liver disease and cholesterol crystals

2.4.1: Fatty liver disease

Fatty liver disease first presents as benign steatosis which includes signatures of TG accumulation and the absence of inflammation[8]. Conditions under the umbrella of metabolic syndrome including dyslipidemia, obesity, and diabetes have been identified as risk factors for the eventual progression of steatosis to NASH[8,10]. Over time, non-resolving inflammation, cholesterol accumulation, and ROS production can all contribute to NASH progression[8]. Transition to NASH can be blunted with lifestyle modifications such as diet and exercise, however, there are limited effective therapeutic strategies[8]. If unresolved, cirrhosis and HCC may develop requiring future liver transplant, reinforcing NASH as the second-highest indication for liver transplantation[119]. Cholesterol has recently been implicated as a major player in NASH pathogenesis[119], and excessive hepatic cholesterol accumulation has been demonstrated to give rise to experimental NASH in animal models[120]. In fact, studies on NASH patients suggest that excessive cholesterol storage and cholesterol crystallization within lipid droplets distinguishes NASH from steatosis[20,25].

2.4.2: Cholesterol crystal nucleation

Crystal nucleation is a fundamental biophysical phenomenon where molecular proto aggregates in a liquid or 2D phase evolve into 3D macroscopic crystals[121]. In other words, macroscopic crystals form using 2D phases as a structural blueprint. However, this process is extremely difficult to study *in vivo* and is therefore challenging to relate it to human diseases. Also, the specific cellular location of CC nucleation has not been fully elucidated. Varsano *et al.* developed a fascinating model to study crystal nucleation using a supported lipid bilayer in a beaker that is supported by a coverslip[80]. Using this model, the group confirmed that 2D lipid bilayer domains provide sufficient nucleating sites for 3D crystal nucleation. Another interesting finding is that lipid bilayers that contain homogenous solutions of cholesterol and other lipids (high dipalmitoylphosphatidylcholine concentration) had reduced CC nucleation, compared to bilayers with less lipids and more cholesterol. It is conceivable that the incorporation of lipids other than

cholesterol into bilayers can disrupt 2D cholesterol microdomain formation, thereby preventing crystal nucleation.

Further studies on crystallization in supported phospholipid bilayers suggest that the process of cholesterol crystallization follows a multistep process known as Ostwald's rule of stages[122]. This heuristic posits that phase transformation in crystallization proceeds down free energy gradients in successive phases to incur the smallest loss of free energy before ultimately reaching the stable ground state. The metastable intermediates such as rods and helical crystals have been observed experimentally[82,83,122] and in rabbit atherosclerotic tissues[84]. It is suggested that these transient intermediates are ultimately requisite steps before forming stable plate-like cholesterol monohydrate crystals[122], which somewhat explains why plate-like crystals are most commonly observed in atherosclerotic lesions. Generally, it is accepted that FC accumulation leads to cholesterol monohydrate crystal formation[13,21,22,65], and there is little evidence indicating CE contribute to crystallization in NASH or atherosclerosis. However, a rare disorder called CE storage disease (CESD), in which there is reduced lysosomal acid lipase function, results in crystals forming in liver lysosomes[123]. These crystals are thought to be composed of CE, so it may be possible that this occurs in NASH. Atherosclerotic lesions were reported to never contain CE crystals, and the crystalline material was identified as cholesterol monohydrate by X-ray diffraction[71]. However, one particular CE known as cholesteryl palmitate that is commonly found in atherosclerotic lesions was hypothesized to be able to induce nucleation of cholesterol monohydrate crystals using a simulation model[124]. Although there is no direct evidence showing that CE can crystallize in liver during NASH or plaques during atherosclerosis, they may have the ability to serve as nucleating agents for cholesterol monohydrate crystal formation.

2.4.3: Cholesterol crystallization in hepatocytes

Hepatic cholesterol overload is known to drive lipotoxicity in NASH pathogenesis and recent reports have supported this perception. Human patients with NASH and mouse models of experimental NASH exhibited robust cholesterol crystallization under PLM when compared to simple steatosis[20,25]. Additionally, aggregates of activated Kupffer cells surrounding necrotic hepatocytes was identified as a defining feature of NASH, leading to the formation of foam cell-like Kupffer cells[25]. Attractively, it was found that the Kupffer cells selectively surround only hepatocyte lipid droplets that have underwent extensive crystallization[24,25]. Ioannou *et al.* used a

clever technique to differentiate the composition of lipid droplets with or without crystallization using osmium tetroxide staining and methylene blue counterstaining. Since osmium tetroxide selectively stains CE (and TG), they posit that the absence of osmium tetroxide staining in crystallized lipid droplets denotes the absence of CE[24,25]. However, it is difficult to agree with this conclusion as the crystals appear to envelop the exterior of the lipid droplet, while identification of the interior is deterred. Simply put, the CE that reside in the lipid droplet interior are likely surrounded by crystallized FC and cannot be detected via osmium tetroxide staining.

Now with the connection between CC and NASH, the same group attempted to resolve crystallization and NASH using cholesterol-lowering drugs. In this study, obese and diabetic mice were fed an atherogenic diet for 16 weeks then administered ezetimibe, atorvastatin, or both for an additional 8 weeks on the atherogenic diet. Compared to vehicle control, the combination of ezetimibe and atorvastatin led to resolution of cholesterol crystallization, crown-like structures, and NASH[125]. They also identified that NLRP3 inflammasome activation by the crystals may play a role in NASH pathogenesis[24]. The same group incubated HCC cell lines with LDL and oleic acid (OA), leading to the conclusion that CC form within human hepatocyte lipid droplets[20,24]. According to their imaging studies, LDL and OA loading led to the direct transport of LDL-derived cholesterol to the lipid droplet through membrane contact sites via the late endosome/lysosome pathway, without transiting to the ER[20]. These studies performed by Ioannou *et al.* provide substantial evidence both *in vivo* and *in vitro* that hepatocyte lipid droplets are organelles capable of intracellular cholesterol crystallization.

To gain a deeper understanding of this process intracellularly, Capua-Shenkar and colleagues utilized cryo-focused ion beam-scanning electron microscopy to image atherosclerotic lesions in rabbits[84]. Their most significant findings suggest that indeed, lipid droplets provide surfaces that enable CC nucleation. Their remarkably high-resolution imaging reveal that the crystals are in close association with the lipid droplets and could have potentially nucleated on the lipid droplet surface. Although there is ample evidence of cholesterol crystallization in NASH, it is unclear whether these crystals are actively involved in NASH pathogenesis or are simply a by-product of hepatic cholesterol overload.

2.4.4: A potential pathway coupled to cholesterol crystallization in liver

The link between CC and NLRP3 inflammasome activation in atherosclerosis is well established, however in NASH the link is unclear. Unexpectedly, pharmacological and genetic inhibition of the NLRP3 inflammasome failed to reduce experimental NASH and seemed to exacerbate cholesterol crystallization[126]. The failure of NLRP3 inhibition to uncouple CC from NASH development suggests an alternative mechanism by which these crystals may contribute to liver disease. One possibility is Mincle (macrophage inducible C-type lectin), a C-type lectin receptor expressed on activated macrophages and dendritic cells[127]. Kiyotake *et al.* reported that Mincle is selectively activated by CC, but not FC, leading to production of inflammatory cytokines which was blocked using an anti-Mincle antibody[128]. Mechanistically, exogenous CC were demonstrated to stimulate Syk and PI3K in macrophages and dendritic cells, leading to IL-1 production and DAMP expression[129]. This concept is in agreement with the model proposed by Ioannou *et al.* where Kupffer cells surround crystallized lipid droplets of necrotic hepatocytes forming crown-like structures[10]. These Kupffer cells are likely to express Mincle on their surface and it may be through this interaction where Mincle potentially contributes to crystal-induced inflammation, independent of the NLRP3 inflammasome. Further investigation will be required to define the role of CC formation in the context of NASH.

2.5: Hypothesis and objectives

Although FC accumulation underlies cholesterol crystallization, the linking mechanism is unknown. Due to the ability of lipid droplets to concentrate cholesterol in the form of esters, we reasoned cholesterol esterification, subsequent lipid droplet localization, and then de-esterification will concentrate FC at the lipid droplet surface to drive cholesterol nucleation and crystal formation. Hence, **we hypothesized that enzymes that mediate cholesterol esterification and enzymes that de-esterify lipid droplet CE are required for intracellular CC formation.** This hypothesis will be tested through the following objectives:

Objective 1: Establish a model of intracellular CC formation in immortalized human hepatocyte and murine macrophage cell lines.

Hep3B and RAW 264.7 cells will be treated with cholesterol or acLDL, respectively, to induce FC accumulation. Cholesterol crystallization will be assessed using PLM and lipids will be extracted to quantify CE levels.

Objective 2: Identify the location of intracellular CC formation/nucleation.

Hep3B and RAW 264.7 cells will be treated with cholesterol or acLDL, respectively, and the location of CC formation/nucleation will be confirmed using fluorescence microscopy to differentiate between different organelles.

Objective 3: Investigate the role of cholesterol ester metabolism in CC formation.

Hep3B and RAW 264.7 cells will be treated with or without cholesterol/acLDL and with or without ACAT inhibitors or an nCEH1 inhibitor. Using CRISPR/Cas9 gene editing technology, ACAT1 and ACAT2-deficient hepatocyte cell lines will be generated. PLM will be used in all cases to assess CC formation.

Chapter 3 – Materials and Methods

3.1: Reagents. Sandoz 58-035/ACAT inhibitor (Sigma-Aldrich, catalog #S9318-5MG), JW480/nCEH inhibitor (Sigma-Aldrich, catalog #SML0792), K604/ACAT1 selective inhibitor (Sigma, catalog #SML1837), dimethyl sulfoxide (DMSO) (Fisher, catalog #BP231-1), Rapamycin/mTOR inhibitor (Tocris, catalog #1292), Simvastatin (Sigma-Aldrich, catalog #S6196), Bardoxolone methyl (CDDO-Me, Sigma, catalog #SMB00376), Tunicamycin (Sigma, catalog #5045700001), U18666a (Sigma-Aldrich, catalog #662015-10MG), TNFα (Abcam, catalog #AB259410), MβCD (Sigma-Aldrich, catalog #C4555-10G), cholesterol (Sigma-Aldrich, catalog #C8667-5G), acetylated low-density lipoprotein (acLDL) (Kalen Biomedical, catalog #770201-4).

3.2: MβCD-Cholesterol complexing. Dry cholesterol power (386.65 g/mol, 1.067 g/mL at 25°C) was solubilized in 100% ethanol at 70°C to a final concentration of 100 mM. 1 mL aliquots of the cholesterol solution were added to 42 mg/mL MβCD (1320 g/mol) in deionized water with constant heating at 70°C to a final concentration of 5 mM cholesterol. The cholesterol-MβCD complexed solution was cooled overnight and sterile filtered. This soluble cholesterol solution will hereon be referred to as cholesterol in all subsequent experiments.

3.3: Cell culture. Hep3B cells (American Type Culture Collection, catalog #HB-8064) and RAW 264.7 cells (American Type Culture Collection, catalog #TIB-71) were cultured in Dulbecco's Modified Eagle Medium (DMEM) (Gibco, catalog #11965-092) supplemented with 10% cosmic calf serum (Cytiva Hyclone, catalog #SH30087.03). Cells were grown at 37°C with 5% CO_2.

3.4: CRISPR/Cas9-based gene editing. Hep3B cells stably expressing Cas9 protein ($Hep3B^{Cas9}$) were generated, and single clonal populations isolated as previously described[130]. $9x10^5$ $Hep3B^{Cas9}$ cells in 3 mL DMEM were infected with 45 μL lentivirus ($1x10^8$ TU/mL) carrying single guide RNA (sgRNA) individually targeting *SOAT1* and *SOAT2* genes, supplemented with 4 ug/mL

polybrene (Sigma-Aldrich, catalog #H9268-10G). The multiplicity of infection (MOI) was 5. Each gene was targeted by two distinct sgRNAs (ThermoFisher Scientific, catalog #A32042 *SOAT1*: CRISPR693296_LV and CRISPR693330_LV, *SOAT2*: CRISPR824991_LV and CRISPR824999_LV). Following addition of the lentivirus, the suspension was incubated for 20 minutes at room temperature, added to a 6 cm dish, and incubated for 1 hour at room temperature, and then transferred to a humidified incubator for 24 hours. Lentivirus and polybrene was then removed from the cells which were refed with complete media for 24 hours. To select for cells that underwent gene editing, DMEM was supplemented with 3 ug/mL puromycin (Sigma-Aldrich, catalog #540411-100MG) and 1 ug/mL blasticidin (Sigma-Aldrich, catalog #15205-25MG) until 100% cell death was observed in Hep3B^{Cas9} cells that did not undergo lentivirus infection. Following selection, heterologous knockout lines were expanded, and lysates were collected to verify absence of the respective protein via immunoblot. Knockout lines were maintained on complete media supplemented with 1 μg/mL puromycin.

3.5: Cholesterol crystal formation and imaging. $4x10^5$ Hep3B cells or $1x10^5$ RAW 264.7 cells were seeded in 3.5 cm glass-bottom poly-D-lysine coated dishes (Mattek, catalog #P35GC-1.5-14-C) and allowed to adhere overnight. To induce cholesterol crystallization, Hep3B cells were treated the following day with cholesterol and RAW 264.7 cells were treated with cholesterol or acLDL. Fresh media and treatments were provided every 24 hours. At the treatment endpoint, media was removed and replaced with phosphate buffered saline (PBS) containing 5 μg/mL Hoechst 33342 (ThermoFisher Scientific, catalog #62249) and incubated at 37°C for 30 min to stain nuclei. CC images of live cells were acquired under polarized light on an Olympus IX73 Inverted Epifluorescence microscope with an Olympus DP73 camera at 20x magnification. Nuclei were imaged in parallel to determine cell number per field of view to normalize CC area to cell number. Images from three distinct locations around the dish were taken to best represent the entire dish. Location of images taken was determined using bright-field view to reduce potential observational bias that may occur by viewing the degree of cholesterol crystallization. All images in the same channel within the same experiment were taken at identical exposures.

3.6: Cholesterol crystal area quantification. CC quantification was performed using ImageJ software (https://imagej.nih.gov/ij/). First, raw CC images were converted from RGB to 8-bit format, then the pixel threshold was set between 20-255 for cholesterol treated cells, and between 15-255 for acLDL treated cells. Next, the image was measured and the % area of CC was recorded. To determine cell number per field of view, Hoechst 33342 images were converted from RGB to 16-bit format. The pixel threshold was set between 7-65535 for Hep3B nuclei and between 15 to 20-65535 for RAW 264.7 nuclei. A watershed was applied to the image to separate overlapping nuclei into individual objects. Next, particle size (pixel^2) was set between 3000-infinity for Hep3B nuclei and 2000-infinity for RAW 264.7 nuclei with circularity set between 0.00-1.00. Particles were measured to determine cell number. Cholesterol crystal$^+$ area/cell (A.U.) was calculated by dividing the % area of CC by cell number. This provides a measure of CC area that is normalized to the number of cells that exhibit crystallization. Means of the three CC images taken per plate represents one biological replicate and is shown as a single data point. Each biological replicate is an independent experiment. Data are presented relative to the control group (set to 1) in all experiments.

3.7: Fluorescence imaging. $1.5x10^5$ Hep3B cells or $1x10^5$ RAW 264.7 cells were seeded in 3.5 cm glass-bottom poly-D-lysine coated dishes and allowed to adhere overnight. Cholesterol crystallization was induced by cholesterol loading for 48 hours in Hep3B cells or 24 hours in RAW 264.7 cells. Fresh media and treatments were provided after 24 hours. At the treatment endpoint, media was removed and replaced with serum-free DMEM containing 5 μg/mL Hoechst 33342 to stain nuclei (blue filter cube – ET DAPI), 2 μM BODIPY 493/503 (Invitrogen, catalog #D3922) to stain lipid droplets (green filter cube – FITC-A-Basic-OFF), and 50 nM LysoTracker Red DND-99 (Invitrogen, catalog #L7528) to stain lysosomes (red filter cube – TRITC-A-Basic-OFF). Cells were incubated at 37°C for 30 minutes. To visualize regions of free cholesterol, Filipin Complex (Sigma-Aldrich, catalog #SAE0088) was added to serum-free DMEM to a concentration of 50 μg/mL and incubated at 37°C for 2 hours. Prior to imaging, staining media was removed and replaced with PBS. Fluorescence images of live cells were acquired alongside CC images under polarized light on an Olympus IX73 Inverted Epifluorescence microscope with an Olympus DP73

camera at 40x magnification. Images containing brightness/contrast enhancements were applied equally to all images within the figure and were not applied prior to image quantification.

3.8: Live/dead imaging assay. Following treatment, media was removed and replaced with PBS containing 5 μg/mL Hoechst 33342 and 5 ug/mL propidium iodide (PI) (ThermoFisher Scientific, catalog #J66584.AB) to stain nonviable cells. Fluorescence images of live cells were acquired on an Olympus IX73 Inverted Epifluorescence microscope with an Olympus DP73 camera at 20x magnification. Nuclei were quantified using the method described above (see cholesterol crystal area quantification) and PI positive cells were quantified manually. The percentage of double positive cells (stained with Hoechst 33342 and PI) was calculated by dividing the number of PI positive cells by the number of Hoechst 33342 positive cells and multiplied by 100.

3.9: Cholesterol crystal solubilization assay. $4x10^5$ Hep3B cells were seeded in 3.5 cm glass-bottom poly-D-lysine coated dishes and allowed to adhere overnight. 48 hours and 96h hours control treatments were identical to the procedure in 'cholesterol crystal formation and imaging'. Dishes requiring induction of cholesterol crystallization and subsequent crystal solubilization were first treated with 200 μM cholesterol for 48 hours to induce CC formation (media changed after 24 hours). CC images were acquired as described above at 48 hours. To avoid exposure to the external environment and potential contamination during imaging, a second glass-bottom dish was placed on top of the first and sealed at the edges with parafilm. Following CC and Hoechst 33342 imaging, cells were trypsinized and re-seeded in a new glass-bottom dish containing either control media or 1.27 mM MβCD to initiate CC solubilization. Media was again changed the following day after 24 hours. At the 96-hour endpoint (48 hours of CC solubilization), CC and Hoechst 33342 images were acquired.

3.10: Lipid extraction and cholesterol quantification. $1x10^6$ Hep3B cells were seeded in 3.5 cm dishes and allowed to adhere overnight. After appropriate treatment, the cells were washed twice with cold PBS, collected in PBS by cell scraping, and centrifuged at 13 000 x g for 10 minutes at 4°C. Cell pellets were resuspended in hexane:isopropanol (3:2, v/v), heated at 75°C for 5 minutes,

and immediately centrifuged at 13 000 x g for 10 minutes at room temperature. The soluble fraction containing lipid was transferred to a new tube and dried at 50°C overnight. Pellets containing proteins were dried, resuspended in 0.2 N sodium hydroxide (NaOH) and solubilized overnight at 37°C. Dried lipids were resuspended in 300 μL of 1x Amplex Red Cholesterol Assay kit reaction buffer (Invitrogen, catalog #A12216) and diluted 10x in 1x buffer. Cholesterol assay was performed according to manufacturer's instructions. Briefly, 50 μL of working solution (containing 1x reaction buffer, 300 μM Amplex Red reagent, 2 U/mL horseradish peroxidase (HRP), 2 U/mL cholesterol oxidase, with or without 0.2 U/mL cholesterol esterase) was added to 50 μL lipid sample resuspended in 1x reaction buffer in a 96-well optical bottom, black walled microplate (Fisher, catalog #12-566-70) and incubated at 37°C for 30 minutes protected from light. Measurement of free cholesterol is achieved by excluding cholesterol esterase in the assay, while measurement of total cholesterol is achieved by including cholesterol esterase in the assay. Esterified cholesterol is obtained by subtracting free cholesterol from total cholesterol. Fluorescence was measured using a Biotek Synergy HT microplate reader using excitation/ emission at 530-560/590 nm. The concentration of unknown samples was determined from a cholesterol standard curve of known concentrations. Measured cholesterol levels were normalized to protein content determined using Pierce bicinchoninic acid (BCA) protein assay kit, with bovine serum albumin (BSA) standards diluted in 0.2 N NaOH.

3.11: Immunoblot analysis. $8x10^5$ Hep3B cells were seeded in 3.5 cm dishes and allowed to adhere overnight. After appropriate treatment, cells were washed twice with cold PBS and lysed in RIPA buffer (150 mM NaCl, 50 mM Tris-HCl pH 7.5, 0.1% w/v sodium dodecyl sulfate (SDS), 0.5% w/v Na-Deoxycholate, 1% v/v Nonidet p40, 1 mM EDTA, 1 mM EGTA, 2.5 mM Na-pyrophosphate, 1 mM $NaVO_4$, 10 mM NaF) supplemented with 1x protease inhibitor cocktail (Sigma-Aldrich, catalog #11873580001), 1x phosphatase inhibitor cocktail 2 (Sigma, catalog #P5726-1ML) and 1% 2-mercaptoethanol. Protein concentration was determined using the Pierce BCA protein assay kit (ThermoFisher Scientific, catalog #23250). Proteins were heated at 100°C for 5 mins in denaturing Laemmli buffer (100 mM Tris, pH 6.8, 2% SDS (w/v), 10% glycerol (v/v), 5% 2-mecaptoethanol, 0.01% bromophenol blue (w/v)) and 10 μg protein was loaded onto Bolt™ 4-12% Bis-Tris mini protein gels (Invitrogen, catalog #NW04125BOX) or Novex™ 14%

Tris-Glycine WedgeWell™ mini protein gels (Invitrogen, catalog #XP00145BOX). Electrophoresis was run at 90 V at neutral pH in NuPAGE™ MOPS SDS running buffer (Invitrogen catalogue# NP0001) or Novex Tris-Glycine SDS Running Buffer (Invitrogen, catalog #LC2675) for 2 hours. Proteins were transferred to nitrocellulose membrane (Bio-Rad, catalog #1620115) in Towbin transfer buffer (25 mM Tris, 192 mM glycine, 20% v/v methanol, pH 8.3) at 10 V for 1.75 hours, blocked in tris-buffered saline containing 0.1% tween 20 (TBST) and 5% powdered skim milk, and incubated overnight at 4°C with primary antibodies (see table 3.1). After three washes with TBST, membranes were incubated with secondary HRP-conjugated antibodies (see table 3.1) at room temperature for 1 hour. Membranes were washed three times with TBST and then incubated with SuperSignal™ West Femto Maximum Sensitivity Substrate (ThermoFisher Scientific, catalog #34096) or SuperSignal™ West Pico PLUS Chemiluminescent Substrate (ThermoFisher Scientific, catalog #34580) to generate chemiluminescence that was detected by a BioRad ChemiDoc MP Imaging System and analyzed using ImageJ software.

Antibody	**Source**	**Molecular Weight (kDa)**	**Host Species/Clonality**	**Dilution**
LC3B	Cell Signaling Technology (catalog #3868)	14, 16	Rabbit mAb	1:1000
GAPDH	Cell Signaling Technology (catalog #2118)	37	Rabbit mAb	1:5000
Anti-Rabbit IgG HRP Conjugated	Santa Cruz Biotechnology (catalog #sc-2357)	N/A	Mouse mAb	1:5000

Table 3.1: Antibodies used for immunoblotting. This table provides a summary of the antibodies used in immunoblot experiments including the source, molecular weight, host species and dilution used.

3.12: Gene expression analysis. $1.2x10^6$ Hep3B cells were seeded in 6cm dishes and allowed to adhere overnight. After appropriate treatment, media was removed and cells were lysed and collected in 500 µL TRIzol Reagent (ThermoFisher Scientific, catalog #15596018) and total RNA was isolated according to manufacturer's protocol. Addition of 100 µl chloroform enabled separation of RNA into the clear upper aqueous phase which was transferred to a new microfuge tube. RNA was precipitated with 250 µL 100% isopropanol. The resulting RNA pellet was washed in 75% ethanol solution and resuspended in 30 µL nuclease free water. 500 ng of purified RNA was used for cDNA synthesis using Maxima H Minus First Strand cDNA Synthesis Kit with dsDNase (ThermoFisher Scientific, catalog #K1672). cDNA was diluted 20x in nuclease free water and 2 µL of diluted cDNA was used as template for quantitative polymerase chain reaction (qPCR) using 0.5 µM of each forward and reverse primers (see table 3.2). qPCR was performed on a Bio-Rad CFX384 Real-Time PCR Detection System using PowerUP™ SYBR™ Green Master Mix (ThermoFisher Scientific, catalog #A25742). Cycle thresholds (Ct) were normalized to glyceraldehyde-3-phosphate dehydrogenase (GAPDH) levels by the ΔΔCt method and reported relative to control.

Gene Name	**Forward Primer (5' → 3')**	**Reverse Primer (5' → 3')**	**Source**
ABCA1	CAGGAAGATTAGACACTGTGG	GAAAGGGGAATGGAGAGAAG	Ananth et al, 2014
FDFT1	CCACCCCGAAGAGTTCTACAA	TGCGACTGGTCTGATTGAGATA	MGH PrimerBank ID: 67089146c1
IDOL	AAACCTGAGAAACCGGATCTCC	GCTCCACGAAGAACTTGACTCTA	MGH PrimerBank ID: 38788242c2
LDLR	CCCGACCCCTACCCACTT	AATAACACAAATGCCAAATGTACACA	Adachi et al, 2014
SOAT1	CAAGGCGCTCTCTCTTAGATG	GGTCCAAACAACGGTAGGAAA	MGH PrimerBank ID: 357430783c3
SOAT2	ATGGAAACACTGAGACGCACA	GGTAGGATTGTATAGCCTCCCG	MGH PrimerBank ID: 125988401c1
nCEH1	TGTTGTACGGGCCACAAAGTA	GCAGGATTGGGGTGTTCACAT	MGH PrimerBank ID: 226423949c1
GAPDH	GAGCCAAAAGGGTCATCATC	TAAGCAGTTGGTGGTGCAGG	

Table 3.2: DNA primer sequences used in qPCR. This table provides a summary of the gene primers used in qPCR gene expression analysis experiments including the forward/reverse sequences and the source.

3.13: Electron microscopy. $1.2x10^6$ Hep3B cells were resuspended in 700 µL of DMEM, and FGP fixative solution (1.25% paraformaldehyde, 2.5% glutaraldehyde, 0.03% picric acid) was added to the suspension at a 1:1 ratio. Cells were fixed for 10 minutes at room temperature. Cells were then centrifuged at 2000 rpm for 5 minutes at 4°C then stored at 4°C. Samples were then provided to our collaborator Dr. Ana Paula Arruda at the University of California Berkeley. Preparation and transmission electron microscope images were taken, in accordance to their recently published work[131].

3.14: Genomic cleavage detection and sequencing. Locus-specific insertion/deletion (INDEL) formation was measured using the Genomic Cleavage Detection Kit according to manufacturer's instructions. Briefly, $3x10^5$ cells were seeded in a 6-well plate, lysed, and DNA extracted after 24 hours. 3 µL of cell lysate was used for PCR amplification. The PCR program was set at 95°C for 10 minutes for one cycle, then 95°C for 30 seconds, 60°C for 30 seconds, and 72°C for 1 minute for a total of 40 cycles. Final extension was set for 7 minutes at 72°C. 3 µL of PCR product was used for denaturing and re-annealing reaction. Lastly, 1 µL detection enzyme was added to the sample and then incubated at 37°C for 1 hour. The digested PCR products were loaded onto a 2% agarose gel to analyze cleavage efficiency. For sequencing, all initial PCR products were loaded onto a 2% agarose gel, and DNA fragments were excised from the gel with X-Tracta Gel Extraction tool (Sigma, catalog #Z722390-100EA) and placed in a 1.5 mL Eppendorf tube. Gel pieces were weighed, and DNA fragments purified using QiAquick gel extraction kit (Qiagen, catalog #28706). Lastly, 5 µL of purified DNA was premixed with 5 µL primer and sent to Eurofinsgenomics for sequencing.

Gene Name and sgRNA Identifier	Forward Primer (5'→3')	Reverse Primer (5' → 3')
SOAT1-296	GAAGACTGTATTTATCTTAGGGCTT	CCTAGAACTCCAATCTGGAAGA
SOAT1-330	CGACCTTGCCATTCTCTACAA	AGGAGCAAGAGAGAGCATAGA
SOAT2-991/999	GGCCTTATCCTTCTGACTGTTT	TTGCAGTGAGCCGAGATTG

Table 3.3: PCR primer sequences used for genomic cleavage detection and sequencing. This table provides a summary of the DNA primers used to verify gene editing of the *SOAT1* and *SOAT2* loci of knockout cells by amplification, genomic cleavage detection, and sequencing. Primer pairs for separate sgRNAs targeting the same gene are listed.

3.15: Statistical analysis. All data analysis was performed using GraphPad PRISM (version 9.5.1). Significance was defined as $p<0.05$ using t-test, one-way or two-way analysis of variance (ANOVA) and Dunnett's or Tukey's post-hoc test as indicated in figure legends. Data are expressed as mean ± standard error of the mean (SEM). Sample size is indicated in each figure. A minimum of three biological replicates (independent experiments) were used for each study.

Chapter 4 – Cholesterol Crystallization Model and Intracellular Localization

4.1: Introductory rationale

Studies done on atherosclerotic mouse models and cell culture models have revealed a tremendous amount of knowledge regarding the role of CC in atherosclerotic plaques. However, few studies have investigated their role in the liver. By weight, hepatocytes make up the majority of the liver composition, are the primary cholesterol metabolizing cells of the liver[34], and CC in hepatocytes are linked to NASH. For these reasons, we deemed a hepatocyte cell culture model is needed to interrogate the mechanisms that promote intracellular cholesterol crystallization. For our studies in this chapter, immortalized human hepatocyte (Hep3B) and mouse macrophage (RAW 264.7) cell lines were used. Previous reports have studied cholesterol crystallization in HepG2 cells by incubating them with LDL and oleic acid for 20 days[20,24]. Although this may be a more physiological approach, it is not an efficient model to probe factors that affect CC formation. Since FC accumulation underlies cholesterol crystallization, we chose to load Hep3B plasma membranes with cholesterol complexed to methyl-β-cyclodextrin (MβCD) and RAW 264.7 cells with acLDL to expedite cholesterol accumulation[66,132,133]. Conversely, cholesterol depletion was achieved by treating with MβCD alone. The use of murine macrophages, rather than human macrophages in our experiments was based on availability and the fact that murine cell culture models are commonly employed in atherosclerosis studies. It is unclear whether CC formation would be affected by any differences in function or response to cholesterol/acLDL loading between murine and human macrophages. Nevertheless, **the first objective of my thesis was to establish a cellular model of intracellular CC formation in hepatocytes and macrophages**.

4.2: Results

4.2.1: Cholesterol crystallization model characterization

To this end, we treated Hep3B cells with or without 200 μM cholesterol for various timepoints and assessed CC formation using PLM. Under polarized light, cells treated with control media did not exhibit any detectable cholesterol crystallization at any timepoints, whereas cholesterol-loaded hepatocytes showed robust crystallization over time (Figure 4.1A). At the 48-

and 96-hour timepoints, cholesterol treatment caused significant levels of crystallization (Figure 4.1B). In a complimentary approach, CCs were also detected in cholesterol treated cells using confocal-polarized light (Appendix C-D). Based on this experiment, the 48-hour timepoint was chosen to further study CC formation.

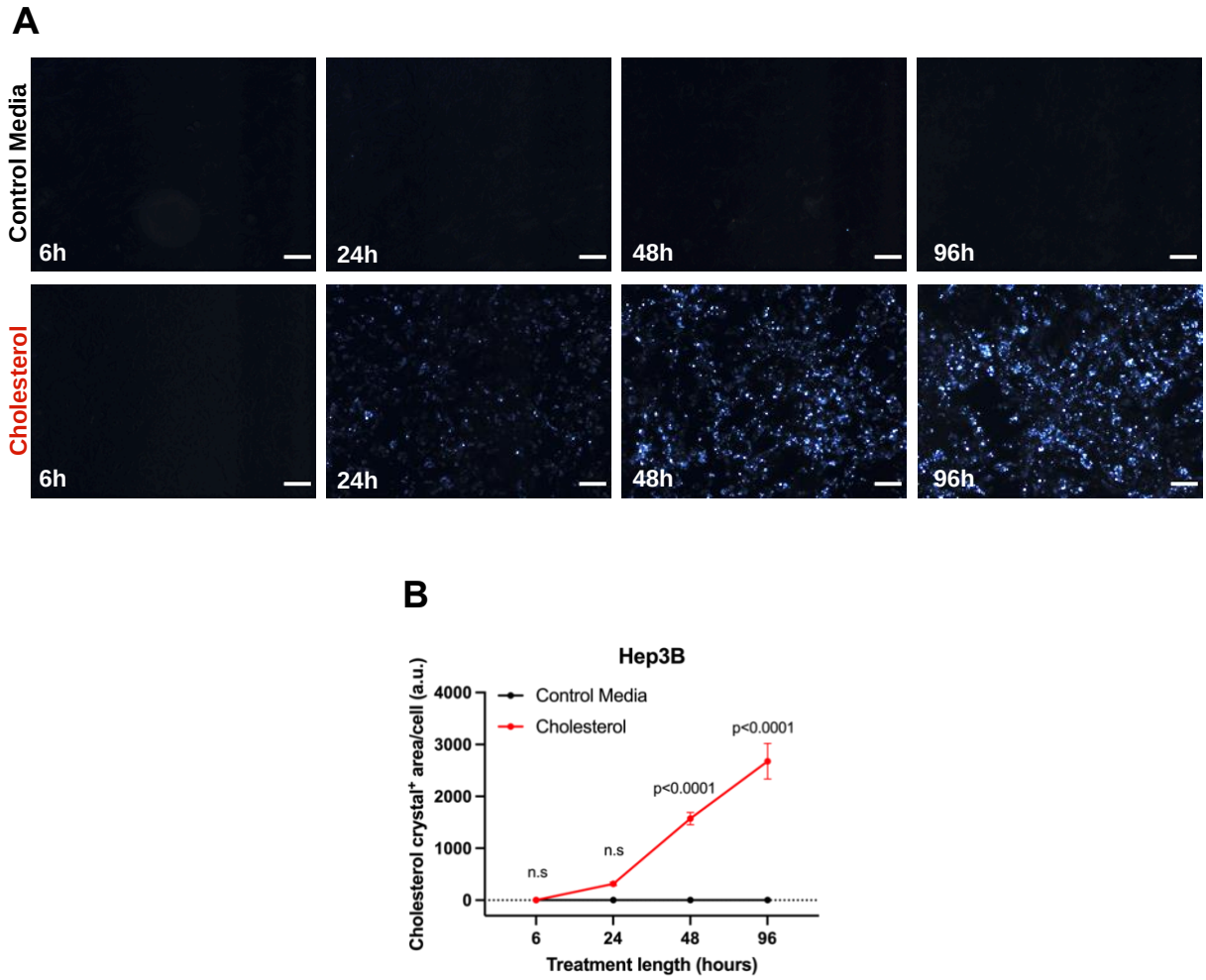

Figure 4.1: Cholesterol loading induces cholesterol crystal formation in a time-dependent manner in hepatocytes.
(A) Representative polarized light images (20x magnification) of live Hep3B cells treated with or without 200 μM cholesterol for 6, 24, 48, or 96h. (B) Quantification of cholesterol crystal formation in (A) (n=3). p-values in (B) were determined by two-way analysis of variance (ANOVA) with Tukey's post-hoc test between treatment groups at the same timepoint. Data in (B) are mean ± SEM. Scale bar = 200 μm.

Next, we examined the dose-dependence of cholesterol treatment on CC formation. Compared to control media (0 μM), higher cholesterol concentrations (50-200 μM) led to greater cholesterol crystallization (Figure 4.2A), and this was significant at the 100 and 200 μM doses (Figure 4.2B). Likewise, the CE content of these cells was elevated by each dose of cholesterol treatment (Figure 4.2C), which is consistent with an expected increase in esterification to prevent FC accumulation in response to cholesterol loading. Interestingly, CE abundance moderately correlated with CC formation (Figure 4.2D), suggesting that cholesterol esterification is linked to CC formation.

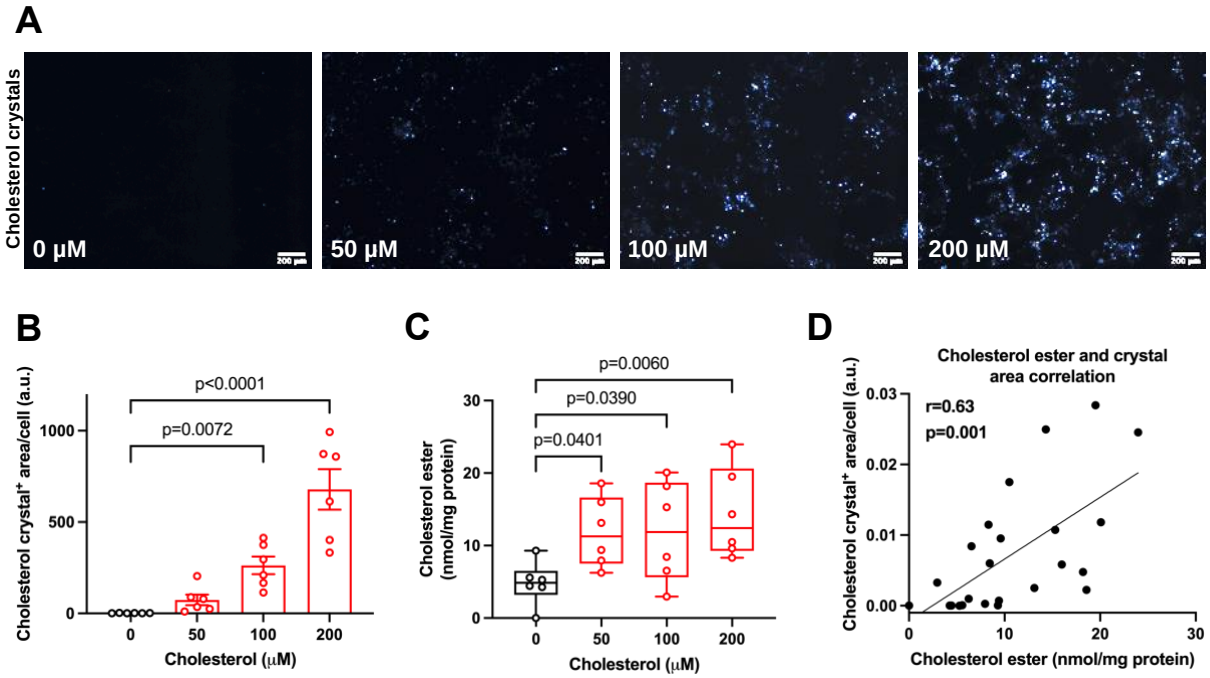

Figure 4.2: Cholesterol esterification is associated with cholesterol crystal formation.
(A) Representative polarized light images (20x magnification) of live Hep3B cells treated with 0-200 μM cholesterol for 48h. (B) Quantification of cholesterol crystal formation in (A) (n=6). (C) Cholesterol ester measurement at 48h (n=6). (D) Correlation plot of cholesterol ester abundance and cholesterol crystal formation. p-values in (B-C) were determined by one-way ANOVA with Dunnett's post-hoc test, and in (D) by two-tailed t-test. r-value in (D) were determined by Pearson r. Data in (B) are mean ± SEM or box and whisker plot in (C). Scale bar = 200 μm.

To verify that our method of cholesterol-MβCD loading was dependent on cholesterol, we tested the effect of removing cholesterol from the media after generating CC. As controls, we treated Hep3B cells with or without cholesterol for 48 or 96 hours. We compared the cholesterol groups to another group that was incubated with cholesterol for 48 hours to pre-form CC, then transitioned to control media for another 48 hours (Figure 4.3A). Removal of cholesterol from cells that contained pre-formed CC resulted in approximately 50% reduction in cholesterol crystallization during the 'resolution' phase compared to 48-hour cholesterol treatment (Figure 4.3B).

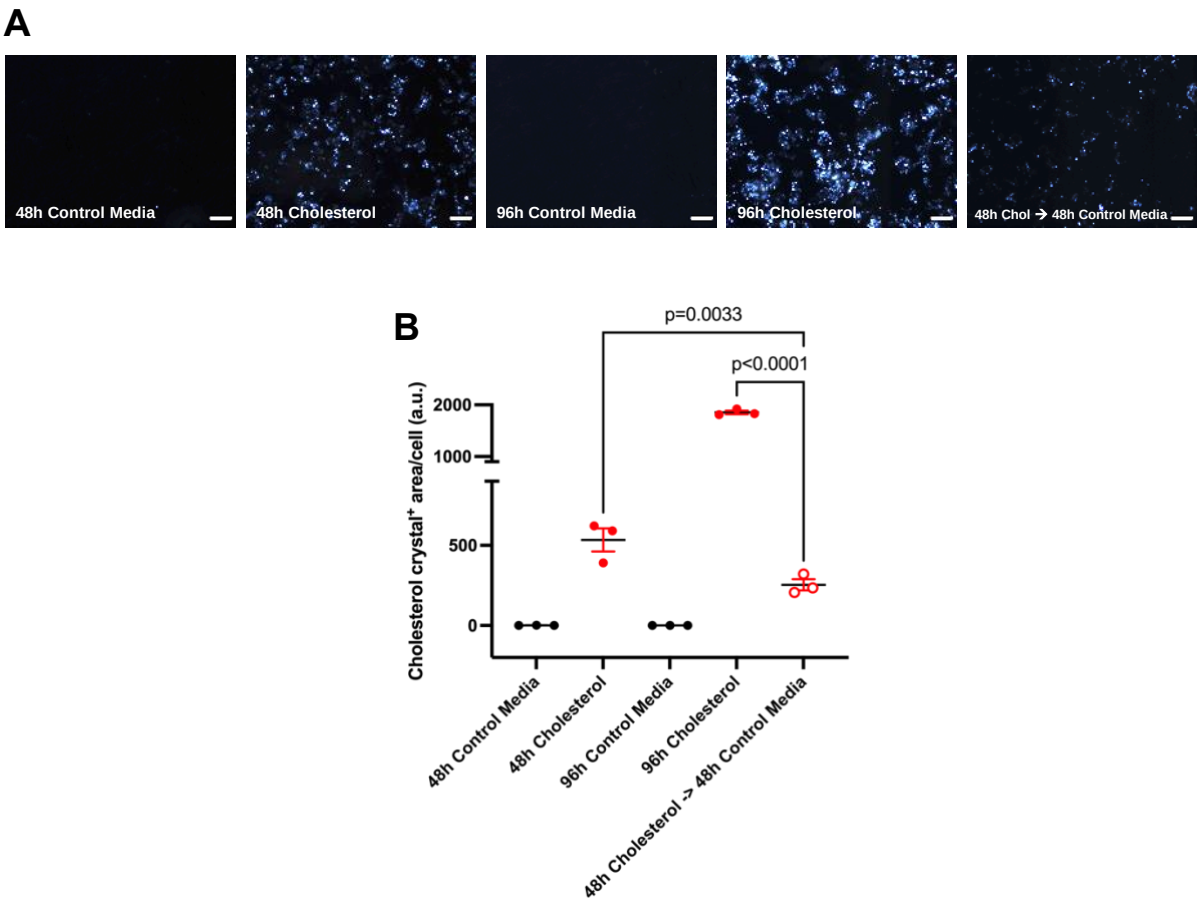

Figure 4.3: Transition to cholesterol-free media is sufficient to solubilize pre-formed cholesterol crystals.
(A) Representative polarized light images (20x magnification) of live Hep3B cells treated with control media, 200 μM cholesterol, or 200 μM cholesterol and transitioned to control media. (B) Quantification of cholesterol crystal formation/solubilization in (A) (n=3). p-values in (B) were determined by one-way ANOVA with Dunnett's post-hoc test. Data in (B) are mean ± SEM. Scale bar = 200 μm.

Similarly, we asked if adding MβCD alone to deplete cholesterol would lead to even less CC. Using the controls listed above and an additional MβCD control, we compared the cholesterol groups to a group that was incubated with cholesterol for 48 hours to pre-form CC and then transitioned to MβCD for 48 hours to deplete cholesterol (Figure 4.4A). Cholesterol depletion from cells with pre-formed CC displayed approximately 50% reduction in cholesterol crystallization compared to 48-hour cholesterol treatment (Figure 4.4B). Surprisingly, cholesterol depletion was not more effective at solubilizing pre-formed CC compared to transition to control media alone (Figure 4.4C-D). Collectively, this work shows that cholesterol loading in hepatocytes efficiently and reliably induces CC formation and establishes this model system for use in further experiments to investigate the mechanisms contributing to intracellular cholesterol crystallization.

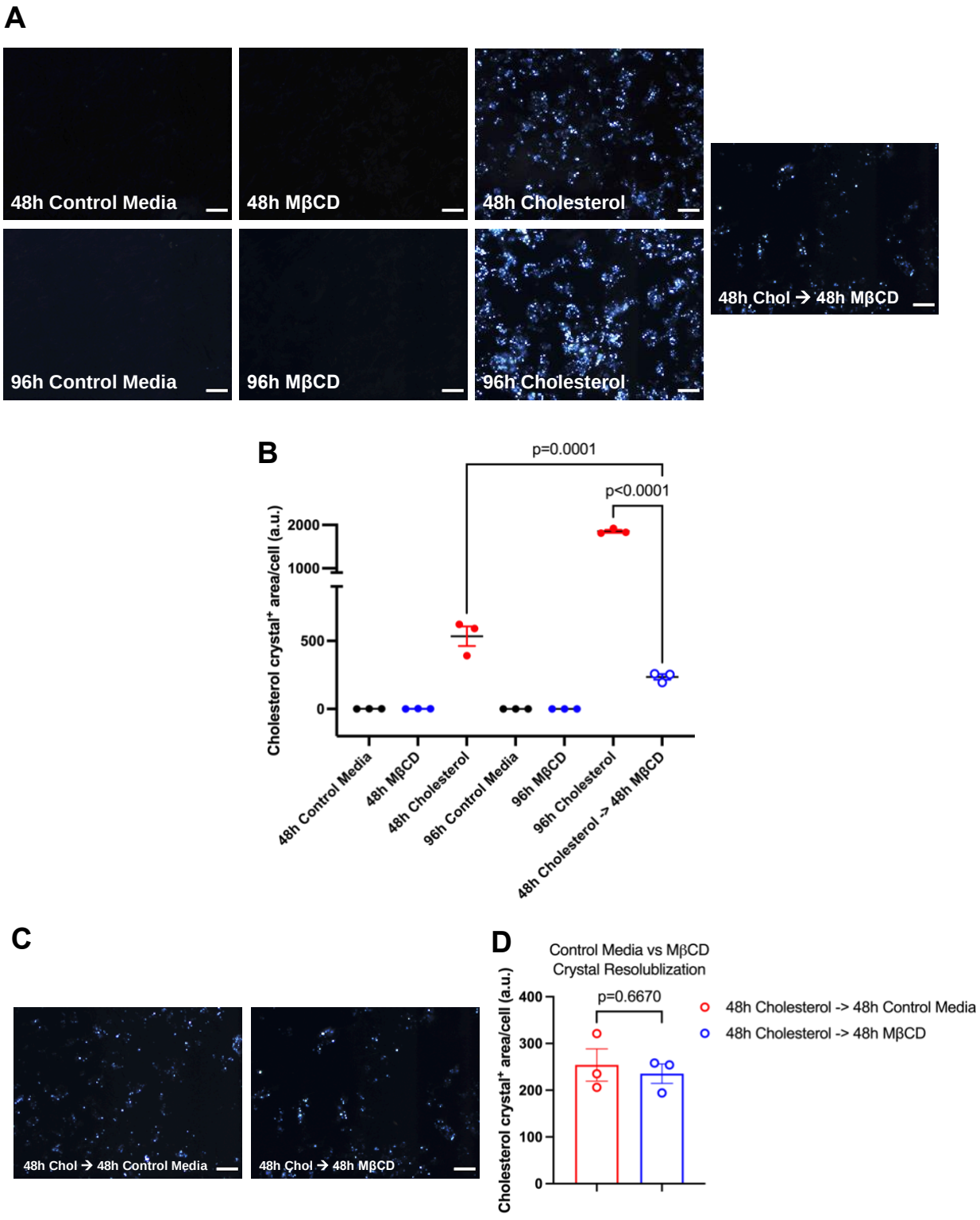

Figure 4.4: Cholesterol depletion is sufficient to solubilize pre-formed cholesterol crystals. A) Representative polarized light images (20x magnification) of live Hep3B cells treated with control media, 1.27 mM MβCD, or 200 μM cholesterol and transitioned to 1.27 mM MβCD. (B) Quantification of cholesterol crystal formation/solubilization in (A) (n=3). (C) Comparison of the ability of control media (from figure 4.3) and MβCD to solubilize pre-formed cholesterol crystals. (D) Crystal solubilization quantification in (C) (n=3). p-values in (B) were determined by one-way ANOVA with Dunnett's post-hoc test and in (D) by t-test. Data in (B) and (D) are mean ± SEM. Scale bar = 200 μm.

Since the vast majority of studies examining intracellular cholesterol crystallization have used macrophages as a model, I deemed it valuable to compare our results in hepatocytes to macrophages. This also allowed us to determine whether cholesterol loading via receptor-mediated uptake also led to cholesterol crystallization. For these studies, we used the RAW 264.7 cell line. Cholesterol loading in macrophages was achieved by incubating with cholesterol or acLDL, which is a modified lipoprotein that is taken up by macrophages in an unregulated fashion via scavenger receptors[66,133].

First, we tested whether CC formation was induced in RAW 264.7 macrophages. This was done by incubating macrophages with acLDL or cholesterol for various timepoints (Figure 4.5A). Compared to control media, 24- and 48-hour incubation was sufficient to cause cholesterol crystallization with both acLDL and cholesterol (Figure 4.5B-C). Although not directly compared, it was clear that cholesterol treatment induced CC formation to a much greater degree than acLDL treatment.

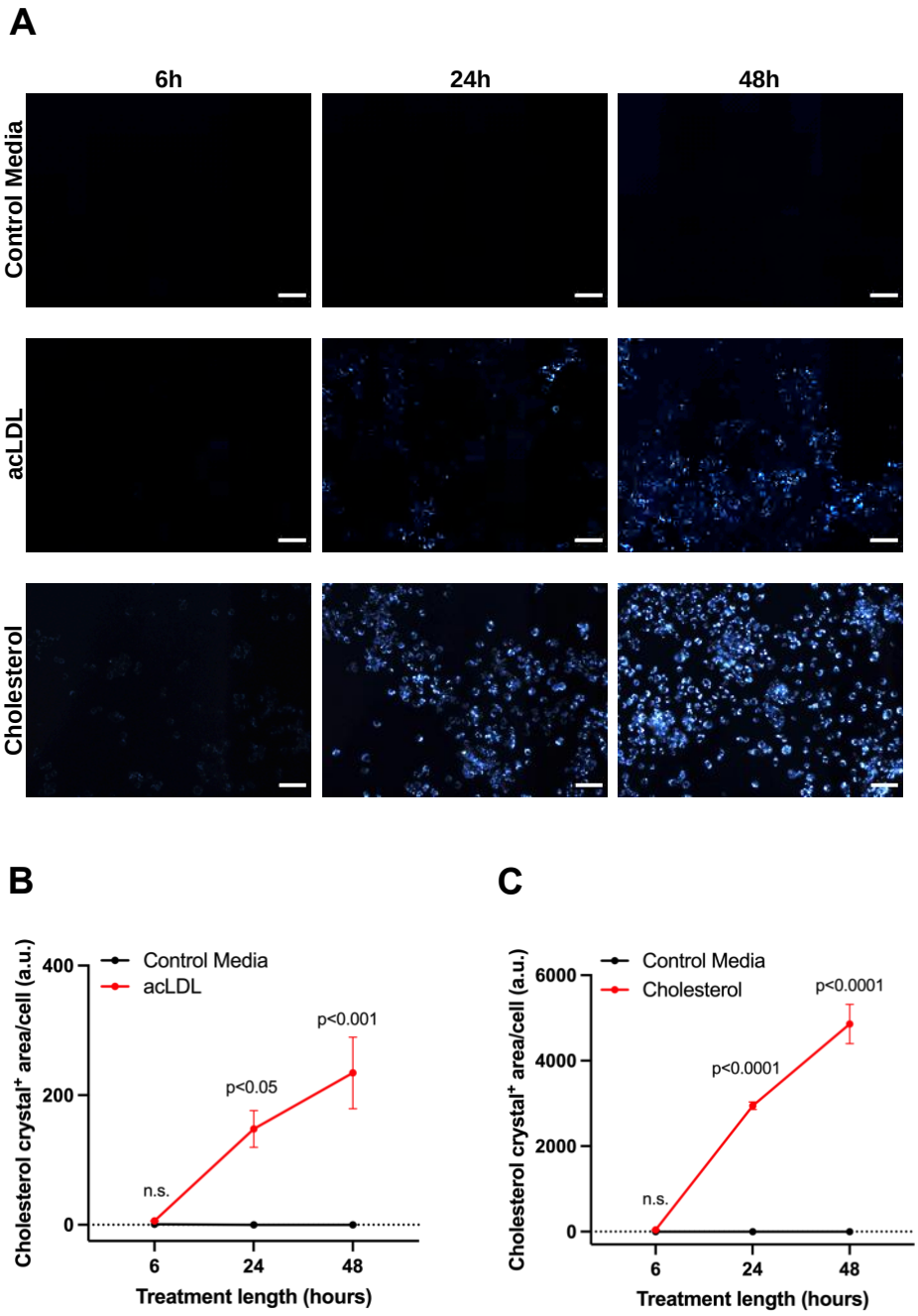

Figure 4.5: acLDL and cholesterol loading induces cholesterol crystal formation in a time-dependent manner in macrophages.
(A) Representative polarized light images (20x magnification) of live RAW 264.7 cells treated with control media, 50 μg/mL acLDL, or 200 μM cholesterol for 6, 24, or 48h. (B) Quantification of acLDL-induced cholesterol crystal formation in (A) (n=3). (C) Quantification of cholesterol-induced cholesterol crystal formation in (A) (n=3). p-values in (B-C) were determined by two-way ANOVA with Tukey's post-hoc test between treatment groups at the same timepoint. Data in (B-C) are mean ± SEM. Scale bar = 200 μm.

4.2.2: Intracellular cholesterol crystal localization

The second objective of my thesis was to identify the location of intracellular CC formation or nucleation. Based on our previous observations that CC formation may be driven by cholesterol esterification (Figure 4.2D) and that lipid droplets concentrate CE, the lipid droplet was a logical organelle to explore. Thus, we treated hepatocytes with or without cholesterol and stained cells with organelle specific fluorophores to be identified using fluorescence microscopy and assessed CC formation with PLM. Incubation of cells with control media resulted in a lack of CC formation as expected, but lipid droplets and lysosomes were detected with BODIPY and LysoTracker staining, respectively (Figure 4.6A [top]). Incubation with cholesterol led to robust CC formation, and merged images show the crystals are intimately associated with the exterior of lipid droplets but not lysosomes (Figure 4.6A[bottom]). Provided that BODIPY is known to stain neutral lipids, is widely used as a lipid droplet marker, and that we observed an increase in lipid droplet size upon cholesterol loading, our imaging demonstrates that intracellular CC formation or nucleation occurs in close association to lipid droplets, and not in lysosomes.

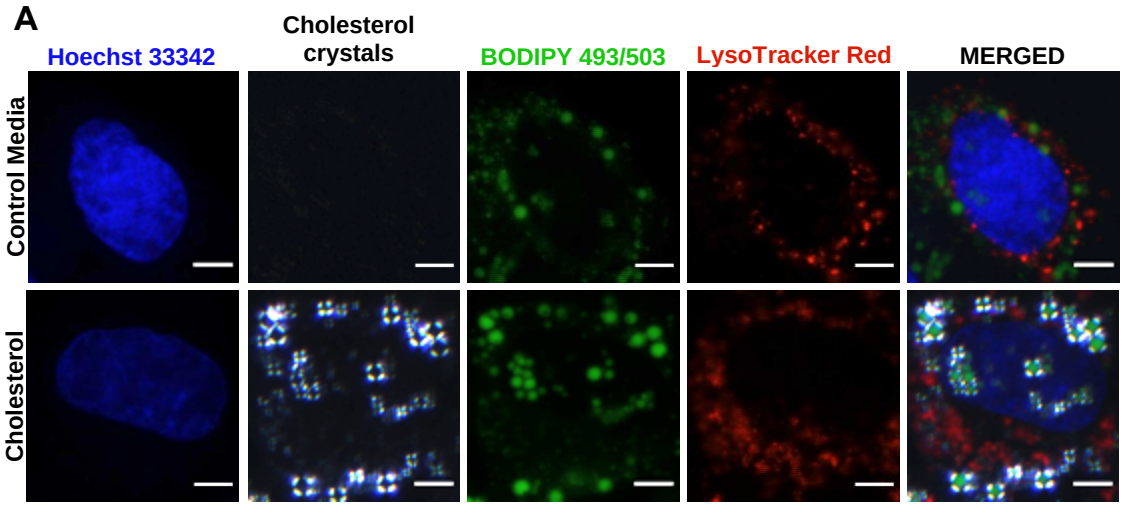

Figure 4.6: Hepatocyte lipid droplets support cholesterol crystallization.
(A) Representative fluorescence and polarized light images (40x magnification) of live Hep3B cells treated with or without 200 μM cholesterol for 48h. Nuclei were stained with Hoechst 33342, cholesterol crystals were detected with polarized light, lipid droplets were stained with BODIPY 493/503, lysosomes were stained with LysoTracker Red DND-99. Images were acquired on an epifluorescence microscope. Scale bar = 50 μm.

Next, the localization of CCs in macrophages was investigated using fluorescence imaging and PLM. Like hepatocytes, control treated macrophages did not display CCs, while cholesterol treated macrophages showed CC formation that was visually consistent with lipid droplet staining (Figure 4.7A). Furthermore, lysosomes did not associate with regions of cholesterol crystallization. Thus, in our hands, cholesterol or acLDL-loaded macrophages also display CC formation and show features comparable to our hepatocyte model, specifically, lipid droplet-localized CCs.

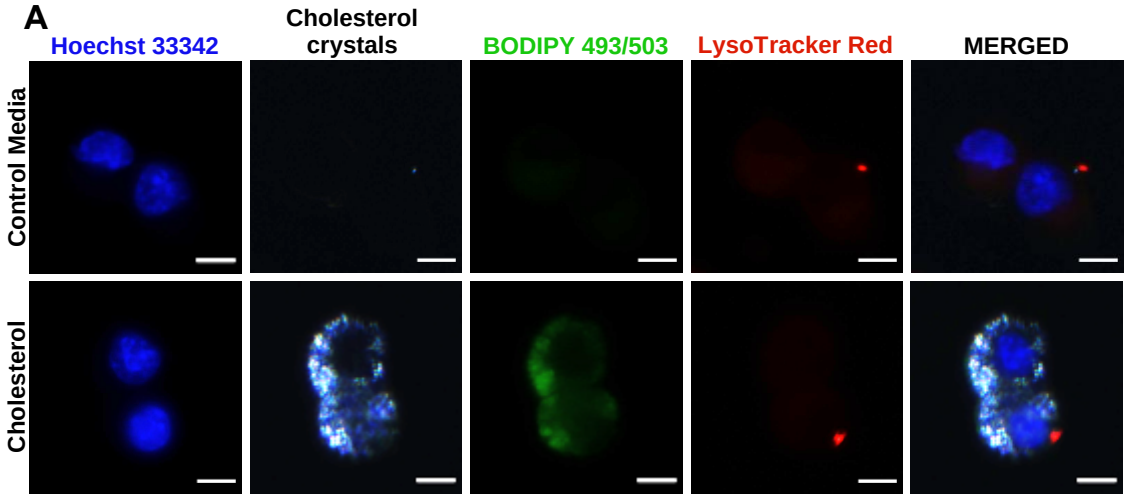

Figure 4.7: Macrophage lipid droplets support cholesterol crystallization.
(A) Representative fluorescence and polarized light images (40x magnification) of live RAW 264.7 cells treated with or without 200 μM cholesterol for 24h. Nuclei were stained with Hoechst 33342, cholesterol crystals were detected with polarized light, lipid droplets were stained with BODIPY 493/503, lysosomes were stained with LysoTracker Red DND-99. Scale bar = 50 μm.

4.3: Conclusion

In summary, our first two objectives have successfully been met in this chapter. First, we established cell culture models of intracellular CC formation in hepatocytes and macrophages and found that we could reliably model the process of cholesterol crystallization, in a manner that is dependent on dose and time of cholesterol loading. Lastly, we demonstrated that CCs are localized to hepatocyte and macrophage lipid droplets, but not lysosomes. These preliminary results lay the groundwork for the bulk of this thesis discussed within chapter 5, which aims to test my hypothesis that enzymes that mediate cholesterol esterification and enzymes that de-esterify lipid droplet CE are required for intracellular CC formation.

Chapter 5 – The Role of Cholesterol Ester Metabolism in Cholesterol Crystal Formation

5.1: Introductory rationale

With our focus set on lipid droplets due to the results in chapter 4, I then sought to explore the mechanistic factors that contribute to CC formation. Given the ability of lipid droplets to store esterified cholesterol, we reasoned that cholesterol esterification and subsequent lipid droplet localization is an essential step in the process leading to cholesterol crystallization. Therefore, **the third objective of my thesis was to investigate the role of cholesterol ester metabolism in intracellular CC formation.**

5.2: Results

5.2.1: Evidence that ACAT1 is required for cholesterol crystal formation

To test the hypothesis that enzymes that mediate cholesterol esterification are required for CC formation, we first treated hepatocytes with a compound named Sandoz 58-035, an established and frequently used nonselective inhibitor of ACAT, to assess its effect on CC formation with PLM. As expected, incubation with control media did not lead to CC formation. However, cells treated with cholesterol alone displayed CC formation after 48 hours. In contrast, crystallization was drastically reduced in cells co-treated with cholesterol and 1 μg/mL of the ACAT inhibitor (Figures 5.1A, B). To determine whether this result may be a confounding factor of altered cell viability, I assessed cell death levels by measuring the percent number of cells stained positive for a nuclei marker, Hoechst 33342, as well as a cell death marker, propidium iodide (PI). Baseline cell death (double positive cells in control treatment) average level was less than 5%, whereas co-treatment increased average cell death to slightly above 5%, and this was not significantly different than cholesterol alone treated cells (Figure 5.1A, C). This indicates reduced CC level in cholesterol loaded cells treated with Sandoz 58-035 was not due to altered cell viability. Moreover, while cholesterol treatment elevated cellular CE abundance, this effect was blunted by Sandoz 58-035 co-treatment, confirming inhibition of cholesterol esterification by ACAT (Figure 5.1D).

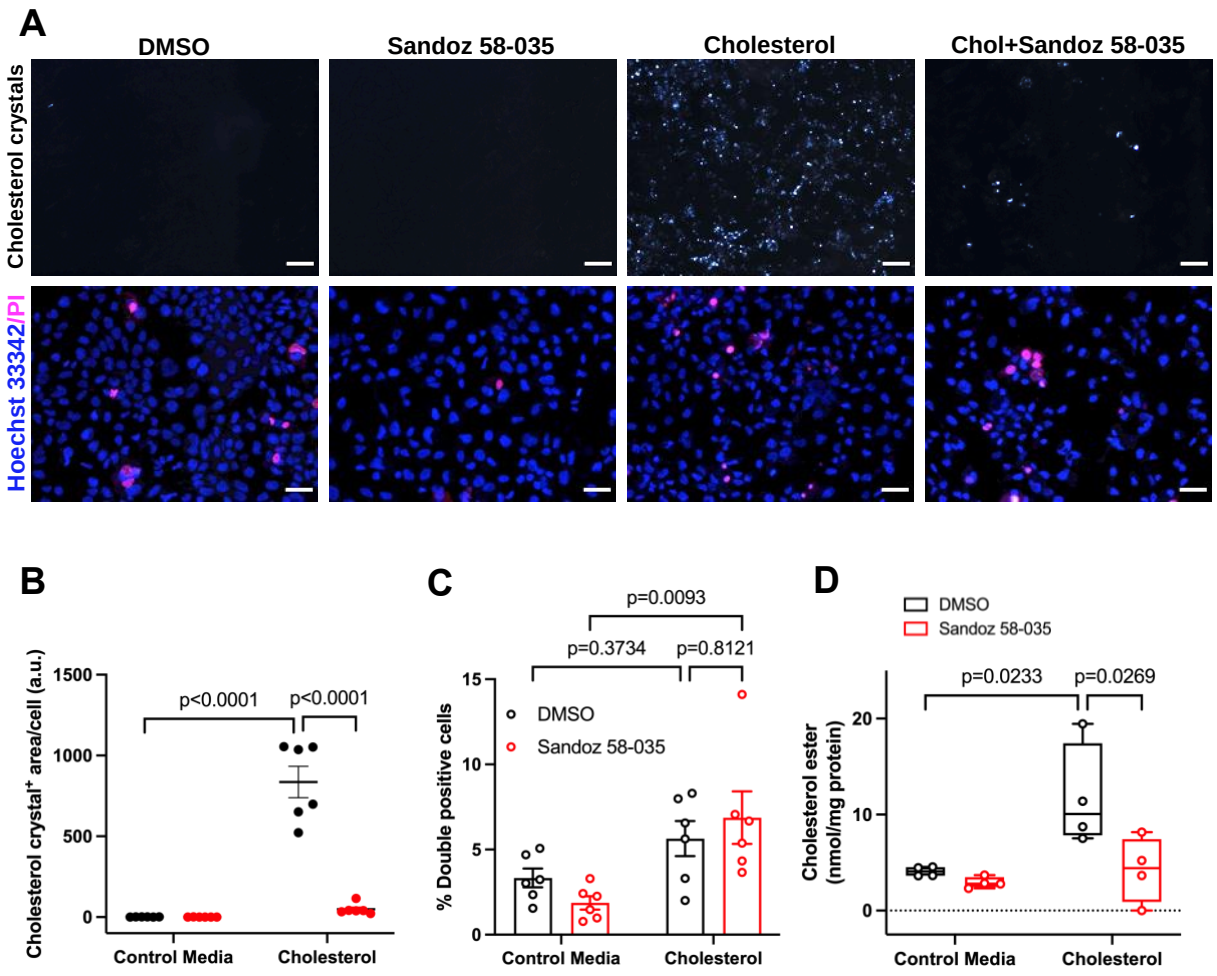

Figure 5.1: Cholesterol esterification and subsequent lipid droplet localization is required for cholesterol crystal formation.
(A) Representative fluorescence (bottom) and polarized light (top) images (20x magnification) of live Hep3B cells treated with or without 200 μM cholesterol and with or without 1 μg/mL Sandoz 58-035 (ACAT inhibitor) for 48 hours. (B) Quantification of cholesterol crystal formation in (A) (n=6). (C) Live/dead imaging assay quantification in (A) (n=6). (D) Cholesterol ester measurement at 24 hours (n=4). p-values in (B-D) were determined by two-way ANOVA with Tukey's post-hoc test. Data in (B-C) are mean ± SEM or box and whisker plot in (D). Scale bar = 200 μm.

Inhibition of ACAT leads to the accumulation of FC within the ER[134], and this should in turn alter transcriptional programming related to cholesterol metabolism. Therefore, I examined the expression of genes that are expected to respond to FC accumulation. In this case, LXR targets *ABCA1* and *IDOL* should be upregulated, while SREBP2 targets *FDFT1* and *LDLR* should be downregulated as a counteracting homeostatic response. I found three genes that were regulated

as expected by cholesterol treatment, with this effect being potentiated by co-treatment (Figure 5.2A). Specifically, *ABCA1* and *IDOL* were enhanced by co-treatment and *FDFT1* was reduced to a greater level. Another effect that can result from FC accumulation is the induction of ER stress[135]. I found two markers of ER stress, *ATF4* and *CHOP*, were upregulated in response to cholesterol, three by co-treatment – *ATF4*, *CHOP*, and *BiP* – and *CHOP* was potentiated by ACAT inhibition (Figure 5.2B). I also examined expression level of genes involved in cholesterol ester metabolism, from which I found only *SOAT2* level was modestly increased by cholesterol treatment (Figure 5.2C). Altogether, these data show that cholesterol treatment without and with ACAT inhibition results in the expected cellular responses, which validates our experimental model.

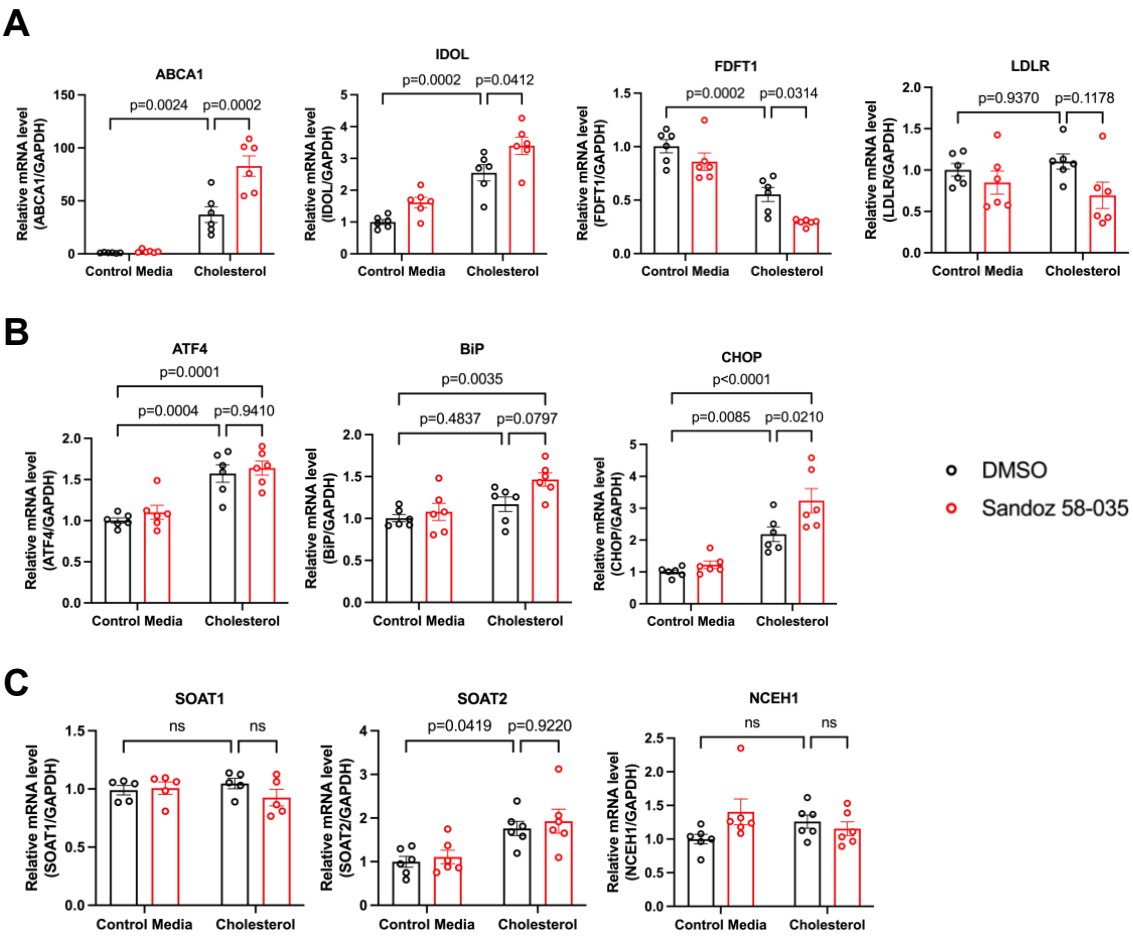

Figure 5.2: Cholesterol loaded hepatocytes display expected homeostatic regulation.
(A) LXR target (ABCA1 and IDOL) and SREBP2 target (FDFT1 and LDLR) gene expression at 18 hours (n=6). (B) ER stress marker gene expression at 18 hours (n=6). (C) Cholesterol ester metabolism gene expression at 18 hours (n=5-6). Hep3B messenger RNA (mRNA) levels were normalized to glyceraldehyde-3-phosphate dehydrogenase (GAPDH) and displayed relative to control. Treatments are consistent with previous experiments. p-values in (A-C) were determined by two-way ANOVA with Tukey's post-hoc test. Data in (A-C) are mean ± SEM.

After establishing that intracellular CC are associated with lipid droplets and finding that esterification appears to be required for CC formation, I next tested whether inhibiting esterification with Sandoz 58-035 would prevent crystal formation at the lipid droplet. Fluorescence imaging and PLM show the CCs associated with lipid droplets in the cholesterol treated cells, while cells co-treated with cholesterol and Sandoz 58-035 lacked CC and had lipid droplets with similar morphology to the control groups (Figure 5.3). As expected, incubation with control media did not lead to CC formation. Hence, these findings confirm that inhibition of ACAT in cholesterol-loaded hepatocytes prevents the formation of lipid droplet-associated cholesterol crystals.

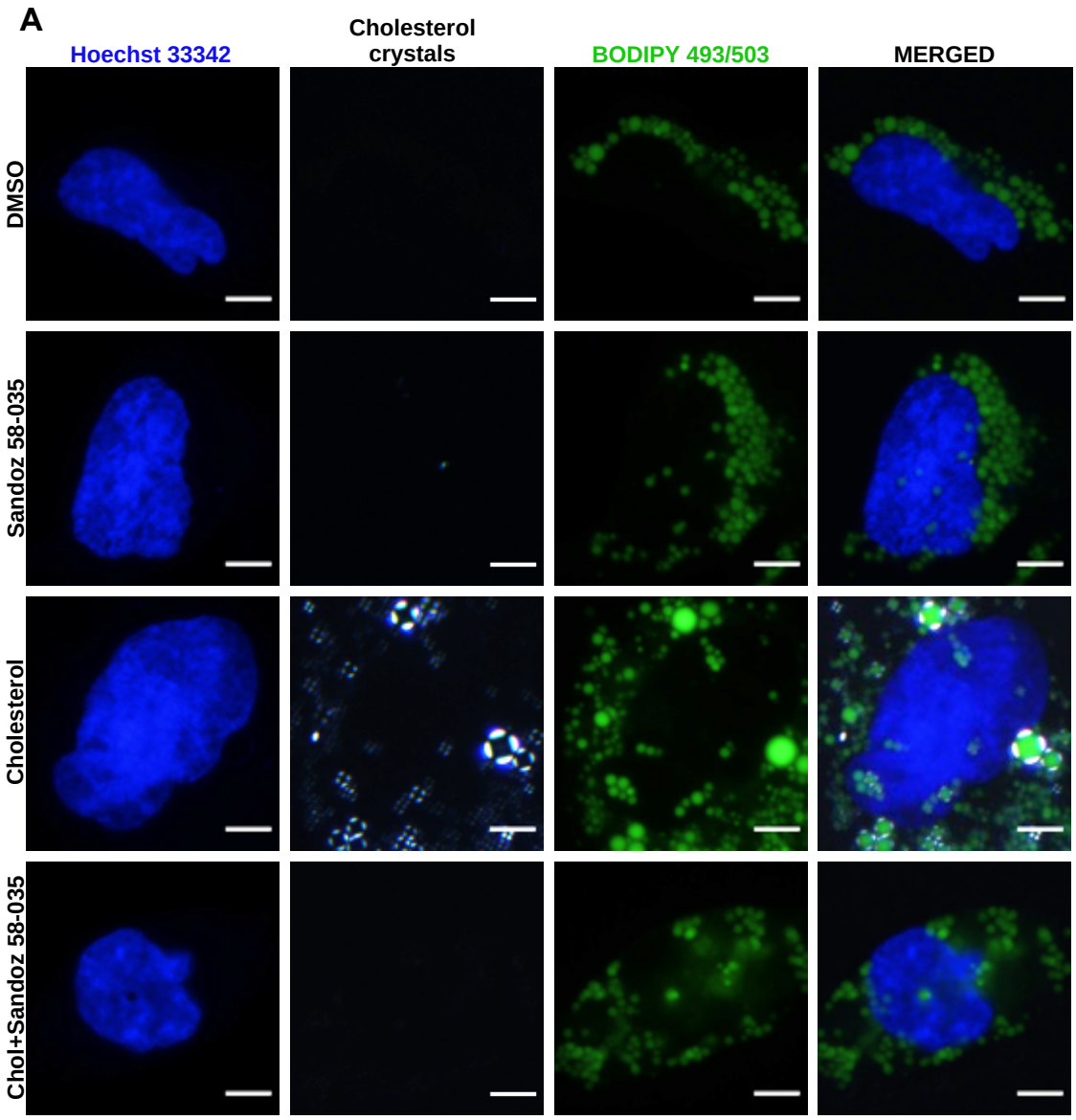

Figure 5.3: ACAT inhibition prevents the formation of lipid droplet-associated cholesterol crystals.
(A) Representative fluorescence and polarized light images (40x magnification) of live Hep3B cells treated with or without 200 μM cholesterol and with or without 1 μg/mL Sandoz 58-035 (ACAT inhibitor) for 48 hours. Nuclei were stained with Hoechst 33342, cholesterol crystals were detected with polarized light, lipid droplets were stained with BODIPY 493/503. Scale bar = 50 μm.

A recent report showed lipid droplets serve as nucleating sites for large intracellular CC in rabbit atherosclerotic lesions[84]. I reasoned that this phenomenon was also possible in hepatocytes. To test this, I treated cells with control media or cholesterol with or without ACAT inhibitor for 48 hours, fixed the cells, and then submitted them to a collaborator for transmission electron microscopy (EM) to examine their sub-cellular architecture. Compared to control, cholesterol treated cells had elevated autophagosome formation as well as exhibited massive void regions within the cytoplasm, indicative of plate-like CC clefts, and these were found next to lipid droplets and autophagosomes (Figure 5.4). These clefts are a classic feature of CC corresponding to empty space in cells that remain after processing for EM with organic solvents[73]. Fascinatingly, there was no detection of CC clefts in cholesterol loaded cells co-treated with Sandoz 58-035 (Figure 5.4). Despite the absence of plate-like CC clefts, autophagosome presence was maintained in co-treated cells, and may be engulfing lipid droplets via lipophagy. This observation was confirmed using fluorescence microscopy and PLM. Cholesterol treated cells exhibited autophagosomes that stain brightly with LysoTracker and are near CCs but are not seen to directly engulf them (Appendix C-A). In contrast, co-treated cells had autophagosomes that appear to be engulfing residual CCs and lipid droplets (Appendix C-A). Moreover, what appears to be a plate-like CC cleft can be observed under polarized light in close association to lipid droplet membranes (Appendix C-B). Other large crystalline structures were observed with bright field microscopy. However, the same structures were not detected under polarized light, nor did they stain with filipin, which detects free cholesterol (Appendix C-C). In fact, while some regions containing CCs stained with filipin, there does not seem to be a clear association between CC formation and filipin staining (Appendix C-C). To our knowledge, we are the first to observe intracellular plate-like CC clefts in hepatocytes. Taken together, our imaging studies reveal that crystallized cholesterol in lipid droplets may nucleate plate-like cholesterol monohydrate crystals, and that ACAT inhibition protects against this process.

A

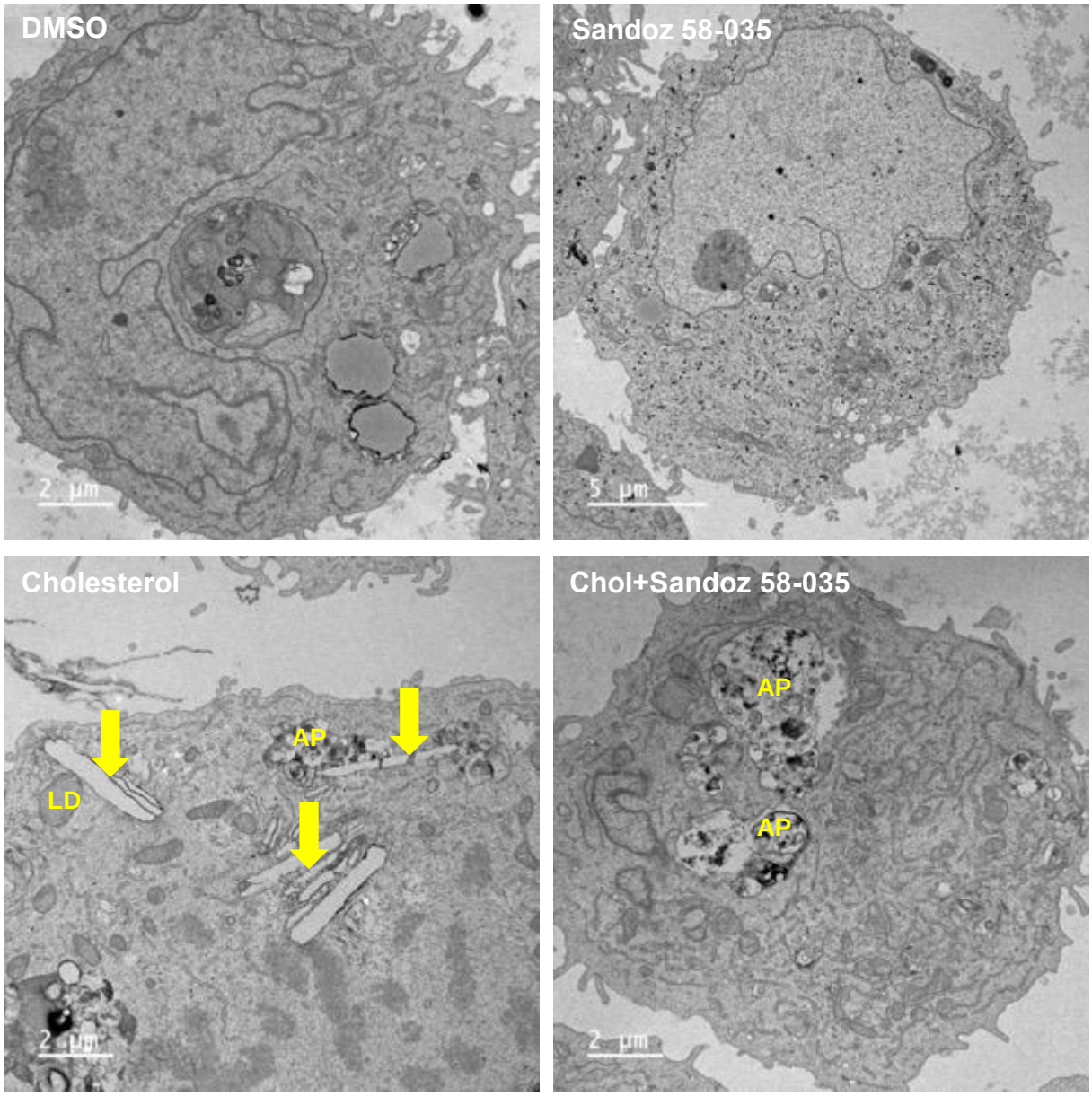

Figure 5.4: Intracellular cholesterol crystal cleft formation in hepatocytes is ameliorated by ACAT inhibition.

(A) Transmission electron microscopy images of representative Hep3B cells treated with or without 200 µM cholesterol and with or without 1 µg/mL Sandoz 58-035 (ACAT inhibitor) for 48 hours. LD = lipid droplet, AP = autophagosome, yellow arrows indicate intracellular plate-like cholesterol crystals. Scale bar length is displayed on each image.

To ensure that our findings with Sandoz 58-035 did not result from unknown off-target effects and because it is a non-selective inhibitor for ACAT1 and ACAT2, we aimed to utilize other methods of reducing ACAT activity and determine which ACAT enzyme may be responsible for mediating CC formation. Given that ACAT1 is generally considered the principal enzyme for generating cholesterol ester that is stored in lipid droplets, we sought ways to target ACAT1. First, we tested the effect of K-604, an ACAT1 selective inhibitor, on cholesterol crystallization in hepatocytes (Figure 5.5A). Cholesterol treatment for 48 hours induced CC formation, while co-treatment with 0.01-1 μM K-604 prevented CC formation (Figure 5.5B), supporting that ACAT1-mediated cholesterol esterification is a critical driver of CC formation.

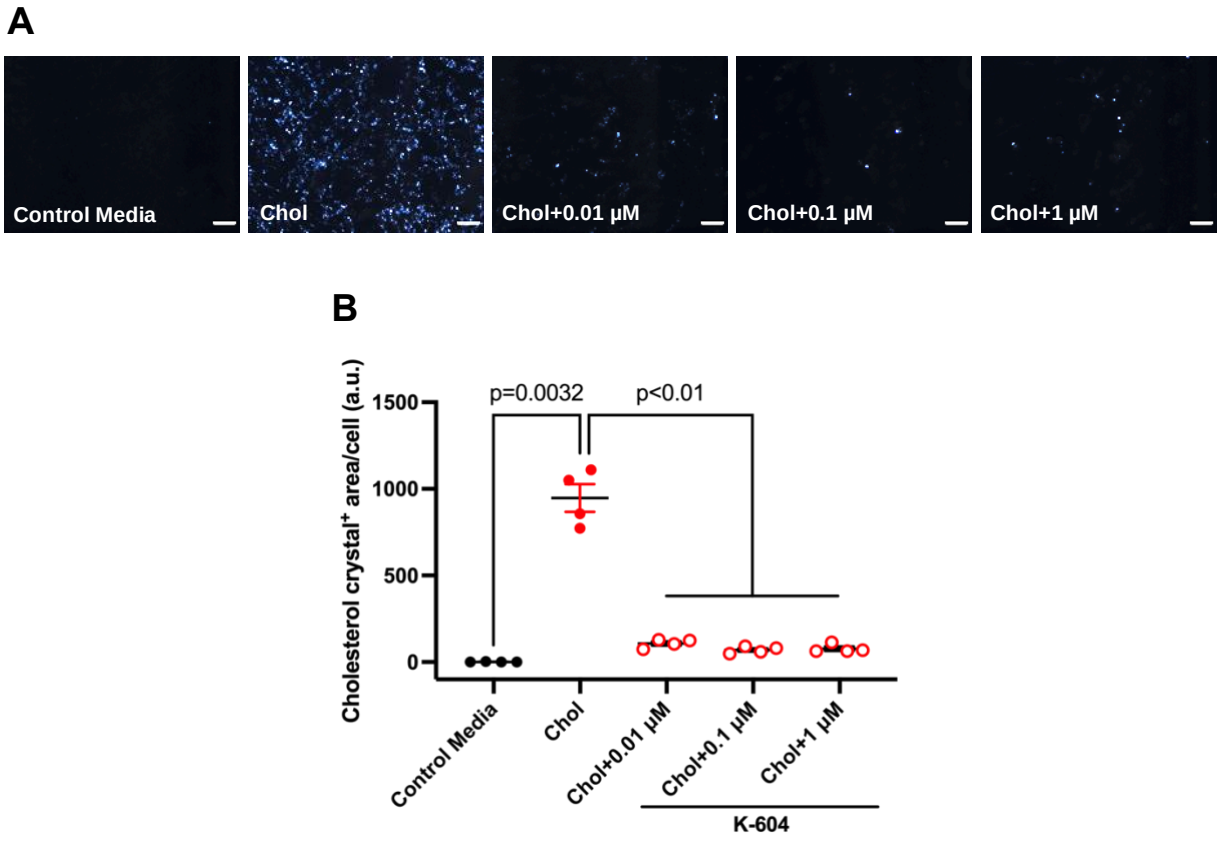

Figure 5.5: Selective ACAT1 inhibition is sufficient to blunt cholesterol crystal formation. (A) Representative polarized light images (20x magnification) of live Hep3B cells treated with control media, 200 μM cholesterol, or 200 μM cholesterol and increasing concentrations of K-604 (selective ACAT1 inhibitor) for 48 hours. (B) Quantification of cholesterol crystal formation in (A) (n=4). p-values in (B) were determined by one-way ANOVA with Dunnett's post-hoc test. Data in (B) are mean ± SEM. Scale bar = 200 μm.

To verify our findings using Sandoz 58-035 and K-604, and to assess the role of SOAT2, we turned to gene deletion as a complimentary loss-of-function approach. We employed clustered regularly interspaced short palindromic repeats (CRISPR)/Cas9 technology to wild-type Hep3B cells that stably express Cas9 protein (Cas9) to generate ACAT1 (gene name *SOAT1*)-deficient ($SOAT1^{KO}$) and ACAT2 (gene name *SOAT2*)-deficient ($SOAT2^{KO}$) Hep3B cells. CRISPR-induced nonsense mutation for *SOAT1* and *SOAT2* to result in truncated loss-of-function mutants was demonstrated by genomic cleavage assay (Appendix D) and genome sequencing of targeted loci for each gene (Appendix E). However, due to lack of quality antibodies, we have not been able to demonstrate ablation of protein. Nevertheless, I proceeded to examine whether $SOAT1^{KO}$ cells or $SOAT2^{KO}$ cells exhibited less CC formation than Cas9 cells following cholesterol treatment. Fascinatingly, cholesterol induced robust CC formation in Cas9 cells, but not in $SOAT1^{KO}$ cells (Figures 5.6A, C). Conversely, $SOAT2^{KO}$ cells had similar induction of CC levels compared to Cas9 cells (Figures 5.6B. D). Despite variable CC formation, there were no genotype or treatment effects on cell death in *SOAT1* or *SOAT2*-deficient cells (Figures 5.6A, B, E, F). These data reveal that SOAT1 is required for CC formation, but SOAT2 is dispensable.

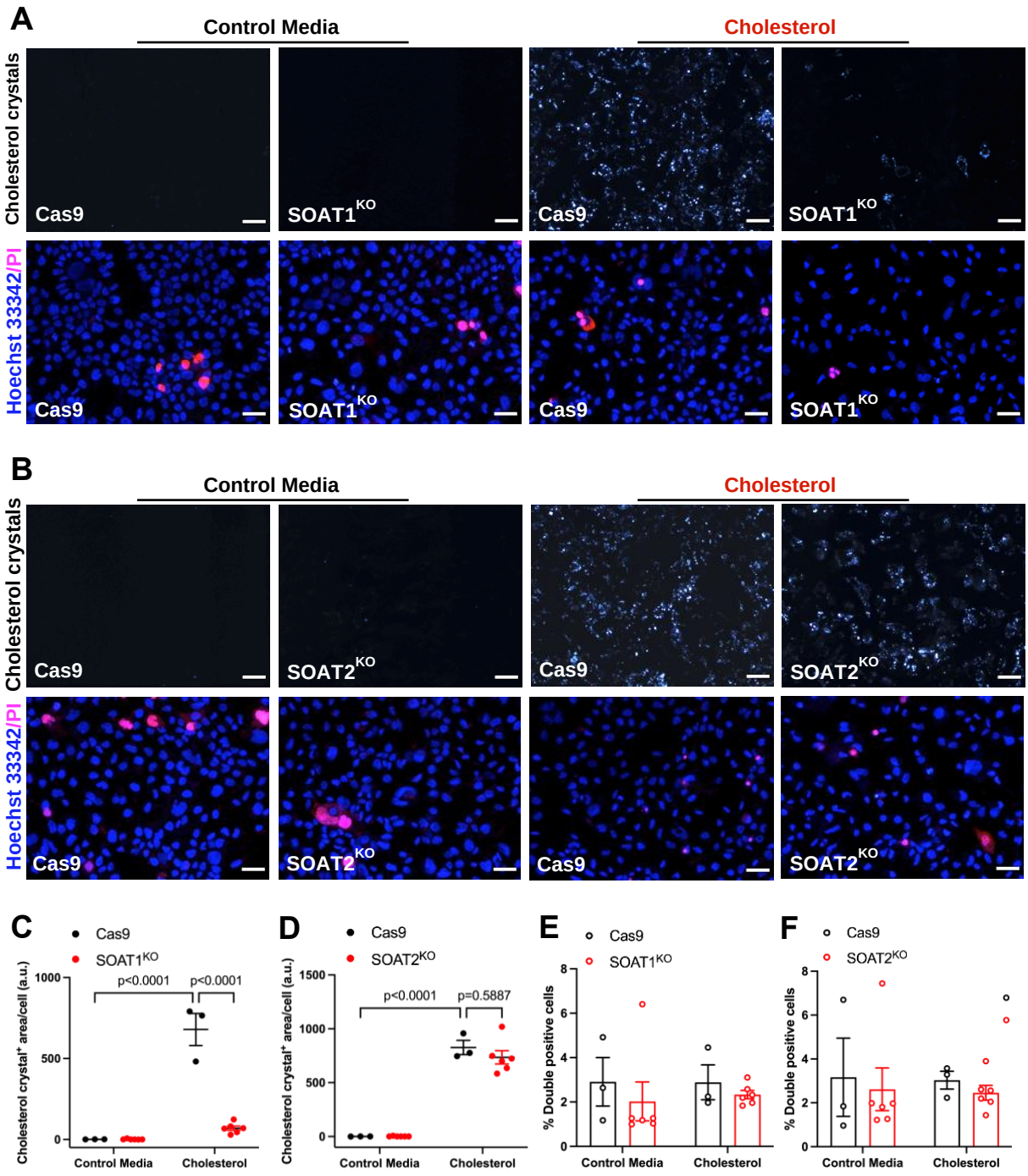

Figure 5.6: *SOAT1*-deficient hepatocytes exhibit reduced cholesterol crystal formation. (A-B) Representative fluorescence (bottom) and polarized light (top) images (20x magnification) of live Hep3B Cas9, SOAT1^{KO}, or SOAT2^{KO} cells treated with or without 200 μM cholesterol for 48 hours. (C-D) Quantification of cholesterol crystal formation in (A-B) (n=3-6). (E-F) Live/dead imaging assay quantification in (A-B) (n=3-6). For all experiments, knockout cell line results were pooled from two independent knockout lines that were infected with gRNAs targeting different regions of the respective gene. p-values in (C-F) were determined by two-way ANOVA with Tukey's post-hoc test. Data in (C-F) are mean ± SEM. Scale bar = 200 μm.

Next, we sought to confirm that deficiency of *SOAT1* would impair lipid droplet expansion and its association with CC. Fluorescence imaging and PLM show expected responses in Cas9 cells treated with cholesterol, consistent with our imaging in wild-type cells (Figure 5.7A [top]). A similar result occurred with SOAT2^{KO} cells (Figure 5.7A [bottom]). In contrast, SOAT1^{KO} cells exhibited an absence of CC and compromised lipid droplet expansion (Figure 5.7A [middle]). Altogether, using multiple imaging modalities as well as pharmacological and genetic methods, our findings clearly show that ACAT1-mediated esterification and subsequent lipid droplet localization is required for CC formation.

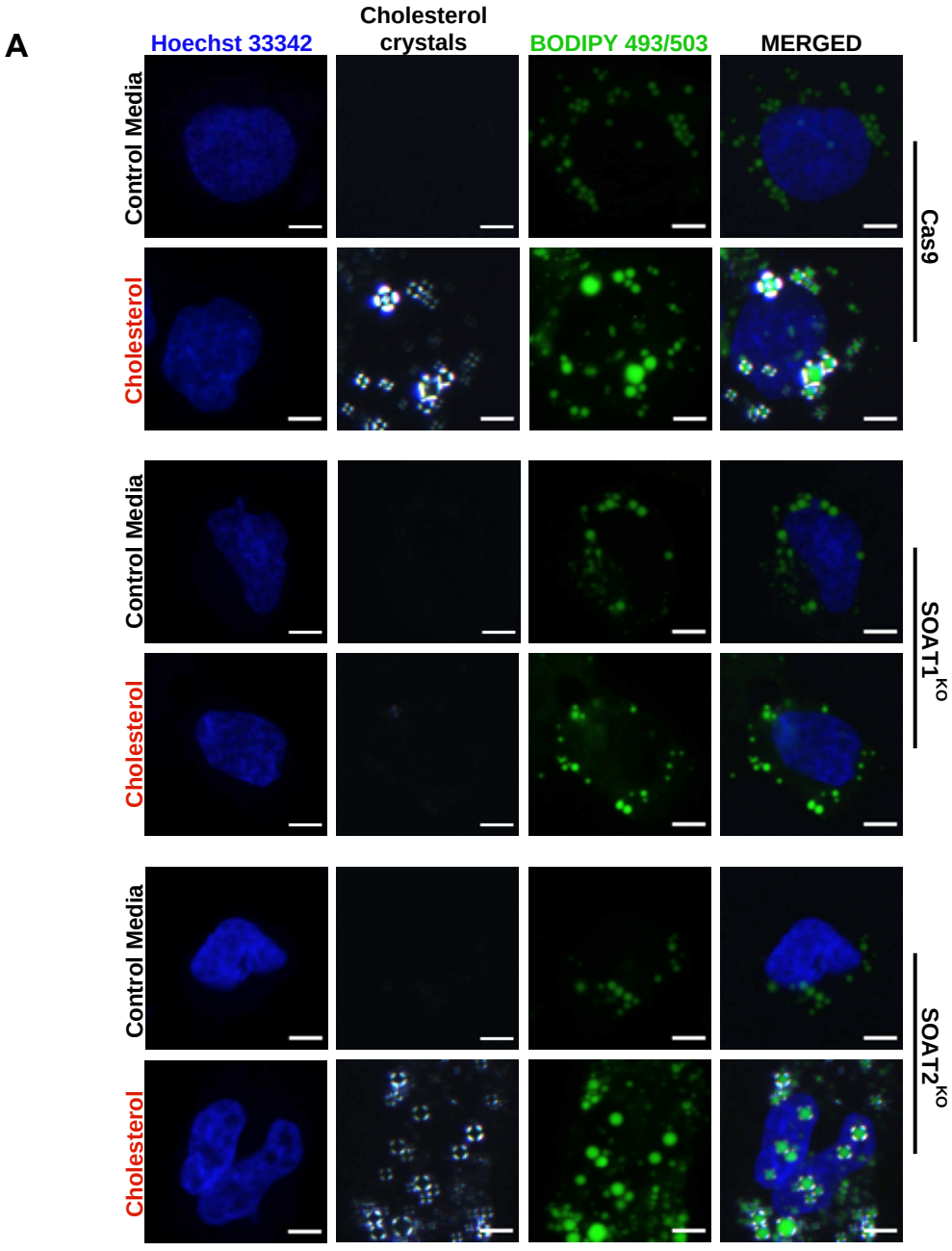

Figure 5.7: *SOAT1*-deficient hepatocytes display altered lipid droplet formation and lack lipid droplet-associated cholesterol crystals.
(A) Representative fluorescence and polarized light images (40x magnification) of live Hep3B Cas9, SOAT1^{KO}, or SOAT2^{KO} cells treated with or without 200 μM cholesterol for 48 hours. Nuclei were stained with Hoechst 33342, cholesterol crystals were detected with polarized light, lipid droplets were stained with BODIPY 493/503. Scale bar = 50 μm.

5.2.2: The contribution of autophagy to cholesterol crystal formation

While inhibiting ACAT likely results in reduced CC formation due to blocking cholesterol esterification, an alternative is that inhibiting ACAT enhances CC solubilization via potentiation of autophagosome activity, which in EM and fluorescence imaging appeared activated in cholesterol treated cells and Sandoz 58-035 co-treated cells (Figure 5.4 and Appendix C). There is precedence for this effect[136]. If this were the case, there should be a potentiated effect on markers of autophagy in co-treated cells. To determine whether Sandoz 58-035 activated autophagy, I performed western blot for LC3B-II, an autophagy marker (Figure 5.8A). Cells incubated with Sandoz 58-035 alone did not have altered LC3B-II level. In contrast, cholesterol markedly increased LC3B-II levels, but this effect was not potentiated by co-treatment with Sandoz 58-035 (Figure 5.8B). Thus, differences in autophagy do not appear to explain differences in CC formation between cholesterol-loaded cells and those co-treated with cholesterol and Sandoz 58-035.

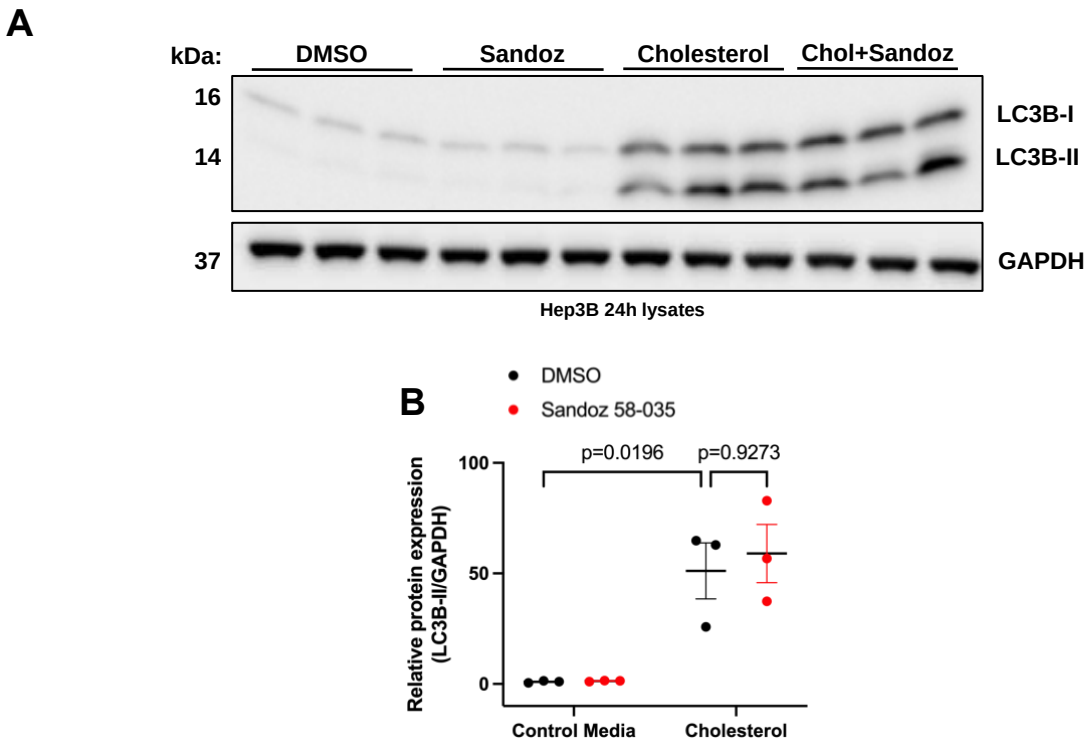

Figure 5.8: Cholesterol accumulation induces autophagy but is not potentiated by ACAT inhibition.
(A) Western blot for autophagy marker LC3B from Hep3B lysates collected at 24 hours. (B) Quantification of LC3B-II protein expression normalized to GAPDH protein expression in (A) and displayed relative to control (n=3). Treatments are consistent with previous experiments. p-values in (B) were determined by two-way ANOVA with Tukey's post-hoc test. Data in (B) are mean ± SEM.

To further test if autophagy may influence CC formation in our model, Hep3B cells were treated with rapamycin, which has been shown to induce autophagy by inhibiting mTORC1[137]. In cholesterol treated cells, rapamycin modestly reduced CC formation (Figure 5.9A, C). Induction of autophagy with the same dose of rapamycin was confirmed by quantifying LC3B-II levels detected via western blot. As expected, rapamycin induced autophagy in cells incubated with control media and cholesterol (Figure 5.9B, D). However, this effect was modest compared to the effect of cholesterol itself. Altogether, differences in autophagy does not appear to underlie the mechanism by which blocking cholesterol esterification reduces CC levels in cholesterol-loaded cellular models.

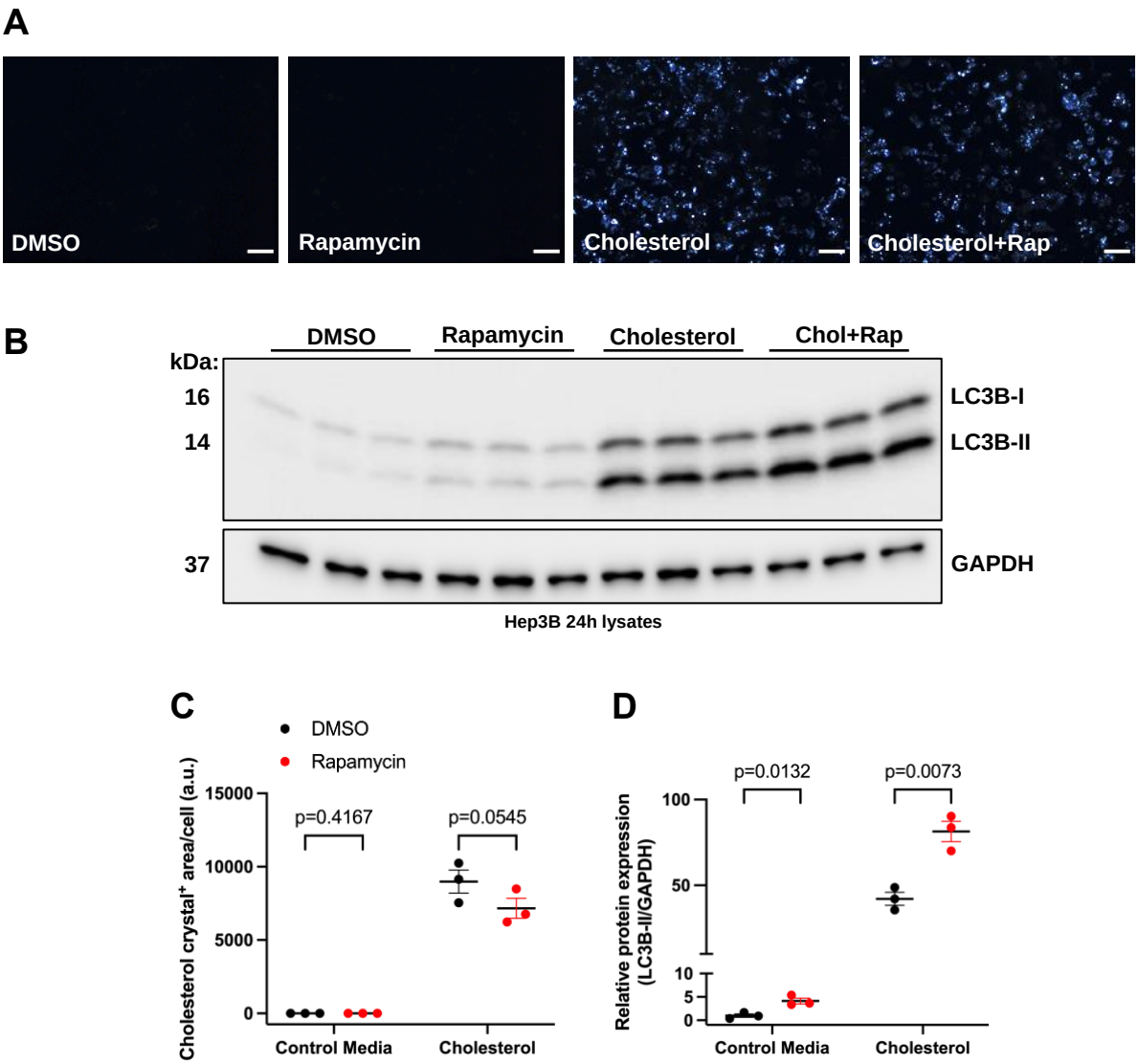

Figure 5.9: Cholesterol crystal formation is slightly affected by autophagy induction.
(A) Representative polarized light images (20x magnification) of live Hep3B cells treated with or without 200 μM cholesterol and with or without 100 nM rapamycin (mTORC1 inhibitor) for 48 hours. (B) Western blot for autophagy marker LC3B from Hep3B lysates collected at 24 hours. (C) Quantification of cholesterol crystal formation in (A) (n=3). (D) Quantification of LC3B-II protein expression normalized to GAPDH protein expression in (B) and displayed relative to control (n=3). p-values in (C-D) were determined by multiple paired t-tests corrected for multiple comparisons. Data in (C-D) are mean ± SEM. Scale bar = 200 μm.

With autophagy excluded as contributing to CC formation, I then examined other factors that could potentially influence crystallization. These included exposing cholesterol loaded cells to tunicamycin to induce ER stress, TNFα to stimulate inflammatory signaling, and U18666a to impair lysosomal cholesterol export. In each case, there was no noticeable effect on CC formation (Appendix A). Similarly, inhibition of cholesterol biosynthesis with Simvastatin, inhibition of cholesterol esterification with K-604, and rapamycin-mediated autophagy induction did not alter the disappearance rate of pre-formed CCs after transitioning to control media (Appendix B).

5.2.3: Evidence that nCEH1 is required for cholesterol crystal formation

Upon further consideration, I realized the results in figures 5.1, 5.4, and 5.6 seem contradictory to current views that cellular cholesterol crystallization is caused by FC accumulation. Yet, we show that inhibiting ACAT, which increases FC accumulation (Figure 5.2A-B), prevents CC formation. We reconciled this discrepancy by theorizing that localized FC accumulation at lipid droplets is critical for CC formation, which is prevented by ACAT inhibition, despite FC levels rising in all other cellular environments. In this case, there may be a factor working in tandem with ACAT1 to trigger CC formation. Such a factor must be able to liberate FC from CE pools stored within lipid droplets. With the recent discovery that nCEH1 is a CE hydrolase in macrophages, we deemed this enzyme an interesting target to consider, particularly since it is not known which enzyme mediates this process in liver. So, we investigated whether lipid droplet CE hydrolysis by nCEH1 is required for CC formation. To test this, CC formation was assessed in control and cholesterol treated Hep3B cells co-treated with or without nCEH1 inhibitor, JW480 (Figure 5.10A). Interestingly, CC formation induced by cholesterol loading was significantly impaired in cells co-treated with cholesterol and JW480 (Figure 5.10B), indicating that nCEH1 may be the second factor required to de-esterify lipid droplet CE to FC, perpetuating the effect of ACAT1 to drive CC formation.

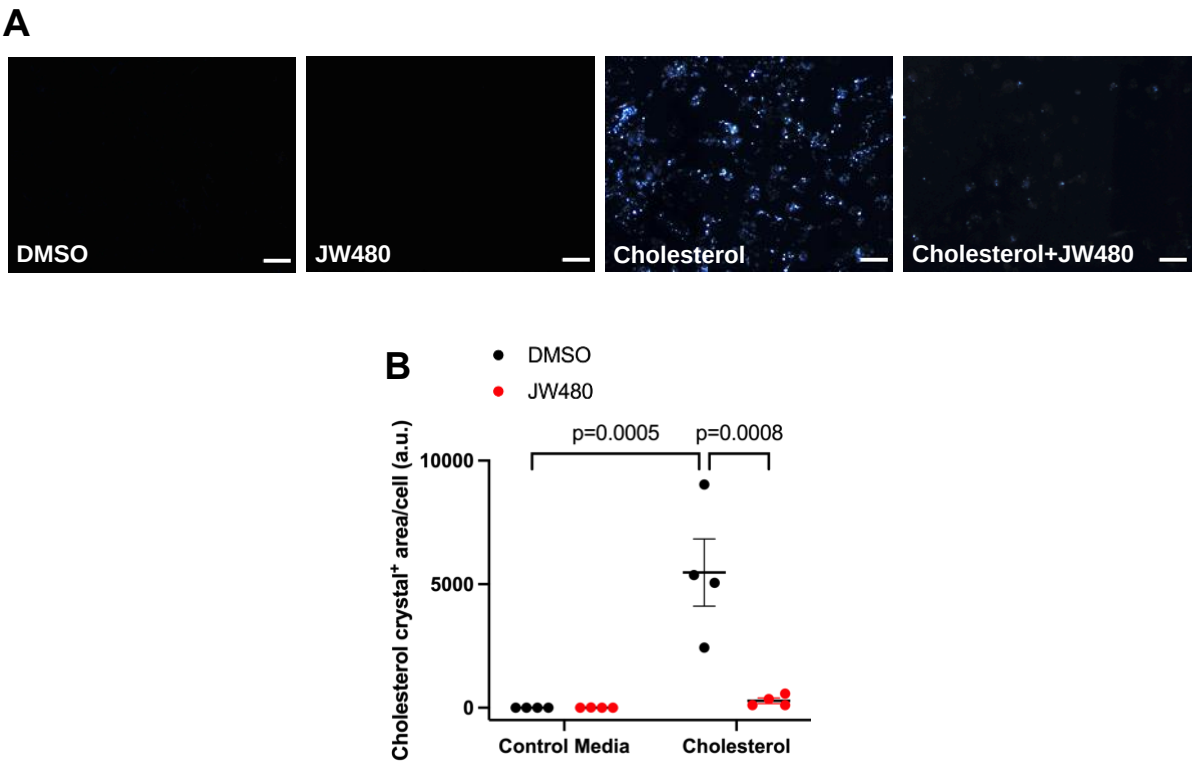

Figure 5.10: Lipid droplet cholesterol ester hydrolysis is required for cholesterol crystal formation.
(A) Representative polarized light images (20x magnification) of live Hep3B cells treated with or without 200 μM cholesterol and with or without 10 μM JW480 (nCEH1 inhibitor) for 48 hours. (B) Quantification of cholesterol crystal formation in (A) (n=4). p-values in (B) were determined by two-way ANOVA with Tukey's post-hoc test. Data in (B) are mean ± SEM. Scale bar = 200 μm.

Next, I wanted to confirm that nCEH1 inhibition with JW480 would also prevent the association of CCs at lipid droplets in a similar fashion to ACAT1 inhibition. Indeed, CCs that were associated with the lipid droplet exterior in cholesterol loaded hepatocytes were absent in those co-treated with cholesterol and JW480 (Figure 5.11A). Consistent with the known function of nCEH1 as a CE hydrolase, the lipid droplets of co-treated cells appear to be enlarged, indicating potential CE accumulation. Also, what appears to be lipid droplet budding from the large lipid droplet can be observed in co-treated cells, which may be a mechanism to defend against lipid droplet overexpansion (Figure 5.11A).

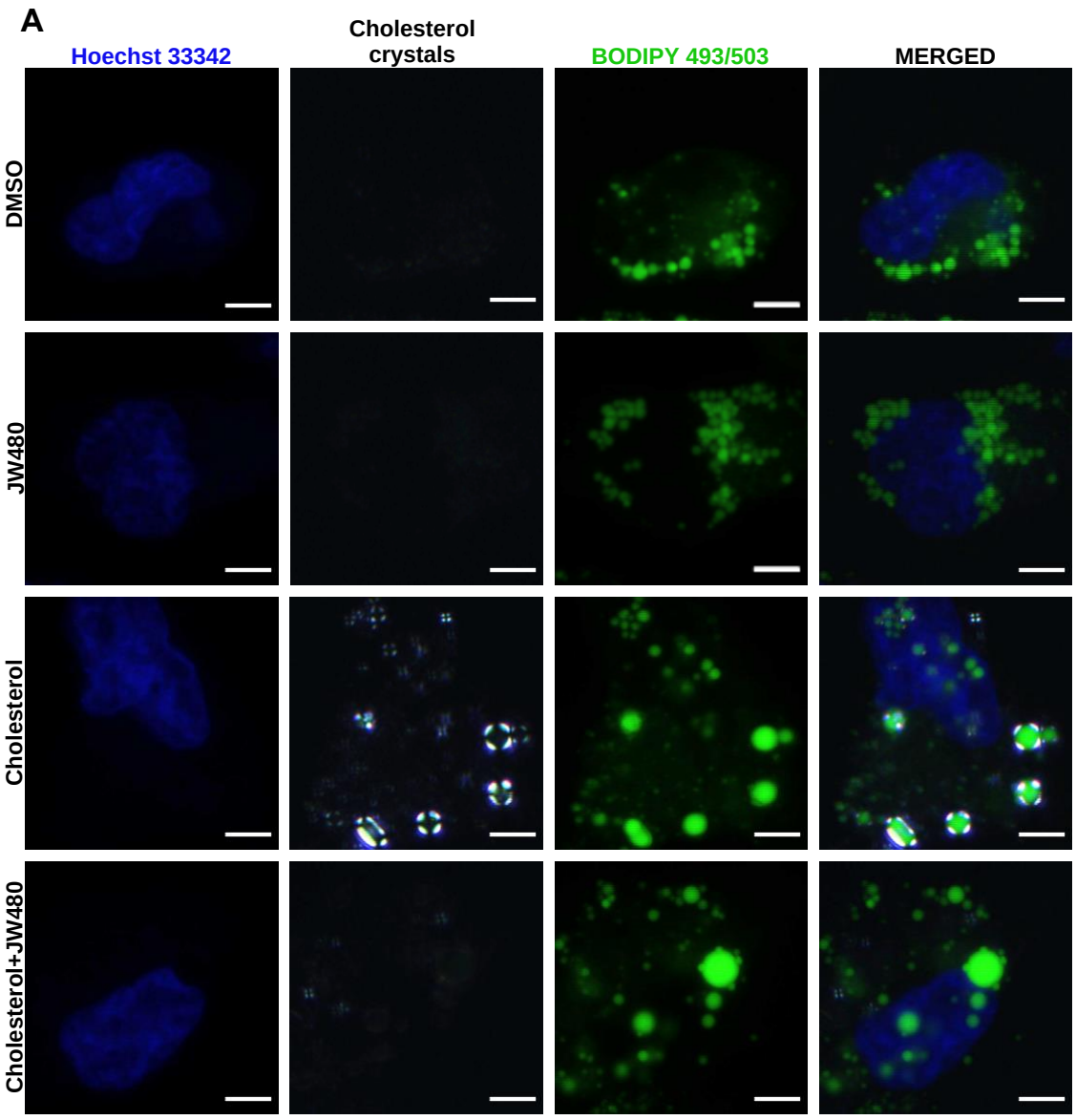

Figure 5.11: nCEH1 inhibition prevents the formation of lipid droplet-associated cholesterol crystals.
(A) Representative fluorescence and polarized light images (40x magnification) of live Hep3B cells treated with or without 200 μM cholesterol and with or without 10 μM JW480 (nCEH1 inhibitor) for 48 hours. Nuclei were stained with Hoechst 33342, cholesterol crystals were detected with polarized light, lipid droplets were stained with BODIPY 493/503. Scale bar = 50 μm.

5.2.4: Replication of results from hepatocytes in macrophages

Based on similar observations in Hep3B hepatocytes and RAW 264.7 macrophages in regard to CC localization, I considered that cholesterol esterification by ACAT may also drive CC formation in macrophages. So, I tested the effect of ACAT inhibition with Sandoz 58-035 on acLDL-loaded macrophages (Figure 5.12A), which is an alternative method of inducing cholesterol accumulation. As with Hep3B cells, co-treatment of RAW 264.7 cells with acLDL and Sandoz 58-035 completely blunted CC formation that was induced when cells were treated with acLDL alone (Figure 5.12B). To ensure that this result was not specific to acLDL, we also loaded RAW 264.7 cells with cholesterol and observed similar effects, albeit at a lower cholesterol dose (100 μM) (Appendix F).

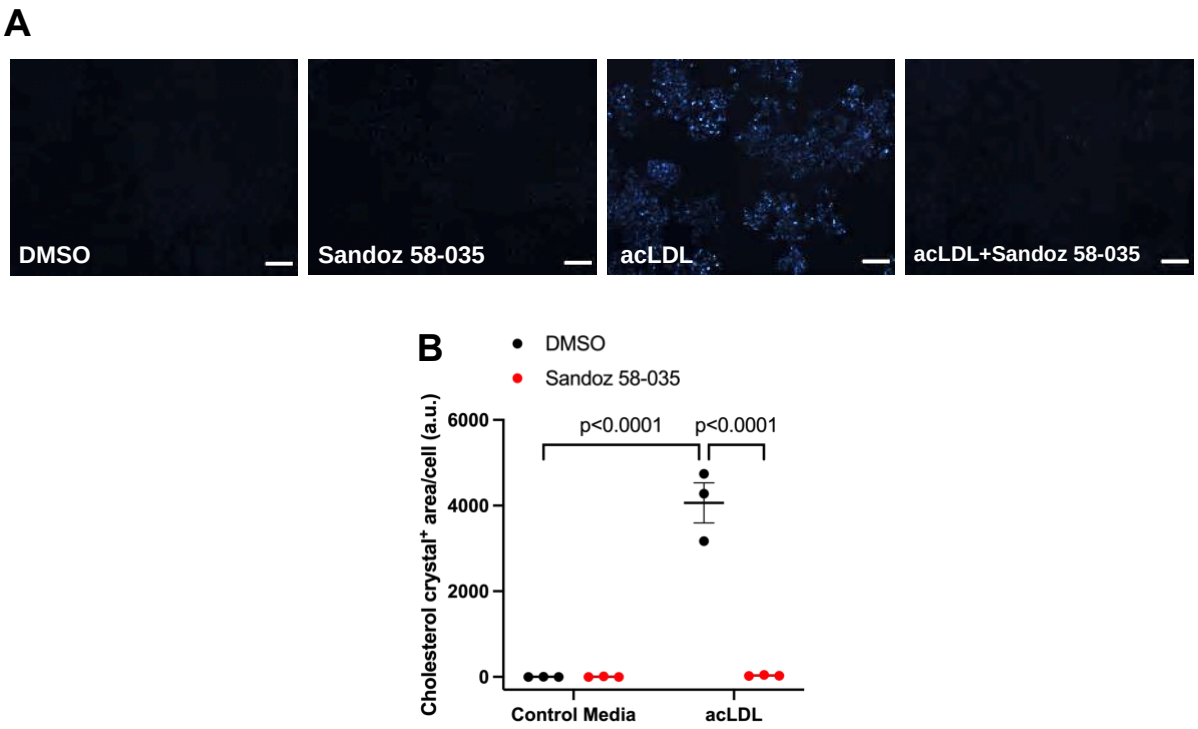

Figure 5.12: ACAT inhibition prevents acLDL-induced cholesterol crystal formation in macrophages.

(A) Representative polarized light images (20x magnification) of live RAW 264.7 cells treated with or without 50 μg/mL acLDL and with or without 1 μg/mL Sandoz 58-035 (ACAT inhibitor) for 48 hours. (B) Quantification of cholesterol crystal formation in (A) (n=3). p-values in (B) were determined by two-way ANOVA with Tukey's post-hoc test. Data in (B) are mean ± SEM. Scale bar = 200 μm.

If the mechanisms contributing to CC formation are conserved between cell types, it would be expected that nCEH1 is also essential for this process in macrophages. Thus, we tested whether JW480 blunted CC formation in RAW 264.7 cells (Figure 5.13A). In contrast to Hep3B hepatocytes, nCEH1 inhibition only reduced CC formation by approximately 50% in RAW 264.7 macrophages (Figure 5.13B). These differences may be explained by variable roles and contribution of nCEH1 to CE hydrolase activity in differing cell types. Altogether, our experiments performed on macrophages predominantly mirror the effects seen in hepatocytes, supporting the notion that ACAT1 and nCEH1 play direct roles in CC formation in the two different cell types. Since similar results were seen in both cells, our findings may be generalizable to cholesterol crystallization that is prominent in NASH and atherosclerosis in humans.

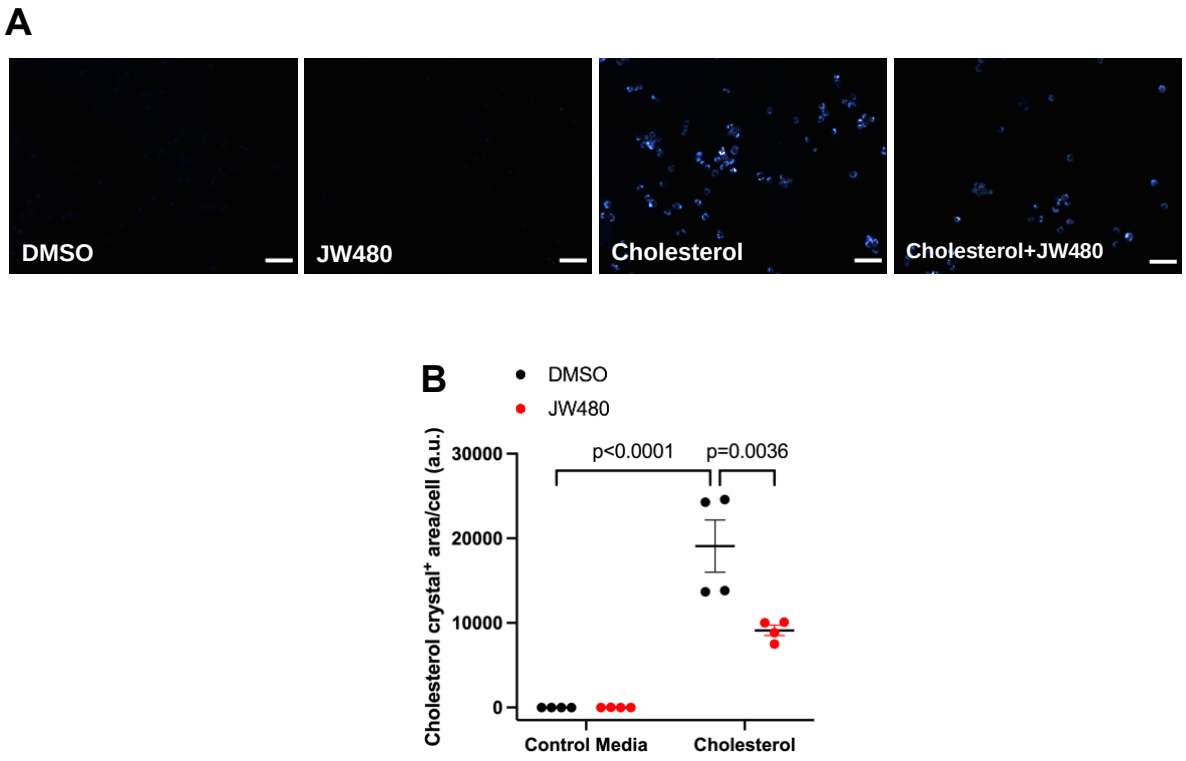

Figure 5.13: nCEH1 inhibition partially reduces cholesterol crystal formation in cholesterol loaded macrophages.
(A) Representative polarized light images (20x magnification) of live RAW 264.7 cells treated with or without 200 μM cholesterol and with or without 10 μM JW480 (nCEH1 inhibitor) for 24 hours. (B) Quantification of cholesterol crystal formation in (A) (n=4). p-values in (B) were determined by two-way ANOVA with Tukey's post-hoc test. Data in (B) are mean ± SEM. Scale bar = 200 μm.

In summary, the third objective of this thesis has successfully been met in this chapter. I explored the role of cholesterol ester metabolism in CC formation and report the exciting discovery that cholesterol esterification and subsequent lipid droplet CE hydrolysis both appear to be required for cholesterol crystallization.

5.3: Conclusion and proposed mechanism

Altogether, my thesis provides evidence that cholesterol esterification, subsequent lipid droplet localization, and CE hydrolysis are critical steps in the formation of CCs in hepatocytes and macrophages. Using pharmacological and genetic techniques to manipulate these factors, I assessed their effect on cholesterol crystallization. Based on the results, I propose a mechanism wherein ACAT1 and nCEH1 operate in a sequential fashion to drive intracellular CC formation (Figure 5.14).

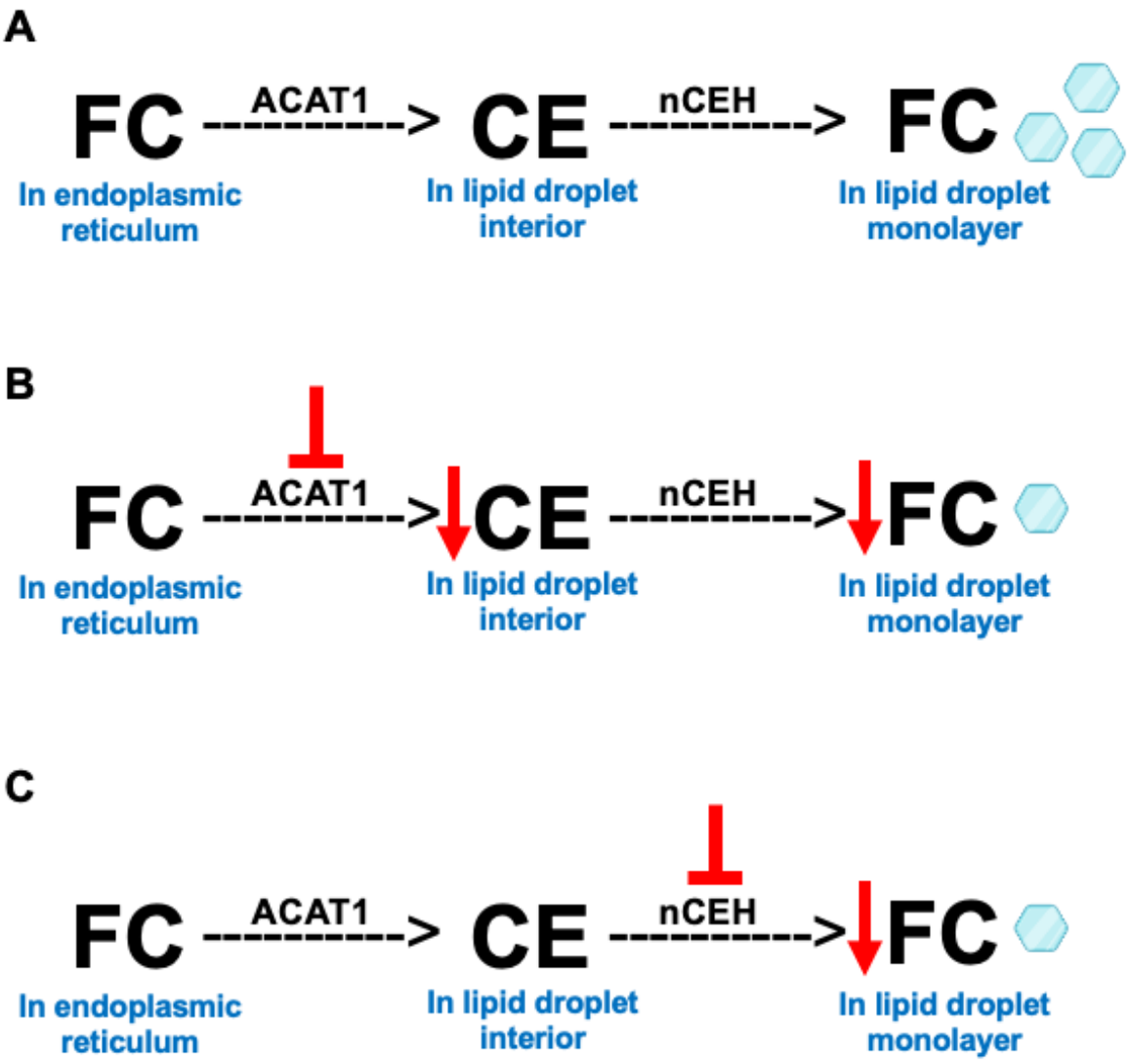

Figure 5.14: Proposed model for intracellular cholesterol crystal formation.
(A) In wild-type cells, cholesterol loading leads to FC accumulation in the ER. As FC levels rise, ACAT1 catalyzes FC conversion to CE which are concentrated in lipid droplets. Subsequent hydrolysis of lipid droplet CE to FC is catalyzed by nCEH promoting FC accumulation within the lipid droplet monolayer, leading to consequent cholesterol crystallization. (B) Pharmacological or genetic targeting of ACAT1 prevents the conversion of FC to CE and subsequent lipid droplet storage, presumably diminishing the pool of CE available to be hydrolyzed by nCEH. Therefore, reduced FC accumulation in the lipid droplet monolayer blunts CC formation. (C) Directly targeting nCEH prevents CE hydrolysis and conversion to FC, thereby reducing FC accumulation in the lipid droplet monolayer and consequent cholesterol crystallization.

Chapter 6 – Discussion

The aim of this thesis was to generate cell culture models of cholesterol crystallization in human hepatocytes and mouse macrophages in order to identify and investigate factors that modulate intracellular CC formation. I hypothesized that enzymes that mediate cholesterol esterification prior to its storage in lipid droplets and enzymes that de-esterify lipid droplet CE are required for intracellular CC formation. Using multiple imaging methods and tools to manipulate cholesterol esterification and de-esterification, we provide evidence supporting this hypothesis. Based on this evidence, I propose that cholesterol esterification by ACAT1 and CE de-esterification by nCEH1 work in series to drive FC accumulation at the lipid droplet surface and subsequent intracellular CC formation/nucleation.

6.1: Cholesterol crystallization in hepatocytes and NASH

6.1.1: General discussion

Since the structure of cholesterol is mainly hydrophobic, it must be complexed to a carrier in order to be delivered to cell membranes. Our studies employed use of cholesterol complexed to MβCD, a cyclic oligosaccharide. We saw a dose- and time-dependent increase in CC formation with cholesterol-MβCD loading in hepatocytes. Similarly, Rong *et al.* also loaded SMCs with cholesterol-MβCD for 48 hours which led to foam cell formation dependent on dose, and was blocked by ACAT inhibition[138]. Based on these observations, it is likely that cholesterol loading by this method leads to FC accumulation within the ER, which has been previously reported[132]. Other methods of loading hepatocytes have been described using LDL and oleic acid treatments for a total of 20 days[20]. This group also reported lipid droplet-associated CC formation using this method. However, it was concluded that cholesterol loading was ER-independent and that lysosome-derived cholesterol drove CC formation through direct membrane contact sites with lipid droplets[20]. This may imply that cholesterol crystallization was not dependent on ACAT1 in this model. However, there are two plausible alternative explanations for these findings. One group was able to detect ACAT1 in ER-derived vesicles that were associated with late endosomes and lysosomes in cholesterol loaded macrophages[139], suggesting that ACAT1 may in fact participate

in lysosome-derived cholesterol esterification outside of the ER. Since cholesterol loading was performed over the course of 20 days, it may also be the case that ER cholesterol was chronically elevated and further cholesterol uptake was shuttled away to prevent ER cholesterol accumulation. Further experiments involving hepatocyte incubation with LDL should be attempted to determine if ACAT1 is also required for CC formation under these conditions.

Determining the composition of the CC detected in our studies is one aspect of this thesis that has not been explored, despite being a critical question. Early studies determined that cholesterol monohydrate was the substance composing cholesterol crystals[37,70,71]. This contributed to the dogma that FC accumulation stimulates CC formation, and there is copious evidence supporting this notion. On the contrary, a group of studies argue that CE promote the formation of liquid-crystalline domains within the lipid droplet interior[140–144]. This ideology was primed by studies in yeast, which reported that CE form distinct ordered shells directly below the phospholipid monolayer, while TG are randomly packed in the lipid droplet interior[145]. Later, polarized third harmonic generation microscopy revealed that lipid droplets with an increased CE/TG ratio displayed greater lipid droplet ordering that may exhibit a crystalline state[140]. These observations prompted other groups to manipulate the CE/TG ratio by depriving cells of glucose to induce lipolysis, where they report that cells under starvation conditions exhibited crystalline lipid droplets and ordered CE shells similar to those identified previously in yeast[141]. Further supporting evidence demonstrated that increased CE/TG ratio drives the formation of liquid-crystalline domains within lipid droplets, and that decreased temperatures favor liquid crystal formation[142]. Of note, this group also identified lipid droplet-associated liquid crystals/cholesterol crystals that reflect our imaging in Figure 4.6. In addition, HeLa cells treated with cholesterol-MβCD complex, but not oleic acid, exhibited birefringent lipid droplets. They also observed liquid crystal formation in yeast upon TG depletion[143]. Another recent article used an identical dose of cholesterol-MβCD to our studies and reported that liquid-crystalline phases appear at physiological temperatures when the CE/TG ratio exceeds 9/1, and this threshold decreases with temperature[144]. Additionally, they proved that seipin participates in CE-rich lipid droplet formation, a role which was only previously described for TG-rich droplets. Based on these studies, it is possible that our PLM imaging detects liquid crystals composed of CE.

While the evidence presented above is appealing, it is possible that lipid droplet-associated CC detected in our experiments and in those described above may be composed of FC rather than CE. The presence of a CE hydrolase functioning at the lipid droplet is, in my view, a more likely factor underlying the formation of crystallized lipid droplets, yet this was not addressed in the studies described above. In this thesis, I investigated an enzyme, nCEH1, that may fulfill this role. Logically, as the ratio of CE/TG increases, nCEH1 activity could also increase proportionally to buffer CE accumulation, consequently causing CC formation due to excessive FC accumulation within the monolayer. For reference, adipocytes primarily store TG within their lipid droplets and have low ACAT expression and activity. However, adipocyte ACAT1 overexpression resulted in the accumulation of FC at the lipid droplet monolayer which appears to be contradictory since ACAT1 generates CE[146]. Again, the presence of enzymes that function to de-esterify CE at the lipid droplet are a likely explanation as to why ACAT1 overexpression led to FC accumulation at the monolayer in this study. In support of this notion, Ioannou *et al*. used osmium tetroxide staining to demonstrate that CC form at the lipid droplet monolayer and not in the interior in hepatocytes[24]. Another area where cholesterol can crystalize is in bile. A review summarizing crystallization in bile posits that liquid crystals and plate-like crystals (composed of unesterified cholesterol monohydrate) exist on a continuum, where the plate-like crystals are more thermodynamically stable and exhibit stronger birefringence[147]. It is difficult to imagine that these two structures are composed of different substances while still existing on a continuum, and the perception that de-esterification drives CC formation is plausible. Taken together, CE liquid crystals might drive intracellular CC formation which may be facilitated by cholesterol de-esterification. Nonetheless, it remains ambiguous as to whether crystallized lipid droplets contain FC, CE, or both. Further biochemical evaluation of the crystalline material in lipid droplets is required to distinguish these characteristics.

Based on our findings, manipulating the lipid content of lipid droplets may be an effective strategy to modulate CC formation. An interesting lipid family to consider are omega-3 fatty acids, specifically eicosapentaenoic acid (EPA) and docosahexaenoic acid (DHA). EPA and DHA have been reported to be protective in atherosclerosis due to their immunomodulatory effects[148], and high dose EPA was found to reduce ischemic events and cardiovascular death in a recent clinical trial[149]. EPA likely mediated these effects by ameliorating lipid oxidation and enhancing normal membrane cholesterol distribution[14]. In contrast, DHA exhibits a higher degree of unsaturation

compared to EPA and may be more effective at increasing membrane fluidity[14]. Optimistically, these lipids may be able to reduce 2D cholesterol microdomain formation in bilayers, increasing the ability of the membrane to carry cholesterol. Intriguingly, DHA was found to inhibit ACAT1 in breast epithelial cells by acting as a poor substrate and reduced CE formation induced by OA[150]. Since excessive cholesterol esterification and crystallization is present in both atherosclerosis and NASH, DHA may have the potential to protect against both features of cholesterol dysregulation. In addition, fatty acid/bile acid conjugates have been found to dissolve pre-existing CC in bile, and prevent gallstone formation[151]. Ioannou has proposed that lipid droplets are organelles that may be particularly susceptible to crystallization due to their lipid monolayer[20]. Indeed, there appears to be fundamental differences between membrane bilayers and monolayers. FC seems to play different roles in membrane tension depending on where it is situated, such as the ER (bilayer) or lipid droplet (monolayer). In bilayers, FC favours hydrophilic pore closing while in monolayers favours hydrophobic pore opening[61]. Moreover, lipid droplet monolayers have been found to contain more phosphatidylcholine (PC) and less sphingomyelin compared to ER bilayers[152]. Interestingly, there have been no reports of CC presence in the ER, though electron microscopy studies are needed to confirm this. These studies support that incorporation of diverse lipids into cholesterol-rich membrane domains could theoretically solubilize these domains and prevent the generation of crystalline material.

Atherosclerosis studies have demonstrated that plate-like CC are present in close association with cytoplasmic lipid droplets,[65,84,85]. Others have shown support for the idea that lipid droplets may provide suitable sites for the nucleation of 3D plate-like CC[80,124]. Similarly, our EM experiment clearly shows clefts of intracellular CC formation in cholesterol loaded hepatocytes that may have nucleated from lipid droplets. To our knowledge, there has been no previous reports identifying 3D plate-like crystals in hepatocytes or in the context of NASH. Additionally, the presence of autophagosomes near plate-like CC might suggest that autophagy is playing a role in the degradation of crystalline material within the cell. Indeed, autophagy is known to be dysfunctional in atherosclerosis, is linked to inflammasome activation[153], and is dysregulated in fatty liver disease[154]. Moreover, dysregulated hepatocyte lipophagy is quickly becoming an attractive area of research in the context of NASH and HCC[34]. Ho-Tin-Noé *et al*. studied CC formation in SMC and found that cholesterol esterification and autophagy were both protective against crystal formation[155]. However, there are fundamental differences in their methodology

compared to ours. Notably, they loaded SMC with aggregated LDL to induce CC formation, then treated with ACAT inhibitor alone for five days. They reported that crystallization was reduced, but this could be attributed to removal of cholesterol in the media, which we have shown can decrease crystallization. In other words, their experiment may be a better measure of crystal resolution than crystal formation. In comparison, we found that autophagy induction only had a modest effect on CC formation, although the presence of autophagosomes near crystalline material suggests that autophagy may contribute to crystal solubilization. Interestingly, they also demonstrated that ACAT1 and nCEH1 gene expression was induced in the intima of aortic segments bearing fatty streaks and fibrolipidic lesions, compared to the media. Further investigation on the role of autophagy in CC solubilization is warranted.

6.1.2: Targeting the liver to treat heart disease

NASH and cardiovascular disease (CVD) share similar risk factors and some groups have proposed a role for heart-liver crosstalk in metabolic disease pathogenesis[156]. In fact, CVD is known to be a leading cause of death in NASH patients[156]. Therapies that simultaneously treat the heart and liver may be attractive options for a broader approach to treating metabolic disease. Fundamentally, the macrophage (heart) and hepatocyte (liver) possess different machinery to handle cholesterol excess. Macrophages rely exclusively on cholesterol efflux and reverse cholesterol transport back to the liver to defend against cholesterol accumulation, while the liver has the ability to excrete cholesterol into bile or package it into lipoproteins to be delivered to other organs and steroidogenic tissues[157]. Since the liver appears to be better equipped to handle cholesterol flux, manipulating liver cholesterol metabolism may be a better option to treat heart disease than targeting the heart itself. These thoughts are based on early preclinical and clinical studies attempting to reduce foam cell formation in atherosclerosis. For example, Delsing *et al.* determined that Avasimibe reduced plasma cholesterol that was attributed to decreased intestinal cholesterol absorption and total ApoB levels, both of which are ACAT2-specific effects[87]. These findings were also confirmed in pigs where Avasimibe blunted ApoB-containing lipoprotein secretion[158]. There is a seeming disconnect between preclinical studies using pharmacologic versus genetic methods to target ACAT1. Almost exclusively, whole body or macrophage ACAT1 deficiency was ineffective[22,102,103], but pharmacologic ACAT1 and ACAT2 inhibition was protective against atherosclerosis[87,99–101]. Not only does this suggest that blocking macrophage

ACAT1 is detrimental due to apparent FC toxicity, but also that nonselective ACAT inhibition may have had protective hepatic effects.

As expected, whole body ACAT2 deficiency was found to be protective against atherosclerosis based on reductions in ACAT2-derived CE and altered VLDL composition that was less atherogenic, instigating a role for a liver enzyme in atherosclerosis[118]. To support this possibility, antisense oligonucleotides were developed specifically targeting hepatic ACAT2 and conferred atheroprotection[159,160], which was mediated in part by non-biliary fecal sterol loss via transintestinal cholesterol efflux[161,162]. Furthermore, pharmacological inhibition of ACAT2 in hyperlipidemic mouse models was found to be anti-atherogenic[163–165]. Evidence of success in human clinical trials has not yet been demonstrated. Nonetheless, the liver emerges as a fascinating therapeutic target in atherosclerosis by virtue of its ability to shuttle excess cholesterol into the feces, something which macrophages cannot do. Lessons learned from the above atherosclerosis studies may also be applied in the context of NASH. Whole body ACAT2 deficiency or knockdown was reported to protect mice from hepatic steatosis, likely by reducing hepatic TG accumulation to compensate for the lack of cholesterol esterification via ACAT2[166]. Also, treatment of rats with Avasimibe increased bile acid synthesis via induction of CYP7A1[167]. Since the liver is a central regulator of cholesterol homeostasis, manipulation of hepatic cholesterol metabolism may be the most effective strategy to treat metabolic disease driven by cholesterol dysregulation. Additionally, the ability of liver to excrete cholesterol into feces provides a mechanism to rid the body of excess cholesterol rather than attempting to alter cholesterol storage.

6.1.3: Potential of targeting ACAT in cancer

The most advanced stage of fatty liver disease is HCC, and progression from NASH to HCC involves multiple immunometabolic factors[8]. In a similar mechanism to atherosclerosis, the storage of excess cholesterol within hepatocyte lipid droplets is facilitated by SOAT1. Thus, targeting SOAT1 may be an attractive therapy for fatty liver disease treatment to prevent cholesterol accumulation associated with the progression of NASH to HCC. Indeed, a fascinating report utilizing proteomics has identified SOAT1 as a potential biomarker for HCC, as it was found to have the highest risk score for HCC mortality prognosis[168,169]. Other studies have identified SOAT1 as a target in cancer immunotherapy as a result of the antitumor effects induced by Avasimibe in promoting CD8+ T-cell activation to supress tumor growth[114,170,171]. Preclinical

studies have established that *SOAT1* is overexpressed in diethylnitrosamine-induced HCC and that inhibition of SOAT1 with Avasimibe suppressed HCC tumor growth[172]. Moreover, hepatocarcinogenesis was found to be exacerbated by tumor suppressor P53 deficiency which conferred dysregulated *SOAT1* activity in HCC, but was ameliorated by Avasimibe administration in mice[173]. Due to a lack of available drugs to target SOAT1 in HCC, Wang *et al.* performed a high-throughput drug screen and identified nilotinib as a potential anti-HCC agent[174]. This high affinity ligand for SOAT1 effectively reduced tumor volume in xenograft models and led to concomitant reprogramming of cholesterol metabolism in tumor cells and enhanced CD8+ T-cell function. Remarkably, nilotinib enhanced bile acid production presumably resulting from decreased cholesterol esterification, underscoring the impression that promoting cholesterol recycling into bile and fecal excretion may be effective in NASH. Downregulation of nCEH1 was coupled to reduced esterification via nilotinib, suggesting that SOAT1 and nCEH1 may be functionally linked, fitting the hypothesis we have proposed. Our strong evidence that SOAT1 drives CC formation in hepatocytes may also explain the efficacy of inhibiting esterification in the context of HCC. However, whether cholesterol crystallization actively contributes to HCC development remains to be explored experimentally.

Besides HCC, various other cancers are also characterized by excessive cholesterol esterification. Glioblastoma is another type of cancer in which high *SOAT1* expression and lipid droplet formation are characteristic[175]. Avasimibe administration or *SOAT1* knockdown resulted in suppressed glioblastoma growth[175], as well as with a SOAT1-specific inhibitor *in v*itro[176]. Additionally, *SOAT1* was found to be highly expressed in clinical colon cancer tissues and *SOAT1* knockdown or Avasimibe suppressed cancer cell viability[177]. Enhanced esterification via SOAT1 was also found promote colorectal tumorigenesis in mice[178]. Recently, elevated *SOAT1* expression was reported to be strongly associated with high risk prostate cancer in humans[179], and *SOAT1* knockdown was protective in prostate cancer cells[180]. Outside the realm of cancer, SOAT inhibition has also been proposed to be an effective therapy for Alzheimer's disease[181].

6.1.4: Role of nCEH1 in cancer

The first link between nCEH1 and cancer was made in a chemical proteomics study on human breast and melanoma cancer lines, where high nCEH1 activity positively correlated with cancer cell invasiveness[182]. Activity-based proteomics and metabolomics techniques were applied

to characterize the novel role of nCEH1 in cancer, which was reported to function by hydrolyzing 2-acetyl monoalkylglycerol to monoalkylglycerol ether (MAGE) in cancer cells[183]. Cravatt and colleagues later developed a specific inhibitor and an shRNA probe targeting nCEH1, and demonstrated reduced MAGE and impaired tumorigenesis of prostate cancer cells *in vitro*[184]. Subsequent studies determined that nCEH1 plays a role in platelet function and thrombosis by regulating ether lipid metabolism[185]. Furthermore, groups using quantitative proteomics[186], gene transcription data[187], and meta-analysis[188] have identified nCEH1 as a potential gastric and pancreatic cancer biomarker. Given the extensive involvement of nCEH1 in various cancers, it is reasonable to consider that it may also be a factor in liver cancer. These insights should prompt further exploration into this aspect.

The apparently low expression of nCEH1 in the liver has likely led researchers to assume that it is also low in liver cancer. However, an interesting aspect of our experimental model is that CC formation was induced in human and mouse immortalized cancer cell lines in all experiments. Provided that the above evidence implicates nCEH1 in cancer, it is possible that nCEH1 is upregulated in our cells. However, studies comparing CC formation and nCEH1 expression in primary cells versus immortalized cell lines are required to verify this postulate.

The ability of nCEH1 inhibition to prevent CC formation is surprising, but not unexpected. The reported localization of nCEH1 within the ER makes it difficult to conceive how it has access to lipid droplet CE with no reported localization to the lipid droplet. It is reasonable to consider that nCEH1 functions during lipid droplet lens formation during the process of initial lipid droplet development rather than after lipid droplet budding from the ER. Theoretically, this would allow access to the CE pool that temporarily forms due to ACAT1 activity prior to lipid droplet formation. Wagner *et al.* also confirmed nCEH1 ER localization via N-terminal GFP-tagged mouse nCEH1 colocalization with a fluorescent ER marker in COS-7 cells[57]. It is surprising that their tagged protein was able to localize to the ER, given that nCEH1 contains an N-terminal ER localization sequence. Moreover, the use of mouse nCEH1 begs the question as to whether human nCEH1 is differentially localized. It was recently suggested that since many lipid droplets remain attached to the ER, nCEH1 may have access to the CE-rich lipid moiety[57]. A complete understanding of nCEH1 localization and dynamics may glean important details regarding its function.

6.2: Cholesterol crystallization in macrophages and atherosclerosis

6.2.1: General discussion

Increasing evidence that CC are associated with poor outcomes in atherosclerosis and thrombosis have fueled recommendations that reducing CC formation may be a valuable therapeutic approach[189]. Many early studies have treated macrophages with synthetically produced CC to model the *in vivo* phenomenon and study the effects of CCs on macrophage inflammation and metabolism[76,77,88,93,94]. Yet, this method does not induce CC formation in these cells. Rather, other groups have incubated macrophages with various modified lipoproteins and imaged them under polarized light[21,36,37,82]. Similar to our results, these groups reported increased CC formation under these conditions. Although, the reported localization of their crystals in some studies are at odds with our data. Whereas we did not detect crystals in association with lysosomes, two studies describe CC formation in lysosomes[36,37]. While we found that ACAT inhibition prevented acLDL-induced CC formation, other groups observed augmented CC formation in the presence of ACAT inhibitors in macrophages[21,79]. Moreover, Baumer and colleagues demonstrated that needle and plate-like CC formation was potentiated by ACAT inhibition[91]. In support of our data, preclinical studies in hyperlipidemic mice show that whole body ACAT1 deficiency, myeloid ACAT1 deficiency, and Avasimibe treatment all effectively reduced the presence of cholesterol clefts in atherosclerotic lesions[22,86,87]. At this point, it is unclear why our results in macrophages are not entirely consistent with previous studies. Differences in cell type or treatment conditions may be the reason.

6.2.2: CE hydrolysis in macrophages

Our data in hepatocytes indicating that nCEH1 is required for CC formation was based on the ability of JW480 to reduce CC formation by approximately 90-95% signifying that nCEH1 may be the primary hepatocyte neutral CE hydrolase. In contrast, JW480 only reduced macrophage CC formation by 50%, implying the contribution of other CE hydrolase enzymes. Ishibashi and colleagues proposed that nCEH1 is the principal neutral CE hydrolase in human macrophages, but this view has faced criticism. Two comment articles have questioned the validity of their claims[190,191]. The first questioned whether their group was justified in concluding that cholesterol ester hydrolase (gene name CES1) did not play a role in neutral CE hydrolase activity, which was attributed to their failure to provide the sequence of the cDNA clone used in their studies[190].

Similarly, the second article did not agree with the statement that "nCEH1 is the only enzyme that requires attention when dealing with neutral CE hydrolase activity in human macrophages", based on their findings that HSL was the primary contributor, rather than nCEH1[191]. Both of these letters to the editor argue that nCEH1 is not the most important contributor to neutral CE hydrolase activity. Nonetheless, in addition to being less effective, nCEH1 inhibition in macrophages would not be advisable in the context of atherosclerosis as nCEH1 is known to promote reverse cholesterol transport, conferring atheroprotection[51,192]. Thus, selectively inhibiting hepatocyte nCEH1 to treat NASH or HCC is more appropriate.

6.2.3: A potential downstream pathway of cholesterol crystallization

The inability of NLRP3 inflammasome inhibition to uncouple CC from experimental NASH implies the existence of an alternative mechanism by which these crystals may contribute to liver disease pathology and progression. As described in section 2.4.4, one such mechanism may be mediated through Mincle. In the context of atherosclerosis, Mincle was found to be highly expressed in mouse and human atherosclerotic lesions and contributed to a proatherogenic macrophage phenotype[193]. Reduction in lipid accumulation, ER stress, and macrophage inflammation were all associated with transplantation of Mincle-null bone marrow into atherosclerotic mice. The role of Mincle was also implicated in acute kidney injury, where it contributed to sustained inflammation and reduced clearance of dead cells[194]. Future studies investigating the role of Mincle and its relationship to CC are needed to clarify its potential role in NASH. Interestingly, Mincle was detected via immunohistochemistry in HCC tissues but its expression decreased with tumor progression[195]. Other C-type lectin 4 (CLEC4) isoforms were reported to play key roles in HCC development, and whether these isoforms can also interact with CC remains to be determined. Exploring if Mincle mediates sterile inflammation in metabolic disease is another appealing avenue to explore[196–198]. To study Mincle *in vivo* and its relevance to CC, humanized transgenic mouse models will need to be developed as human, but not mouse Mincle was found to bind CC[128].

6.3 Limitations

While care was taken in experimental design, I acknowledge there are limitations. First, my experiments were carried out on human and mouse immortalized cell lines, which may have

acquired adaptations or exhibit an altered gene expression profile that poorly reflect the *in vivo* scenario. Future studies using primary cells, animal models, and human subjects will be necessary to establish the clinical significance of my findings. Second, my cholesterol loading protocol in both cell types was designed to rapidly 'flood' cells with cholesterol to induce cholesterol crystallization in an efficient manner. While this enabled me to gain mechanistic insights, LDL loading would better recapitulate physiological conditions. However, this would take a much longer period to induce intracellular crystals and may involve distinct mechanisms. Third, Shimobayashi *et al*. show that temperature affects liquid crystalline phase transition[142]. A caveat of our experimental design is that temperature was not controlled for during live cell imaging, which was done at room temperature and thus may have varied between treatment groups, as well from day to day. Furthermore, while we provide endpoint analyses of CC formation, we did not assay formation at the early stages, nor did we track formation over time. It is possible that critical information is not being captured at these early stages of CC formation. Lastly, we do not determine whether the CC in our experiments contain FC or CE, which would be beneficial to support the perception that FC underlies CC formation.

6.4: Future directions

Potential future directions are as follows. (1) Determine whether CC are pathological in liver disease and if they actively promote NASH development and/or progression to HCC. (2) Investigate CC formation in a mouse model of NASH and determine if ACAT inhibition also protects against crystallization *in vivo*. (3) Overexpress ACAT1 and nCEH1 in Hep3B cells to ascertain whether this exacerbates CC formation. (4) Induce CC formation in Hep3B cells using LDL loading. (5) Explore the ability of autophagy to promote CC solubilization.

Although not officially proposed in the literature, it is interesting to question if lipid droplets can become 'stressed' following CC formation or development of liquid crystals. Stress could mean altered surface tension within the lipid droplet monolayer, which may affect protein association and function[61,199]. Given that lipid droplets are tightly integrated with ER stress responses[200] and that lipid droplets are decorated with an abundance of metabolic proteins[64], it is tempting to consider that stressed or dysfunctional lipid droplets may induce the unfolded protein response independent of misfolded proteins within the ER. Intriguingly, ACAT1 overexpression

in adipocytes led to increased FC levels on the lipid droplet surface and impaired lipid droplet metabolic functions such as lipolysis and insulin signaling[146]. Conceivably, FC accumulation at the lipid droplet surface has detrimental consequences for metabolism.

6.5 Conclusions

Cholesterol crystallization is a serious consequence of cholesterol dysregulation present in heart and liver disease. FC accumulation is known to be linked to CC formation, but the mechanisms that underlie this process have not been elucidated. **Chapter 1** introduces the context of this thesis and the rationale for our experiments. **Chapter 2** discusses the current body of knowledge surrounding crystallization in atherosclerosis and NASH and introduces our hypothesis that enzymes that mediate cholesterol esterification and enzymes that de-esterify lipid droplet CE are required for intracellular CC formation. **Chapter 3** outlines the materials and methods used to test our hypothesis. In **Chapter 4**, we investigate crystallization in hepatocytes and macrophages and determine that CC formation occurs in close association with lipid droplets. In **Chapter 5**, we report that cholesterol esterification, subsequent lipid droplet localization, and CE hydrolysis are required for intracellular CC formation. **Chapter 6** discusses the relevance of our findings in the context of NASH, HCC, and atherosclerosis, and proposes future directions of study. In conclusion, this thesis proposes that CE metabolism governs intracellular CC formation, driven by ACAT1 and nCEH1 which work in unison to concentrate FC at the lipid droplet surface.

References

1. Sánchez López de Nava, A. & Raja, A. Physiology, Metabolism. in *StatPearls* (StatPearls Publishing, 2023). http://www.ncbi.nlm.nih.gov/books/NBK546690/.
2. Lemmer, I. L., Willemsen, N., Hilal, N. & Bartelt, A. A guide to understanding endoplasmic reticulum stress in metabolic disorders. *Mol Metab* **47**, 101169 (2021).
3. Hruby, A. & Hu, F. B. The Epidemiology of Obesity: A Big Picture. *Pharmacoeconomics* **33**, 673–689 (2015).
4. Government of Canada, S. C. Leading causes of death, total population, by age group. https://www150.statcan.gc.ca/t1/tbl1/en/cv.action?pid=1310039401 (2021).
5. World Health Organization. Cardiovascular diseases (CVDs). https://www.who.int/news-room/fact-sheets/detail/cardiovascular-diseases-(cvds).
6. Libby, P. *et al.* Atherosclerosis. *Nat Rev Dis Primers* **5**, 1–18 (2019).
7. Ioannou, G. N. Epidemiology and risk-stratification of NAFLD-associated HCC. *Journal of Hepatology* **75**, 1476–1484 (2021).
8. Akl, M. G. & Widenmaier, S. B. Immunometabolic factors contributing to obesity-linked hepatocellular carcinoma. *Frontiers in Cell and Developmental Biology* **10**, (2023).
9. Luo, J., Yang, H. & Song, B.-L. Mechanisms and regulation of cholesterol homeostasis. *Nat Rev Mol Cell Biol* **21**, 225–245 (2020).
10. Ioannou, G. N. The Role of Cholesterol in the Pathogenesis of NASH. *Trends Endocrinol Metab* **27**, 84–95 (2016).
11. Tabas, I. Consequences of cellular cholesterol accumulation: basic concepts and physiological implications. *J Clin Invest* **110**, 905–911 (2002).
12. Maxfield, F. R. & Tabas, I. Role of cholesterol and lipid organization in disease. *Nature* **438**, 612–621 (2005).
13. Janoudi, A., Shamoun, F. E., Kalavakunta, J. K. & Abela, G. S. Cholesterol crystal induced arterial inflammation and destabilization of atherosclerotic plaque. *Eur Heart J* **37**, 1959–1967 (2016).
14. John Chapman, M. & Preston Mason, R. Cholesterol crystals and atherosclerotic plaque instability: Therapeutic potential of Eicosapentaenoic acid. *Pharmacol Ther* **240**, 108237 (2022).
15. Shi, X. *et al.* Cholesterol Crystals are Associated with Carotid Plaque Vulnerability: An Optical Coherence Tomography Study. *Journal of Stroke and Cerebrovascular Diseases* **29**, 104579 (2020).
16. Abela, G. S. & Aziz, K. Cholesterol crystals cause mechanical damage to biological membranes: a proposed mechanism of plaque rupture and erosion leading to arterial thrombosis. *Clin Cardiol* **28**, 413–420 (2005).
17. Abela, G. S. Cholesterol crystals piercing the arterial plaque and intima trigger local and systemic inflammation. *J Clin Lipidol* **4**, 156–164 (2010).
18. Abela, G. S. & Aziz, K. Cholesterol crystals rupture biological membranes and human plaques during acute cardiovascular events--a novel insight into plaque rupture by scanning electron microscopy. *Scanning* **28**, 1–10 (2006).
19. Luo, Y. *et al.* Modeling of Mechanical Stress Exerted by Cholesterol Crystallization on Atherosclerotic Plaques. *PLoS One* **11**, e0155117 (2016).
20. Ioannou, G. N. *et al.* Cholesterol Crystals in Hepatocyte Lipid Droplets Are Strongly Associated With Human Nonalcoholic Steatohepatitis. *Hepatol Commun* **3**, 776–791 (2019).

21. Kellner-Weibel, G. *et al.* Crystallization of Free Cholesterol in Model Macrophage Foam Cells. *Arteriosclerosis, Thrombosis, and Vascular Biology* **19**, 1891–1898 (1999).
22. Accad, M. *et al.* Massive xanthomatosis and altered composition of atherosclerotic lesions in hyperlipidemic mice lacking acyl CoA:cholesterol acyltransferase 1. *J Clin Invest* **105**, 711–719 (2000).
23. Chang, T.-Y., Chang, C. C. Y., Ohgami, N. & Yamauchi, Y. Cholesterol Sensing, Trafficking, and Esterification. *Annual Review of Cell and Developmental Biology* **22**, 129–157 (2006).
24. Ioannou, G. N. *et al.* Cholesterol crystallization within hepatocyte lipid droplets and its role in murine NASH. *J Lipid Res* **58**, 1067–1079 (2017).
25. Ioannou, G. N., Haigh, W. G., Thorning, D. & Savard, C. Hepatic cholesterol crystals and crown-like structures distinguish NASH from simple steatosis. *J Lipid Res* **54**, 1326–1334 (2013).
26. Craig, M., Yarrarapu, S. N. S. & Dimri, M. Biochemistry, Cholesterol. in *StatPearls* (StatPearls Publishing, 2023).
27. Maxfield, F. R. & van Meer, G. Cholesterol, the central lipid of mammalian cells. *Current Opinion in Cell Biology* **22**, 422–429 (2010).
28. CROCKETT, E. L. Cholesterol Function in Plasma Membranes from Ectotherms: Membrane-Specific Roles in Adaptation to Temperature1. *American Zoologist* **38**, 291–304 (1998).
29. Menon, A. K. Sterol gradients in cells. *Current Opinion in Cell Biology* **53**, 37–43 (2018).
30. Zhang, L. *et al.* Significance and Mechanism of CYP7a1 Gene Regulation during the Acute Phase of Liver Regeneration. *Molecular Endocrinology* **23**, 137–145 (2009).
31. Ding, C. *et al.* A Cell-type-resolved Liver Proteome. *Mol Cell Proteomics* **15**, 3190–3202 (2016).
32. Bilzer, M., Roggel, F. & Gerbes, A. L. Role of Kupffer cells in host defense and liver disease. *Liver Int* **26**, 1175–1186 (2006).
33. Winau, F., Quack, C., Darmoise, A. & Kaufmann, S. H. E. Starring stellate cells in liver immunology. *Curr Opin Immunol* **20**, 68–74 (2008).
34. Schulze, R. J., Schott, M. B., Casey, C. A., Tuma, P. L. & McNiven, M. A. The cell biology of the hepatocyte: A membrane trafficking machine. *Journal of Cell Biology* **218**, 2096–2112 (2019).
35. Baumer, Y. *et al.* Chronic skin inflammation accelerates macrophage cholesterol crystal formation and atherosclerosis. *JCI Insight* **3**, e97179, 97179 (2018).
36. Klinkner, A. M., Waites, C. R., Kerns, W. D. & Bugelski, P. J. Evidence of foam cell and cholesterol crystal formation in macrophages incubated with oxidized LDL by fluorescence and electron microscopy. *J Histochem Cytochem* **43**, 1071–1078 (1995).
37. Tangirala, R. K. *et al.* Formation of cholesterol monohydrate crystals in macrophage-derived foam cells. *Journal of Lipid Research* **35**, 93–104 (1994).
38. Rogers, M. A. *et al.* Acyl-CoA:cholesterol acyltransferases (ACATs/SOATs): Enzymes with multiple sterols as substrates and as activators. *J Steroid Biochem Mol Biol* **151**, 102–107 (2015).
39. Chang, T.-Y., Li, B.-L., Chang, C. C. Y. & Urano, Y. Acyl-coenzyme A:cholesterol acyltransferases. *Am J Physiol Endocrinol Metab* **297**, E1-9 (2009).

40. Chang, C. C., Huh, H. Y., Cadigan, K. M. & Chang, T. Y. Molecular cloning and functional expression of human acyl-coenzyme A:cholesterol acyltransferase cDNA in mutant Chinese hamster ovary cells. *J Biol Chem* **268**, 20747–20755 (1993).
41. Catherine C. Y., C. *et al.* Regulation and Immunolocalization of Acyl-Coenzyme A:Cholesterol Acyltransferase in Mammalian Cells as Studied with Specific Antibodies (*). *Journal of Biological Chemistry* **270**, 29532–29540 (1995).
42. Meiner, V. L. *et al.* Disruption of the acyl-CoA:cholesterol acyltransferase gene in mice: evidence suggesting multiple cholesterol esterification enzymes in mammals. *Proc Natl Acad Sci U S A* **93**, 14041–14046 (1996).
43. Cases, S. *et al.* ACAT-2, a second mammalian acyl-CoA:cholesterol acyltransferase. Its cloning, expression, and characterization. *J Biol Chem* **273**, 26755–26764 (1998).
44. Oelkers, P., Behari, A., Cromley, D., Billheimer, J. T. & Sturley, S. L. Characterization of two human genes encoding acyl coenzyme A:cholesterol acyltransferase-related enzymes. *J Biol Chem* **273**, 26765–26771 (1998).
45. Anderson, R. A. *et al.* Identification of a form of acyl-CoA:cholesterol acyltransferase specific to liver and intestine in nonhuman primates. *J Biol Chem* **273**, 26747–26754 (1998).
46. Repa, J. J., Buhman, K. K., Farese Jr., R. V., Dietschy, J. M. & Turley, S. D. ACAT2 deficiency limits cholesterol absorption in the cholesterol-fed mouse: Impact on hepatic cholesterol homeostasis. *Hepatology* **40**, 1088–1097 (2004).
47. Buhman, K. K. *et al.* Resistance to diet-induced hypercholesterolemia and gallstone formation in ACAT2-deficient mice. *Nat Med* **6**, 1341–1347 (2000).
48. Chang, C. C. *et al.* Immunological quantitation and localization of ACAT-1 and ACAT-2 in human liver and small intestine. *J Biol Chem* **275**, 28083–28092 (2000).
49. Joyce, C., Skinner, K., Anderson, R. A. & Rudel, L. L. Acyl-coenzyme A: cholesteryl acyltransferase 2. *Current Opinion in Lipidology* **10**, 89 (1999).
50. Okazaki, H. *et al.* Identification of neutral cholesterol ester hydrolase, a key enzyme removing cholesterol from macrophages. *J Biol Chem* **283**, 33357–33364 (2008).
51. Sekiya, M. *et al.* Ablation of Neutral Cholesterol Ester Hydrolase 1 Accelerates Atherosclerosis. *Cell Metabolism* **10**, 219–228 (2009).
52. Buchebner, M. *et al.* Cholesteryl ester hydrolase activity is abolished in HSL-/- macrophages but unchanged in macrophages lacking KIAA1363. *J Lipid Res* **51**, 2896–2908 (2010).
53. Igarashi, M. *et al.* The Critical Role of Neutral Cholesterol Ester Hydrolase 1 in Cholesterol Removal From Human Macrophages. *Circulation Research* **107**, 1387–1395 (2010).
54. Sekiya, M. *et al.* Absence of Nceh1 augments 25-hydroxycholesterol-induced ER stress and apoptosis in macrophages. *J Lipid Res* **55**, 2082–2092 (2014).
55. Sakai, K. *et al.* Critical role of neutral cholesteryl ester hydrolase 1 in cholesteryl ester hydrolysis in murine macrophages. *J Lipid Res* **55**, 2033–2040 (2014).
56. Nomura, D. K. *et al.* Serine hydrolase KIAA1363: toxicological and structural features with emphasis on organophosphate interactions. *Chem Res Toxicol* **19**, 1142–1150 (2006).
57. Wagner, C. *et al.* KIAA1363 affects retinyl ester turnover in cultured murine and human hepatic stellate cells. *J Lipid Res* **63**, 100173 (2022).
58. Quiroga, A. D. & Lehner, R. Role of endoplasmic reticulum neutral lipid hydrolases. *Trends in Endocrinology & Metabolism* **22**, 218–225 (2011).
59. Igarashi, M. *et al.* Targeting of neutral cholesterol ester hydrolase to the endoplasmic reticulum via its N-terminal sequence. *J Lipid Res* **51**, 274–285 (2010).

60. Hodges, B. D. M. & Wu, C. C. Proteomic insights into an expanded cellular role for cytoplasmic lipid droplets[S]. *Journal of Lipid Research* **51**, 262–273 (2010).
61. Thiam, A. R., Farese Jr, R. V. & Walther, T. C. The biophysics and cell biology of lipid droplets. *Nat Rev Mol Cell Biol* **14**, 775–786 (2013).
62. Thiam, A. R. & Dugail, I. Lipid droplet–membrane contact sites – from protein binding to function. *Journal of Cell Science* **132**, jcs230169 (2019).
63. Olzmann, J. A. & Carvalho, P. Dynamics and functions of lipid droplets. *Nat Rev Mol Cell Biol* **20**, 137–155 (2019).
64. Xu, S., Zhang, X. & Liu, P. Lipid droplet proteins and metabolic diseases. *Biochimica et Biophysica Acta (BBA) - Molecular Basis of Disease* **1864**, 1968–1983 (2018).
65. Chistiakov, D. A., Bobryshev, Y. V. & Orekhov, A. N. Macrophage-mediated cholesterol handling in atherosclerosis. *J Cell Mol Med* **20**, 17–28 (2016).
66. Goldstein, J. L., Ho, Y. K., Basu, S. K. & Brown, M. S. Binding site on macrophages that mediates uptake and degradation of acetylated low density lipoprotein, producing massive cholesterol deposition. *Proc Natl Acad Sci U S A* **76**, 333–337 (1979).
67. Bäck, M., Yurdagul, A., Tabas, I., Öörni, K. & Kovanen, P. T. Inflammation and its resolution in atherosclerosis: mediators and therapeutic opportunities. *Nat Rev Cardiol* **16**, 389–406 (2019).
68. Gui, Y., Zheng, H. & Cao, R. Y. Foam Cells in Atherosclerosis: Novel Insights Into Its Origins, Consequences, and Molecular Mechanisms. *Frontiers in Cardiovascular Medicine* **9**, (2022).
69. Bailey, C. H. ATHEROMA AND OTHER LESIONS PRODUCED IN RABBITS BY CHOLESTEROL FEEDING. *J Exp Med* **23**, 69–84 (1916).
70. Bogren, H. & Larsson, K. An X-ray-diffraction study of crystalline cholesterol in some pathological deposits in man. *Biochimica et Biophysica Acta* **75**, 65–69 (1963).
71. Katz, S. S., Shipley, G. G. & Small, D. M. Physical chemistry of the lipids of human atherosclerotic lesions. Demonstration of a lesion intermediate between fatty streaks and advanced plaques. *J Clin Invest* **58**, 200–211 (1976).
72. Suhalim, J. L. *et al.* Characterization of cholesterol crystals in atherosclerotic plaques using stimulated Raman scattering and second-harmonic generation microscopy. *Biophys J* **102**, 1988–1995 (2012).
73. Nasiri, M. *et al.* Role of cholesterol crystals in atherosclerosis is unmasked by altering tissue preparation methods. *Microsc Res Tech* **78**, 969–974 (2015).
74. Cho, S. *et al.* High-Contrast Imaging of Cholesterol Crystals in Rabbit Arteries Ex Vivo Using LED-Based Polarization Microscopy. *Sensors (Basel)* **18**, 1258 (2018).
75. Douplik, A., Saiko, G., Schelkanova, I. & Tuchin, V. V. 3 - The response of tissue to laser light. in *Lasers for Medical Applications* (ed. Jelínková, H.) 47–109 (Woodhead Publishing, 2013). doi:10.1533/9780857097545.1.47.
76. Duewell, P. *et al.* NLRP3 inflammasomes are required for atherogenesis and activated by cholesterol crystals. *Nature* **464**, 1357–1361 (2010).
77. Rajamäki, K. *et al.* Cholesterol crystals activate the NLRP3 inflammasome in human macrophages: a novel link between cholesterol metabolism and inflammation. *PLoS One* **5**, e11765 (2010).
78. Perl-Treves, D., Kessler, N., Izhaky, D. & Addadi, L. Monoclonal antibody recognition of cholesterol monohydrate crystal faces. *Chem Biol* **3**, 567–577 (1996).

79. Jin, X. *et al.* Macrophages Shed Excess Cholesterol in Unique Extracellular Structures Containing Cholesterol Microdomains. *Arterioscler Thromb Vasc Biol* **38**, 1504–1518 (2018).
80. Varsano, N., Fargion, I., Wolf, S. G., Leiserowitz, L. & Addadi, L. Formation of 3D Cholesterol Crystals from 2D Nucleation Sites in Lipid Bilayer Membranes: Implications for Atherosclerosis. *J. Am. Chem. Soc.* **137**, 1601–1607 (2015).
81. Varsano, N. *et al.* Development of Correlative Cryo-soft X-ray Tomography and Stochastic Reconstruction Microscopy. A Study of Cholesterol Crystal Early Formation in Cells. *J Am Chem Soc* **138**, 14931–14940 (2016).
82. Varsano, N. *et al.* Two polymorphic cholesterol monohydrate crystal structures form in macrophage culture models of atherosclerosis. *Proc Natl Acad Sci U S A* **115**, 7662–7669 (2018).
83. Varsano, N. *et al.* The Effect of the Phospholipid Bilayer Environment on Cholesterol Crystal Polymorphism. *Chempluschem* **84**, 338–344 (2019).
84. Capua-Shenkar, J. *et al.* Examining atherosclerotic lesions in three dimensions at the nanometer scale with cryo-FIB-SEM. *Proceedings of the National Academy of Sciences* **119**, e2205475119 (2022).
85. Baumer, Y., Mehta, N. N., Dey, A. K., Powell-Wiley, T. M. & Boisvert, W. A. Cholesterol crystals and atherosclerosis. *Eur Heart J* **41**, 2236–2239 (2020).
86. Melton, E. M. *et al.* Myeloid Acat1/Soat1 KO attenuates pro-inflammatory responses in macrophages and protects against atherosclerosis in a model of advanced lesions. *J Biol Chem* **294**, 15836–15849 (2019).
87. Delsing, D. J. *et al.* Acyl-CoA:cholesterol acyltransferase inhibitor avasimibe reduces atherosclerosis in addition to its cholesterol-lowering effect in ApoE*3-Leiden mice. *Circulation* **103**, 1778–1786 (2001).
88. Sheedy, F. J. *et al.* CD36 coordinates NLRP3 inflammasome activation by facilitating intracellular nucleation of soluble ligands into particulate ligands in sterile inflammation. *Nat Immunol* **14**, 812–820 (2013).
89. Ho-Tin-Noé, B. *et al.* Cholesterol crystallization in human atherosclerosis is triggered in smooth muscle cells during the transition from fatty streak to fibroatheroma. *The Journal of Pathology* **241**, 671–682 (2017).
90. Baumer, Y. *et al.* Hyperlipidemia-induced cholesterol crystal production by endothelial cells promotes atherogenesis. *Nat Commun* **8**, 1129 (2017).
91. Baumer, Y. *et al.* Hyperlipidaemia and IFNgamma/TNFalpha Synergism are associated with cholesterol crystal formation in Endothelial cells partly through modulation of Lysosomal pH and Cholesterol homeostasis. *EBioMedicine* **59**, 102876 (2020).
92. Halkias, C. *et al.* An advanced method for quantitative measurements of cholesterol crystallization. *Biochimica et Biophysica Acta (BBA) - Molecular and Cell Biology of Lipids* **1866**, 158872 (2021).
93. O'Rourke, S. A. *et al.* Cholesterol crystals drive metabolic reprogramming and M1 macrophage polarisation in primary human macrophages. *Atherosclerosis* **352**, 35–45 (2022).
94. Zimmer, S. *et al.* Cyclodextrin promotes atherosclerosis regression via macrophage reprogramming. *Sci Transl Med* **8**, 333ra50 (2016).
95. Grebe, A. & Latz, E. Cholesterol Crystals and Inflammation. *Curr Rheumatol Rep* **15**, 313 (2013).

96. Abela, G. S. *et al.* Effect of Cholesterol Crystals on Plaques and Intima in Arteries of Patients With Acute Coronary and Cerebrovascular Syndromes. *The American Journal of Cardiology* **103**, 959–968 (2009).
97. Xue, C. *et al.* The relationships between cholesterol crystals, NLRP3 inflammasome, and coronary atherosclerotic plaque vulnerability in acute coronary syndrome: An optical coherence tomography study. *Front Cardiovasc Med* **9**, 905363 (2022).
98. Goldstein, J. L., Dana, S. E. & Brown, M. S. Esterification of low density lipoprotein cholesterol in human fibroblasts and its absence in homozygous familial hypercholesterolemia. *Proc Natl Acad Sci U S A* **71**, 4288–4292 (1974).
99. Kusunoki, J. *et al.* Acyl-CoA:Cholesterol Acyltransferase Inhibition Reduces Atherosclerosis in Apolipoprotein E–Deficient Mice. *Circulation* **103**, 2604–2609 (2001).
100. Bocan, T. M. *et al.* The ACAT inhibitor avasimibe reduces macrophages and matrix metalloproteinase expression in atherosclerotic lesions of hypercholesterolemic rabbits. *Arterioscler Thromb Vasc Biol* **20**, 70–79 (2000).
101. Nicolosi, R. J., Wilson, T. A. & Krause, B. R. The ACAT inhibitor, CI-1011 is effective in the prevention and regression of aortic fatty streak area in hamsters. *Atherosclerosis* **137**, 77–85 (1998).
102. Yagyu, H. *et al.* Absence of ACAT-1 attenuates atherosclerosis but causes dry eye and cutaneous xanthomatosis in mice with congenital hyperlipidemia. *J Biol Chem* **275**, 21324–21330 (2000).
103. Fazio, S. *et al.* Increased atherosclerosis in LDL receptor-null mice lacking ACAT1 in macrophages. *J Clin Invest* **107**, 163–171 (2001).
104. Tardif, J.-C. *et al.* Effects of the Acyl Coenzyme A:Cholesterol Acyltransferase Inhibitor Avasimibe on Human Atherosclerotic Lesions. *Circulation* **110**, 3372–3377 (2004).
105. Nissen, S. E. *et al.* Effect of ACAT Inhibition on the Progression of Coronary Atherosclerosis. *New England Journal of Medicine* **354**, 1253–1263 (2006).
106. Meuwese, M. C. *et al.* ACAT inhibition and progression of carotid atherosclerosis in patients with familial hypercholesterolemia: the CAPTIVATE randomized trial. *JAMA* **301**, 1131–1139 (2009).
107. Sahi, J. *et al.* Avasimibe Induces CYP3A4 and Multiple Drug Resistance Protein 1 Gene Expression through Activation of the Pregnane X Receptor. *J Pharmacol Exp Ther* **306**, 1027–1034 (2003).
108. Rong, J. X. *et al.* ACAT inhibition reduces the progression of pre-existing, advanced atherosclerotic mouse lesions without plaque or systemic toxicity. *Arterioscler Thromb Vasc Biol* **33**, 4–12 (2013).
109. Terasaka, N. *et al.* ACAT inhibitor pactimibe sulfate (CS-505) reduces and stabilizes atherosclerotic lesions by cholesterol-lowering and direct effects in apolipoprotein E-deficient mice. *Atherosclerosis* **190**, 239–247 (2007).
110. Ikenoya, M. *et al.* A selective ACAT-1 inhibitor, K-604, suppresses fatty streak lesions in fat-fed hamsters without affecting plasma cholesterol levels. *Atherosclerosis* **191**, 290–297 (2007).
111. Yoshinaka, Y. *et al.* A selective ACAT-1 inhibitor, K-604, stimulates collagen production in cultured smooth muscle cells and alters plaque phenotype in apolipoprotein E-knockout mice. *Atherosclerosis* **213**, 85–91 (2010).

112. Huang, L.-H. *et al.* Myeloid Acyl-CoA:Cholesterol Acyltransferase 1 Deficiency Reduces Lesion Macrophage Content and Suppresses Atherosclerosis Progression. *J Biol Chem* **291**, 6232–6244 (2016).
113. Wakabayashi, T. *et al.* Inflammasome Activation Aggravates Cutaneous Xanthomatosis and Atherosclerosis in ACAT1 (Acyl-CoA Cholesterol Acyltransferase 1) Deficiency in Bone Marrow. *Arteriosclerosis, Thrombosis, and Vascular Biology* **38**, 2576–2589 (2018).
114. Yang, W. *et al.* Potentiating the antitumour response of CD8(+) T cells by modulating cholesterol metabolism. *Nature* **531**, 651–655 (2016).
115. Yamazaki, H. *et al.* Loss of ACAT1 Attenuates Atherosclerosis Aggravated by Loss of NCEH1 in Bone Marrow-Derived Cells. *Journal of Atherosclerosis and Thrombosis* **26**, 246–259 (2019).
116. Rogers, M. A. *et al.* Acat1/Soat1 knockout extends the mutant Npc1 mouse lifespan and ameliorates functional deficiencies in multiple organelles of mutant cells. *Proc Natl Acad Sci U S A* **119**, e2201646119 (2022).
117. Perrey, S. *et al.* Preferential pharmacological inhibition of macrophage ACAT increases plaque formation in mouse and rabbit models of atherogenesis. *Atherosclerosis* **155**, 359–370 (2001).
118. Willner, E. L. *et al.* Deficiency of acyl CoA:cholesterol acyltransferase 2 prevents atherosclerosis in apolipoprotein E-deficient mice. *Proceedings of the National Academy of Sciences* **100**, 1262–1267 (2003).
119. Horn, C. L., Morales, A. L., Savard, C., Farrell, G. C. & Ioannou, G. N. Role of Cholesterol-Associated Steatohepatitis in the Development of NASH. *Hepatol Commun* **6**, 12–35 (2022).
120. Wouters, K. *et al.* Intrahepatic cholesterol influences progression, inhibition and reversal of non-alcoholic steatohepatitis in hyperlipidemic mice. *FEBS Lett* **584**, 1001–1005 (2010).
121. Gavezzotti, A. Chapter 8 - Organic crystal nucleation and growth: Little knowledge, much mystery. in *Theoretical and Computational Chemistry* (ed. Gavezzotti, A.) vol. 20 201–229 (Elsevier, 2021).
122. Park, S., Sut, T. N., Ma, G. J., Parikh, A. N. & Cho, N.-J. Crystallization of Cholesterol in Phospholipid Membranes Follows Ostwald's Rule of Stages. *J. Am. Chem. Soc.* **142**, 21872–21882 (2020).
123. Bernstein, D. L., Hülkova, H., Bialer, M. G. & Desnick, R. J. Cholesteryl ester storage disease: Review of the findings in 135 reported patients with an underdiagnosed disease. *Journal of Hepatology* **58**, 1230–1243 (2013).
124. Shepelenko, M. *et al.* Polymorphism, Structure, and Nucleation of Cholesterol·H2O at Aqueous Interfaces and in Pathological Media: Revisited from a Computational Perspective. *J. Am. Chem. Soc.* **144**, 5304–5314 (2022).
125. Ioannou, G. N. *et al.* Cholesterol-lowering drugs cause dissolution of cholesterol crystals and disperse Kupffer cell crown-like structures during resolution of NASH. *J Lipid Res* **56**, 277–285 (2015).
126. Ioannou, G. N. *et al.* Genetic deletion or pharmacologic inhibition of the Nlrp3 inflammasome did not ameliorate experimental NASH. *J Lipid Res* **64**, 100330 (2023).
127. Matsumoto, M. *et al.* A novel LPS-inducible C-type lectin is a transcriptional target of NF-IL6 in macrophages. *J Immunol* **163**, 5039–5048 (1999).
128. Kiyotake, R. *et al.* Human Mincle Binds to Cholesterol Crystals and Triggers Innate Immune Responses. *J Biol Chem* **290**, 25322–25332 (2015).

129. Corr, E. M., Cunningham, C. C. & Dunne, A. Cholesterol crystals activate Syk and PI3 kinase in human macrophages and dendritic cells. *Atherosclerosis* **251**, 197–205 (2016).
130. McDonald, S. Systematic Sudy of Cellular Cholesterol Homeostasis. *MSc Thesis* **University of Saskatchewan**, (2022).
131. Parlakgül, G. *et al.* Regulation of liver subcellular architecture controls metabolic homeostasis. *Nature* **603**, 736–742 (2022).
132. Radhakrishnan, A., Goldstein, J. L., McDonald, J. G. & Brown, M. S. Switch-like control of SREBP-2 transport triggered by small changes in ER cholesterol: a delicate balance. *Cell Metab* **8**, 512–521 (2008).
133. Brown, M. S., Goldstein, J. L., Krieger, M., Ho, Y. K. & Anderson, R. G. Reversible accumulation of cholesteryl esters in macrophages incubated with acetylated lipoproteins. *J Cell Biol* **82**, 597–613 (1979).
134. Hai, Q. & Smith, J. D. Acyl-Coenzyme A: Cholesterol Acyltransferase (ACAT) in Cholesterol Metabolism: From Its Discovery to Clinical Trials and the Genomics Era. *Metabolites* **11**, 543 (2021).
135. Devries-Seimon, T. *et al.* Cholesterol-induced macrophage apoptosis requires ER stress pathways and engagement of the type A scavenger receptor. *J Cell Biol* **171**, 61–73 (2005).
136. Shibuya, Y. *et al.* Acyl-CoA:cholesterol acyltransferase 1 blockage enhances autophagy in the neurons of triple transgenic Alzheimer's disease mouse and reduces human P301L-tau content at the pre-symptomatic stage. *Neurobiol Aging* **36**, 2248–2259 (2015).
137. Sekiguchi, A., Kanno, H., Ozawa, H., Yamaya, S. & Itoi, E. Rapamycin promotes autophagy and reduces neural tissue damage and locomotor impairment after spinal cord injury in mice. *J Neurotrauma* **29**, 946–956 (2012).
138. Rong, J. X., Kusunoki, J., Oelkers, P., Sturley, S. L. & Fisher, E. A. Acyl-coenzymeA (CoA):cholesterol acyltransferase inhibition in rat and human aortic smooth muscle cells is nontoxic and retards foam cell formation. *Arterioscler Thromb Vasc Biol* **25**, 122–127 (2005).
139. Lei, X. *et al.* Association of ACAT1-positive vesicles with late endosomes/ lysosomes in cholesterol-rich human macrophages. *J Atheroscler Thromb* **17**, 740–750 (2010).
140. Bautista, G. *et al.* Polarized THG microscopy identifies compositionally different lipid droplets in mammalian cells. *Biophys J* **107**, 2230–2236 (2014).
141. Mahamid, J. *et al.* Liquid-crystalline phase transitions in lipid droplets are related to cellular states and specific organelle association. *Proc Natl Acad Sci U S A* **116**, 16866–16871 (2019).
142. Shimobayashi, S. F. & Ohsaki, Y. Universal phase behaviors of intracellular lipid droplets. *Proceedings of the National Academy of Sciences* **116**, 25440–25445 (2019).
143. Rogers, S. *et al.* Triglyceride lipolysis triggers liquid crystalline phases in lipid droplets and alters the LD proteome. *Journal of Cell Biology* **221**, e202205053 (2022).
144. Dumesnil, C. *et al.* Cholesterol esters form supercooled lipid droplets whose nucleation is facilitated by triacylglycerols. *Nat Commun* **14**, 915 (2023).
145. Czabany, T. *et al.* Structural and Biochemical Properties of Lipid Particles from the Yeast Saccharomyces cerevisiae*. *Journal of Biological Chemistry* **283**, 17065–17074 (2008).
146. Xu, Y., Du, X., Turner, N., Brown, A. J. & Yang, H. Enhanced acyl-CoA:cholesterol acyltransferase activity increases cholesterol levels on the lipid droplet surface and impairs adipocyte function. *J Biol Chem* **294**, 19306–19321 (2019).
147. Portincasa, P. *et al.* Pathways of cholesterol crystallization in model bile and native bile. *Digestive and Liver Disease* **35**, 118–126 (2003).

148. So, J. *et al.* EPA and DHA differentially modulate monocyte inflammatory response in subjects with chronic inflammation in part via plasma specialized pro-resolving lipid mediators: A randomized, double-blind, crossover study. *Atherosclerosis* **316**, 90–98 (2021).
149. Bhatt, D. L. *et al.* Cardiovascular Risk Reduction with Icosapent Ethyl for Hypertriglyceridemia. *N Engl J Med* **380**, 11–22 (2019).
150. Antalis, C. J., Arnold, T., Lee, B., Buhman, K. K. & Siddiqui, R. A. Docosahexaenoic acid is a substrate for ACAT1 and inhibits cholesteryl ester formation from oleic acid in MCF-10A cells. *Prostaglandins, Leukotrienes and Essential Fatty Acids* **80**, 165–171 (2009).
151. Gilat, T. *et al.* Arachidyl amido cholanoic acid (aramchol) is a cholesterol solubilizer and prevents the formation of cholesterol gallstones in inbred mice. *Lipids* **36**, 1135–1140 (2001).
152. Tauchi-Sato, K., Ozeki, S., Houjou, T., Taguchi, R. & Fujimoto, T. The Surface of Lipid Droplets Is a Phospholipid Monolayer with a Unique Fatty Acid Composition*. *Journal of Biological Chemistry* **277**, 44507–44512 (2002).
153. Razani, B. *et al.* Autophagy links inflammasomes to atherosclerotic progression. *Cell Metab* **15**, 534–544 (2012).
154. Filali-Mouncef, Y. *et al.* The ménage à trois of autophagy, lipid droplets and liver disease. *Autophagy* **18**, 50–72.
155. Ho-Tin-Noé, B. *et al.* Cholesterol crystallization in human atherosclerosis is triggered in smooth muscle cells during the transition from fatty streak to fibroatheroma. *The Journal of Pathology* **241**, 671–682 (2017).
156. Njoku, D. B., Schilling, J. D. & Finck, B. N. Mechanisms of nonalcoholic steatohepatitis-associated cardiomyopathy: key roles for liver–heart crosstalk. *Current Opinion in Lipidology* **33**, 295 (2022).
157. Brewer, H. B. The lipid-laden foam cell: an elusive target for therapeutic intervention. *J Clin Invest* **105**, 703–705 (2000).
158. Burnett, J. R. *et al.* Inhibition of ACAT by avasimibe decreases both VLDL and LDL apolipoprotein B production in miniature pigs. *J Lipid Res* **40**, 1317–1327 (1999).
159. Bell, T. A. *et al.* Liver-specific inhibition of acyl-coenzyme a:cholesterol acyltransferase 2 with antisense oligonucleotides limits atherosclerosis development in apolipoprotein B100-only low-density lipoprotein receptor-/- mice. *Arterioscler Thromb Vasc Biol* **26**, 1814–1820 (2006).
160. Melchior, J. T. *et al.* Targeted Knockdown of Hepatic SOAT2 With Antisense Oligonucleotides Stabilizes Atherosclerotic Plaque in ApoB100-only LDLr-/- Mice. *Arterioscler Thromb Vasc Biol* **35**, 1920–1927 (2015).
161. Brown, J. M. *et al.* Targeted depletion of hepatic ACAT2-driven cholesterol esterification reveals a non-biliary route for fecal neutral sterol loss. *J Biol Chem* **283**, 10522–10534 (2008).
162. Marshall, S. M. *et al.* Acute sterol o-acyltransferase 2 (SOAT2) knockdown rapidly mobilizes hepatic cholesterol for fecal excretion. *PLoS One* **9**, e98953 (2014).
163. Ohshiro, T. *et al.* Pyripyropene A, an Acyl–Coenzyme A:Cholesterol Acyltransferase 2–Selective Inhibitor, Attenuates Hypercholesterolemia and Atherosclerosis in Murine Models of Hyperlipidemia. *Arteriosclerosis, Thrombosis, and Vascular Biology* **31**, 1108–1115 (2011).
164. Ohshiro, T. *et al.* New pyripyropene A derivatives, highly SOAT2-selective inhibitors, improve hypercholesterolemia and atherosclerosis in atherogenic mouse models. *J Pharmacol Exp Ther* **355**, 299–307 (2015).
165. Ohshiro, T. *et al.* The Anti-atherogenic Activity of Beauveriolide Derivative BVD327, a Sterol O-Acyltransferase 2-Selective Inhibitor, in Apolipoprotein E Knockout Mice. *Biol Pharm Bull* **43**, 951–958 (2020).

166. Alger, H. M. *et al.* Inhibition of acyl-coenzyme A:cholesterol acyltransferase 2 (ACAT2) prevents dietary cholesterol-associated steatosis by enhancing hepatic triglyceride mobilization. *J Biol Chem* **285**, 14267–14274 (2010).
167. Post, S. M. *et al.* Acyl-coenzyme A:cholesterol acyltransferase inhibitor, avasimibe, stimulates bile acid synthesis and cholesterol 7alpha-hydroxylase in cultured rat hepatocytes and in vivo in the rat. *Hepatology* **30**, 491–500 (1999).
168. Jiang, Y. *et al.* Proteomics identifies new therapeutic targets of early-stage hepatocellular carcinoma. *Nature* **567**, 257–261 (2019).
169. Khatib, S. A. & Wang, X. W. Proteomic heterogeneity reveals SOAT1 as a potential biomarker for hepatocellular carcinoma. *Transl Gastroenterol Hepatol* **4**, 37 (2019).
170. Li, M. *et al.* Enhanced chemo-immunotherapy against melanoma by inhibition of cholesterol esterification in CD8+ T cells. *Nanomedicine* **14**, 2541–2550 (2018).
171. Pan, J. *et al.* Potentiation of Kras peptide cancer vaccine by avasimibe, a cholesterol modulator. *EBioMedicine* **49**, 72–81 (2019).
172. Ren, M., Xu, H., Xia, H., Tang, Q. & Bi, F. Simultaneously targeting SOAT1 and CPT1A ameliorates hepatocellular carcinoma by disrupting lipid homeostasis. *Cell Death Discov.* **7**, 125 (2021).
173. Zhu, Y. *et al.* P53 deficiency affects cholesterol esterification to exacerbate hepatocarcinogenesis. *Hepatology* (2022) doi:10.1002/hep.32518.
174. Wang, Z. *et al.* High-affinity SOAT1 ligands remodeled cholesterol metabolism program to inhibit tumor growth. *BMC Med* **20**, 292 (2022).
175. Geng, F. *et al.* Inhibition of SOAT1 Suppresses Glioblastoma Growth via Blocking SREBP-1–Mediated Lipogenesis. *Clinical Cancer Research* **22**, 5337–5348 (2016).
176. Ohmoto, T. *et al.* K604, a specific acyl-CoA:cholesterol acyltransferase 1 inhibitor, suppresses proliferation of U251-MG glioblastoma cells. *Mol Med Rep* **12**, 6037–6042 (2015).
177. Xu, H., Xia, H., Zhou, S., Tang, Q. & Bi, F. Cholesterol activates the Wnt/PCP-YAP signaling in SOAT1-targeted treatment of colon cancer. *Cell Death Discov.* **7**, 1–13 (2021).
178. Zhu, Y. *et al.* Ceramide-mediated gut dysbiosis enhances cholesterol esterification and promotes colorectal tumorigenesis in mice. *JCI Insight* **7**, e150607 (2022).
179. Eckhardt, C. *et al.* High expression of Sterol-O-Acyl transferase 1 (SOAT1), an enzyme involved in cholesterol metabolism, is associated with earlier biochemical recurrence in high risk prostate cancer. *Prostate Cancer Prostatic Dis* **25**, 484–490 (2022).
180. Liu, Y., Wang, Y., Hao, S., Qin, Y. & Wu, Y. Knockdown of sterol O-acyltransferase 1 (SOAT1) suppresses SCD1-mediated lipogenesis and cancer procession in prostate cancer. *Prostaglandins Other Lipid Mediat* **153**, 106537 (2021).
181. Chang, T. Y. *et al.* Blocking cholesterol storage to treat Alzheimer's disease. *Explor Neuroprotective Ther* **1**, 173–184 (2021).
182. Jessani, N., Liu, Y., Humphrey, M. & Cravatt, B. F. Enzyme activity profiles of the secreted and membrane proteome that depict cancer cell invasiveness. *Proc Natl Acad Sci U S A* **99**, 10335–10340 (2002).
183. Chiang, K. P., Niessen, S., Saghatelian, A. & Cravatt, B. F. An enzyme that regulates ether lipid signaling pathways in cancer annotated by multidimensional profiling. *Chem Biol* **13**, 1041–1050 (2006).
184. Chang, J. W., Nomura, D. K. & Cravatt, B. F. A potent and selective inhibitor of KIAA1363/AADACL1 that impairs prostate cancer pathogenesis. *Chem Biol* **18**, 476–484 (2011).

185. Holly, S. P. *et al.* Ether lipid metabolism by AADACL1 regulates platelet function and thrombosis. *Blood Adv* **3**, 3818–3828 (2019).
186. Xiao, Y. *et al.* NAD(P)-dependent steroid dehydrogenase-like protein and neutral cholesterol ester hydrolase 1 serve as novel markers for early detection of gastric cancer identified using quantitative proteomics. *J Clin Lab Anal* **35**, e23652 (2021).
187. Lu, Y., Zhang, L., Chen, X. & Zhang, Q. NCEH1 may be a prognostic biomarker for pancreatic cancer. *Int J Clin Exp Pathol* **13**, 2746–2752 (2020).
188. Bai, R., Rebelo, A., Kleeff, J. & Sunami, Y. Identification of prognostic lipid droplet-associated genes in pancreatic cancer patients via bioinformatics analysis. *Lipids Health Dis* **20**, 58 (2021).
189. Nidorf, S. M., Eikelboom, J. W. & Thompson, P. L. Targeting Cholesterol Crystal-Induced Inflammation for the Secondary Prevention of Cardiovascular Disease. *J Cardiovasc Pharmacol Ther* **19**, 45–52 (2014).
190. Ghosh, S. Important Considerations for Evaluating the Data Presented by Igarashi et al. *Circulation Research* **108**, e6–e7 (2011).
191. Kratky, D. Neutral cholesterol ester hydrolases in macrophages: still a matter of debate. *Circ Res* **108**, e13 (2011).
192. Sekiya, M., Osuga, J.-I., Igarashi, M., Okazaki, H. & Ishibashi, S. The role of neutral cholesterol ester hydrolysis in macrophage foam cells. *J Atheroscler Thromb* **18**, 359–364 (2011).
193. Clément, M. *et al.* Necrotic Cell Sensor Clec4e Promotes a Proatherogenic Macrophage Phenotype Through Activation of the Unfolded Protein Response. *Circulation* **134**, 1039–1051 (2016).
194. Tanaka, M. *et al.* C-type lectin Mincle mediates cell death-triggered inflammation in acute kidney injury. *J Exp Med* **217**, e20192230 (2020).
195. Zhang, Y. *et al.* CLEC4s as Potential Therapeutic Targets in Hepatocellular Carcinoma Microenvironment. *Front Cell Dev Biol* **9**, 681372 (2021).
196. Patin, E. C., Orr, S. J. & Schaible, U. E. Macrophage Inducible C-Type Lectin As a Multifunctional Player in Immunity. *Front Immunol* **8**, 861 (2017).
197. Tanaka, M. Molecular mechanism of obesity-induced adipose tissue inflammation; the role of Mincle in adipose tissue fibrosis and ectopic lipid accumulation. *Endocr J* **67**, 107–111 (2020).
198. Yamasaki, S. *et al.* Mincle is an ITAM-coupled activating receptor that senses damaged cells. *Nat Immunol* **9**, 1179–1188 (2008).
199. Kim, S., Oh, M. I. & Swanson, J. M. J. Stressed Lipid Droplets: How Neutral Lipids Relieve Surface Tension and Membrane Expansion Drives Protein Association. *J. Phys. Chem. B* **125**, 5572–5586 (2021).
200. Jarc, E. & Petan, T. Lipid Droplets and the Management of Cellular Stress. *Yale J Biol Med* **92**, 435–452 (2019).

Appendix

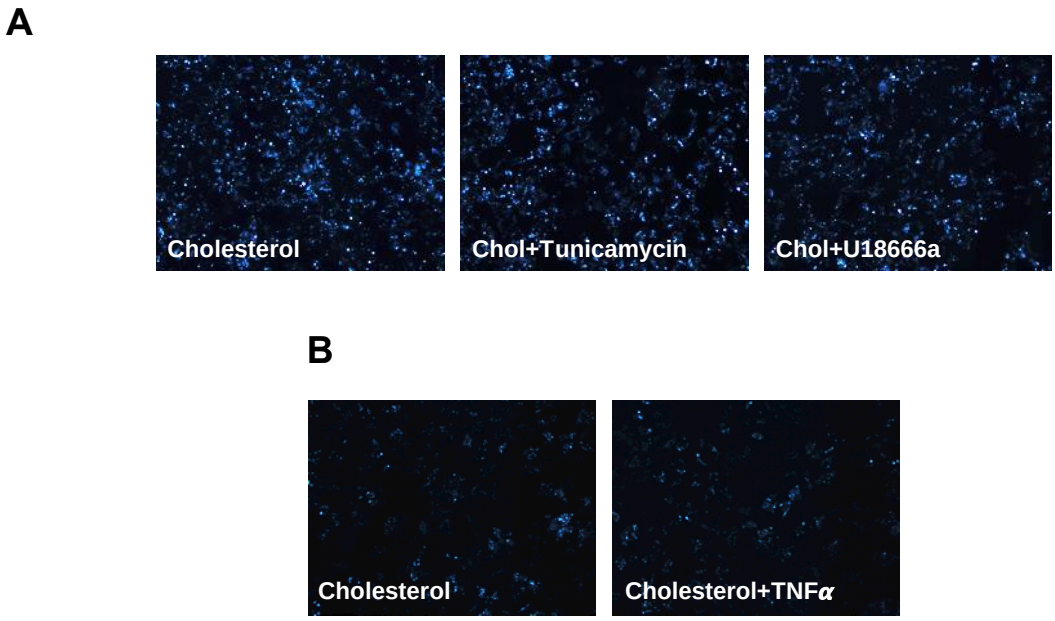

Appendix A: Testing potential factors that may affect hepatocyte CC formation.

A

48h Cholesterol → 48h Control Media
48h K604 (0.1 μM)
48h Rapamycin (100 nM)
48h Simvastatin (1 μM)

B

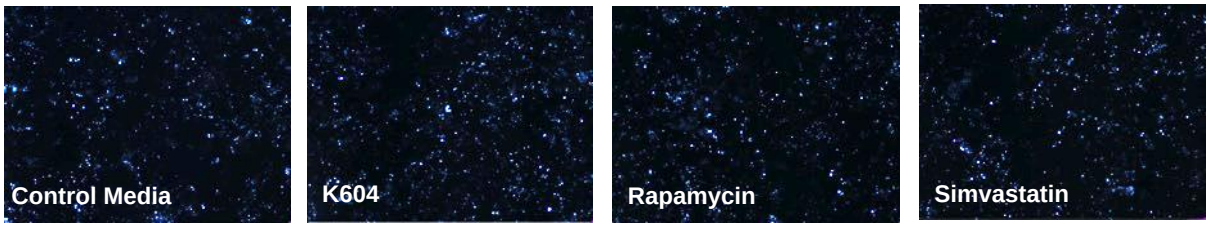

Appendix B: Testing potential factors that may contribute to the resolution of hepatocyte cholesterol crystallization.

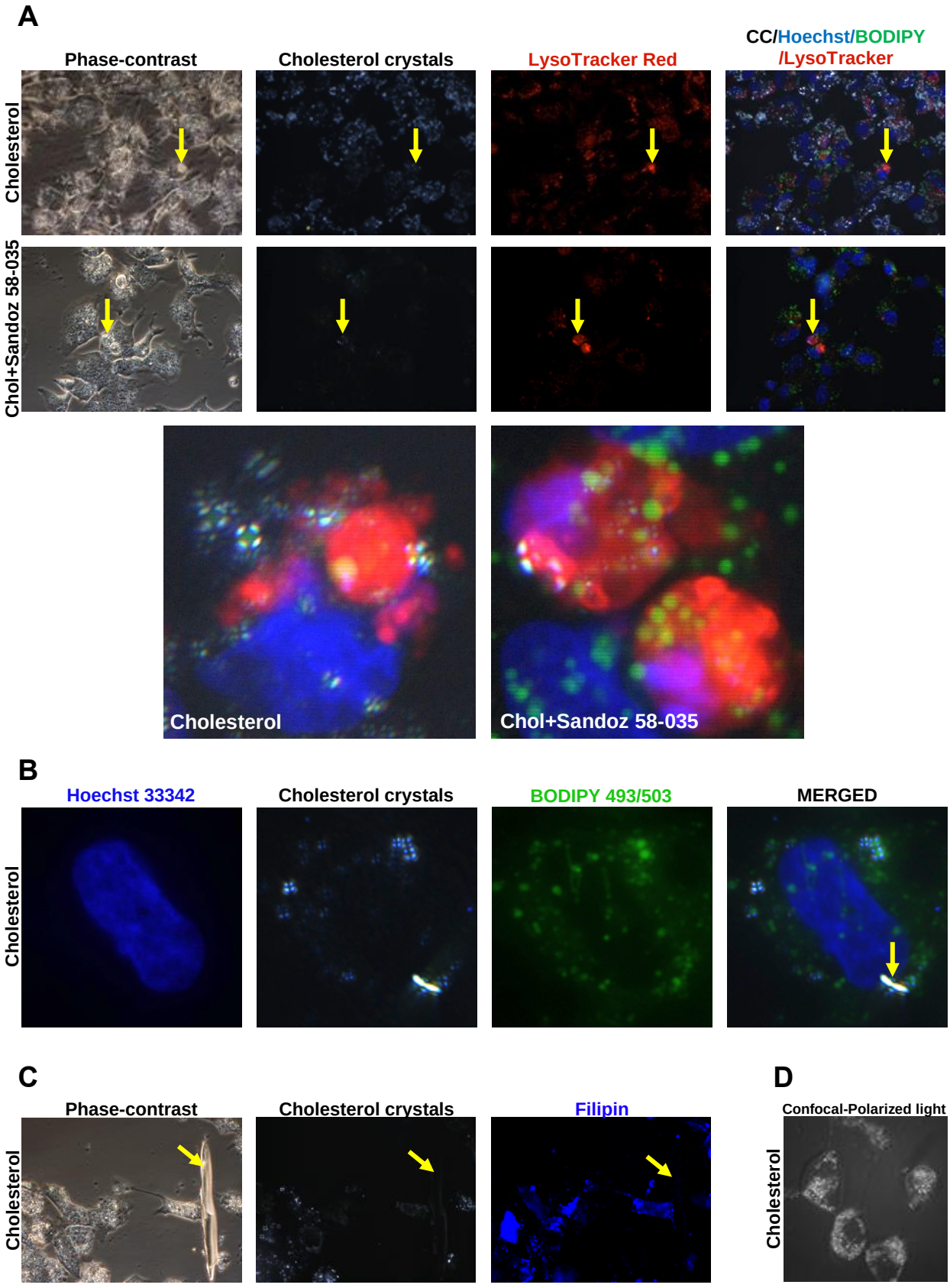

Appendix C: Identification of autophagosomes and plate-like cholesterol crystals.

A

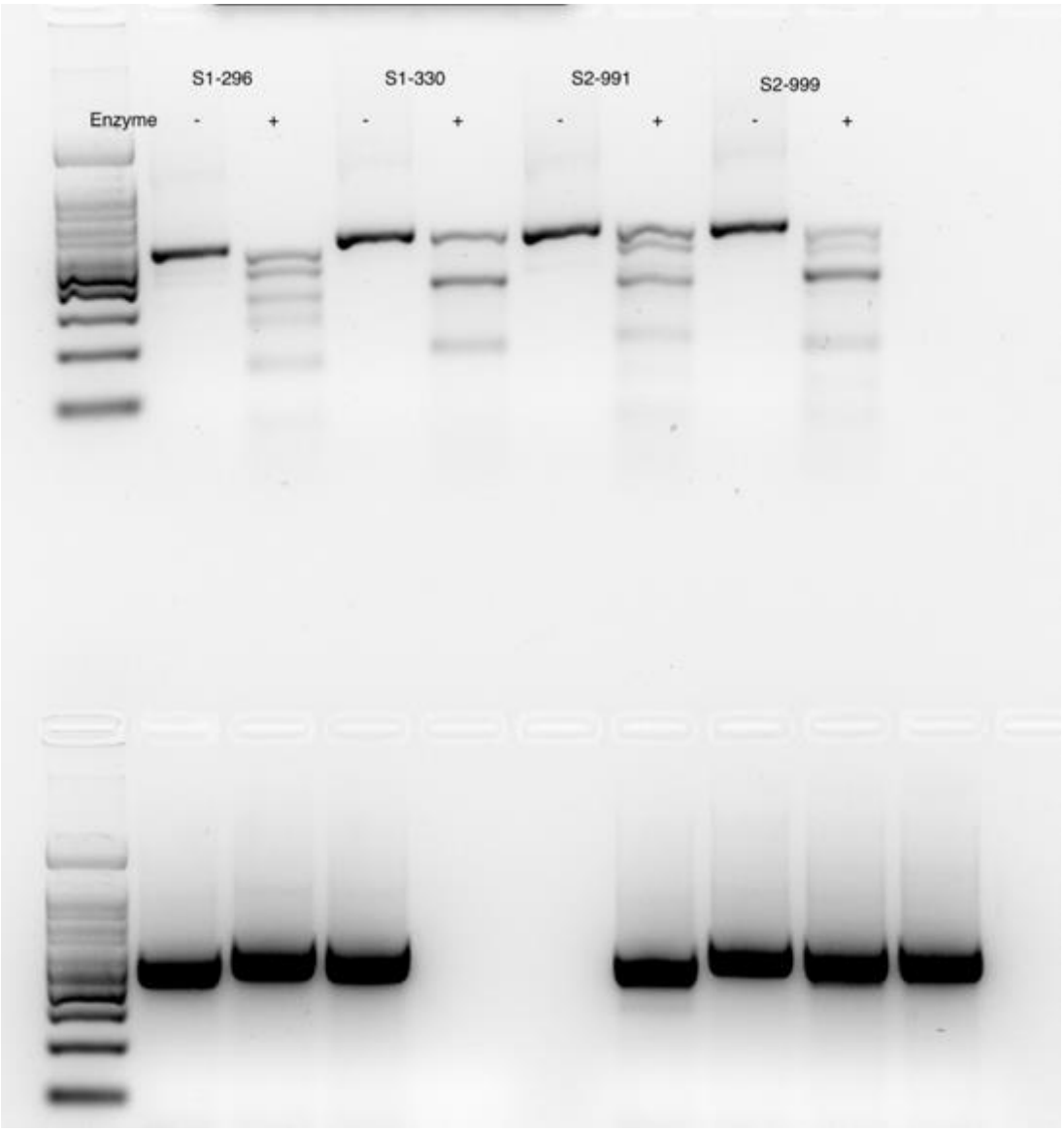

Appendix D: Genomic cleavage assay verifying gene editing in SOAT1/2^{KO} lines.

A

SOAT1: gRNA #296

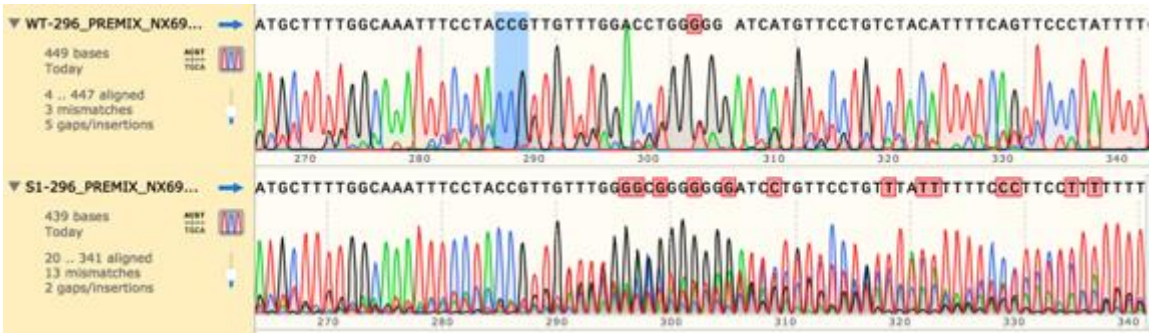

SOAT1: gRNA #330

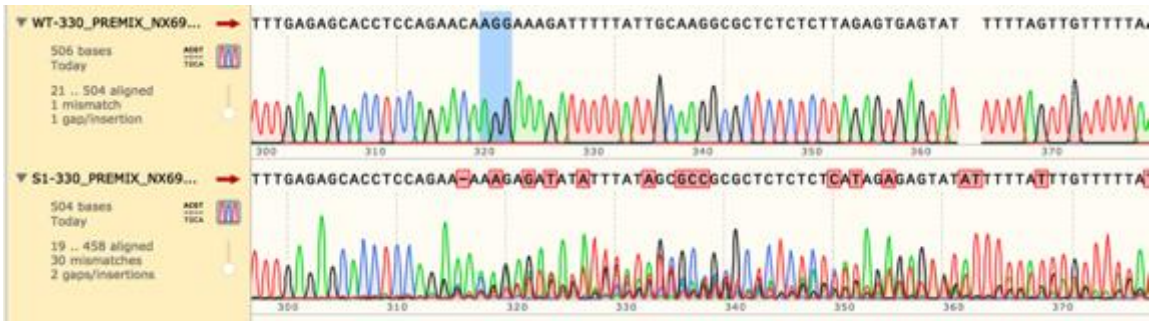

SOAT2: gRNA #991

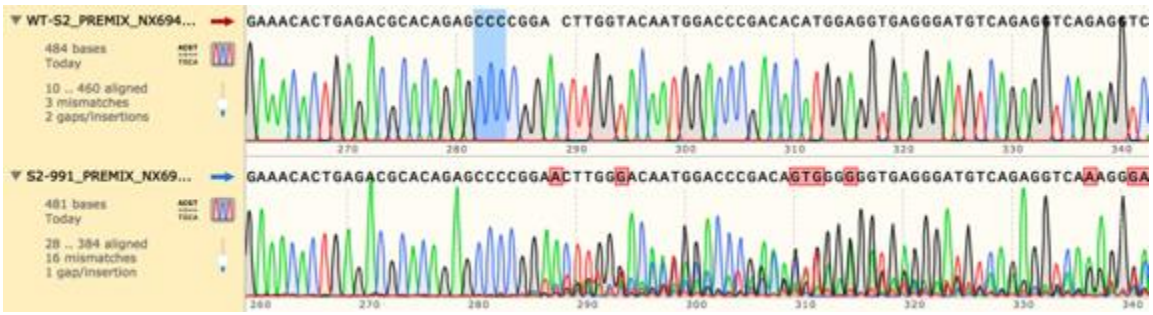

SOAT2: gRNA #999

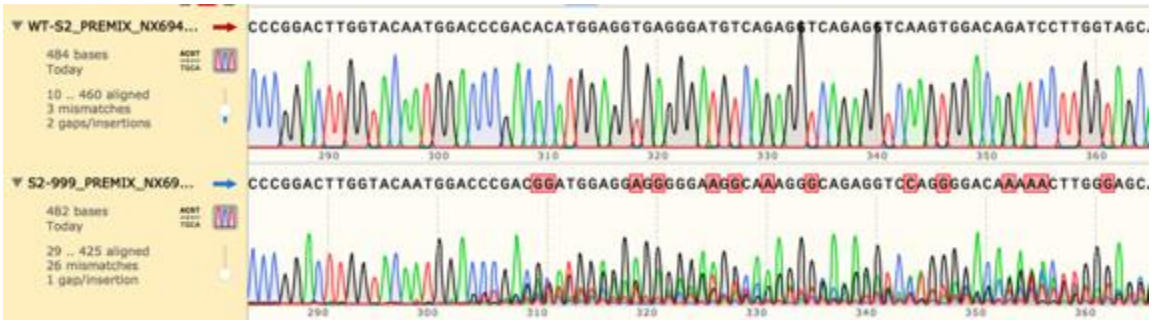

Appendix E: Sequencing verifying gene editing in SOAT1/2^{KO} lines.

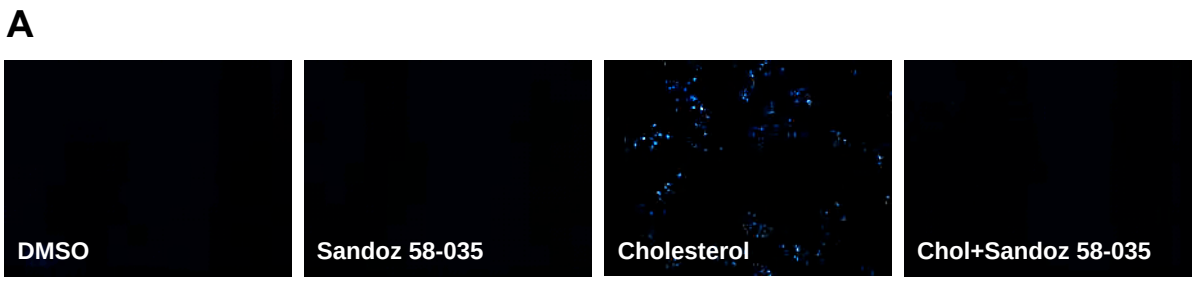

Appendix F: ACAT inhibition prevents cholesterol-induced CC formation in macrophages.